UiT
THE ARCTIC UNIVERSITY OF NORWAY

Faculty of Science and Technology

Department of Geosciences

Deposits and processes on the tide-influenced fjord-head delta in Dicksonfjorden, Svalbard

—

Maria Huse Kvam

Master thesis in Sedimentology and Quaternary Geology (GEO-3900)

May 2018

UNIS

UNIVERSITY OF TROMSØ

Abstract

This study investigates for the first time the tide-influenced fjord-head delta in Dicksonfjorden, a fjord in central Spitsbergen, Svalbard. In order to examine the deposits and processes, sediment cores, surface observations and bulk samples have been obtained. Sedimentary facies, log transects and composite logs are presented. Sediment cores are dated with the ^{210}Pb dating method to provide an average sedimentation rate for the intertidal zone. High-resolution aerial images are used to produce a geomorphological map of the area. Landforms and surface features are identified, described and interpreted. Sedimentological trends of the delta are described and interpreted. An aerial photo from 1938 is used to describe and discuss the development of the delta.

Tidal flats, tidal channel, tidal bars, rill channels and cheniers are identified. 7 facies are identified which belong to tidal flat deposits or tidal bar deposits. The tidal flat deposits generally consist of muddy and sometimes sandy laminations, indicating mostly deposition from suspension during high tide. Deformational structures are common and together with circular depressions on the tidal flats they indicate shore ice influence. The tidal bar deposits generally consist of cross-laminated and structureless sand, indicating rapid deposition from a relatively strong heavy sediment-laden current. Heterolithic horizontal laminations, bedforms, reactivation surfaces and desiccation cracks together serve as a strong indicator of tidal influence. The wave-protected setting in which the delta is situated allows a microtidal range to be sufficient for influencing the deposits. Tidal flat deposits transition from mud flat to mixed sand-mud flats moving in a channel-ward direction, indicating a decrease of tidal current speed due to friction against the tidal flat. ^{210}Pb profiles indicate non-steady deposition in the intertidal zone and an average sediment accumulation rate of 0,3 cm/year during the last century. Rill channels develop on tidal flats due to erosion by ebb tide and their distribution can therefor be used to determine the boundary between the intertidal and supratidal zone. Grain-sizes increasing towards the outskirts of the delta indicate a sediment input coming from the surrounding mountains, in addition to Dicksonelva. Because of this and the lack of sand flat deposits in the channel proximal areas of the tidal flats, the delta does not show a good correlation with the previously published facies model from Dalrymple (1992). The aerial photo from 1938 reveals that major tidal channels are located at approximately the same positions as today, indicating that the channel system is quite stable. This is probably linked to the cohesive properties of the muddy tidal flat deposits. Due to relative sea level fall since the last glaciation, the delta represents a forced regressive deposit. The forced regression causes the supratidal part of the delta to slowly increase. Fluvial downcutting and transport of older deposits out on the delta front and slope is likely to be occurring.

Acknowledgements

I want to start by thanking my supervisor, Maria Jensen (UNIS), for giving me the opportunity to have my MSs project on Svalbard. It has been two fantastic summers with fieldwork and life lasting memories. Thanks also for giving me the opportunity to participate in conferences, and great support and feedback. I would also like to thank my other supervisor, Matthias Forwick (UiT) for all the advice and feedback I have received. Witold Szczuciński (Adam Mickiewicz University in Poznan) is thanked for great advise and help with the ^{210}Pb and ^{137}Cs dating interpretation. Kyungsik Choi (Seoul National University) is thanked for great discussions and advice.

The fieldwork could not have been done without my co-field workers and field assistants. A big thanks to fellow master student Max Holthuis for help with planning and organizing fieldwork, for great discussions and for always being happy! Dagmar Schou, Martha Schou, Tyler Steward, Marine Ilg, Maiken Rian and Astrid Fuglseth Rasmussen are thanked for their contribution to the fieldwork and good team spirit. A big thanks to Trine Merete Dahl, Karina Monsen, Ingvild Hald and Sigrun Kvenbø Hegestad for laboratory assistance at UiT. Thanks to Lise Gjellstad for being the best student adviser one can have.

Thank you to all the amazing people at UNIS, especially Cristina, Hugo, Kristine, Vanessa Ditte, Matilda, Juliane and Michael for making this place into what it is.

Finally, I want to thank my amazing family who always is there for me when I need them.

The study was funded by the Research Council in Norway, Svalbard Science Forum's strategic grants (257581) and supported by Polish National Science Centre grant no 2013/10/E/ST10/00166.

Table of Contents

List of Figures

List of Tables

1. Introduction

1.1 Motivation, aim and approach

Only a few studies exist from cold region tidal flats (e.g. Dionne 1988 and Dashtgard *et al.* 2014), and the only studies of tidal flats in Svalbard are those from Boròwka (1989), Wlodarska-Kowalczuk *et al*. (2007), Eriksen (2013) and Jensen *et al.* (2014). Due to the presence of shore ice and frost action, tidal flats in cold regions differ greatly from those in temperate and warm regions. Much better coverage is needed to provide generalized facies models, which can be a useful tool for interpreting environmental and climatic conditions in which ancient sediments may have been deposited.

The aim of this study is to examine processes and deposits the tide influenced fjord-head delta in Dicksonfjorden. This study provides for the first time a geomorphological map of the fjord-head delta, as well as sedimentological data obtained from short sediment cores, surface observations and grain-size samples.

This study is a part of the research project "Sediment flux from source to sink – the coastal link", which aims at increasing the understanding of how sediments are transported from land to fjord basins in fjords of Svalbard, as well as evaluating the impact of changing sediment supply on marine life. This is done through comparing a glaciated fjord (Kongsfjorden) and a non-glaciated fjord (Dicksonfjorden).

2. Background

2.1 Tidal cycles

The moon exerts gravitational forces on the Earth and everything on the surface of it, including the water masses in the oceans. The water that is closest to the Moon experiences the largest gravitational pull, and this creates a bulge of water, a tidal bulge. On the opposite side of the Earth, another bulge is created because the Moon is pulling the Earth away from the water masses (Nichols 2012[1]).

If the Earth was a perfect sphere without large continents, every point on the Earth could experience two equally proportioned high and low tide every day. The large continents block the westward route of the tidal bulges as the Earth rotates about its axis. Unable to move freely, the tidal bulges create complex tidal patterns within every ocean basin. Most of the Earths coastlines have semidiurnal tides, which means two high and two low tides every day. Some coasts only have one high and one low tide (diurnal tides), and some have a combination of these two, called mixed semidiurnal tides (Sumich 1996).

In addition to the influence of continents, the Coriolis force is also affecting the tidal bulges. Water masses moving in the northern hemisphere are turned towards the right and in the southern hemisphere to the left (Nichols 2012[1]).

Neap-Spring cycles are caused by variations in the effect of the gravitational pull of the Moon and the Sun during the Moon's monthly orbit. Spring tides are created when the Moon and the Sun are in line and the gravitational effects of these two objects on the Earth are added together. This increases the height of the tidal bulge and causes stronger flood and ebb tides. Neap tides are created when the Moon is 90° to the line joining the Sun and the Earth and the tidal bulge caused by the Sun partially cancels out the bulge caused by the Moon. This decreased the height of the tidal bulge and causes weaker flood and ebb tides. During the 28 days of the Moon´s orbit, the Moon and the Sun is twice in line (spring tide) and at right angles to each other (neap tide) (Nichols 2012[1]).

On top of the semidiurnal/diurnal and neap-spring cycles is an annual tidal cycle caused by the elliptical nature of the Earth´s orbit around the Sun. At the autumn and spring equinoxes, the Earth is closest to the Sun and the gravitational effect is strongest. The highest tides of the year occur during spring tides in the equinoxes (Nichols 2012[1]).

2.2 Modern tidal flats

Tidal flats are low-relief (< 0,1°) coastal environments generally consisting of fine-grained sediments such as mud and sand. Tidal flats are situated in the intertidal zone, meaning that they are submerged during high tide and subaerially exposed during low tide. The subtidal zone lies below the mean low tide, while the supratidal zone lies above the mean high tide, but may be flooded during exceptionally high tides (Dalrymple 1992, 2010).

Davies (1964) classifies coastlines based on their tidal range. Macrotidal coasts have a tidal range greater than 4 m, mesotidal coasts have a tidal range of 2-4 meter, and microtidal coasts have a tidal range less than 2 m.

The formation of tidal flats is controlled by the relative influence of tidal currents, which is a product of the tidal range and current speed, as well as the amount of wave action. Waves can rework tidal deposits and geomorphology and prevent the formation of tidal flats (Davies 1964).

Tidal flats generally occur in environmental systems sheltered from large waves and swells, such as estuaries, embayments and lagoons (Fan 2012), and are therefore most often associated with transgressive coastlines. Even small, microtidal ranges are sufficient for the formation of tidal flats, in these protected coastlines.

Tidal flats can also form in more open and exposed environmental systems on prograding/ regressive coasts, such as deltas and coastal plains (Dalrymple 1992, 2010), if the coast is exposed to large tidal ranges and/or high tidal current speeds overrunning the wave action (Fig. 1).

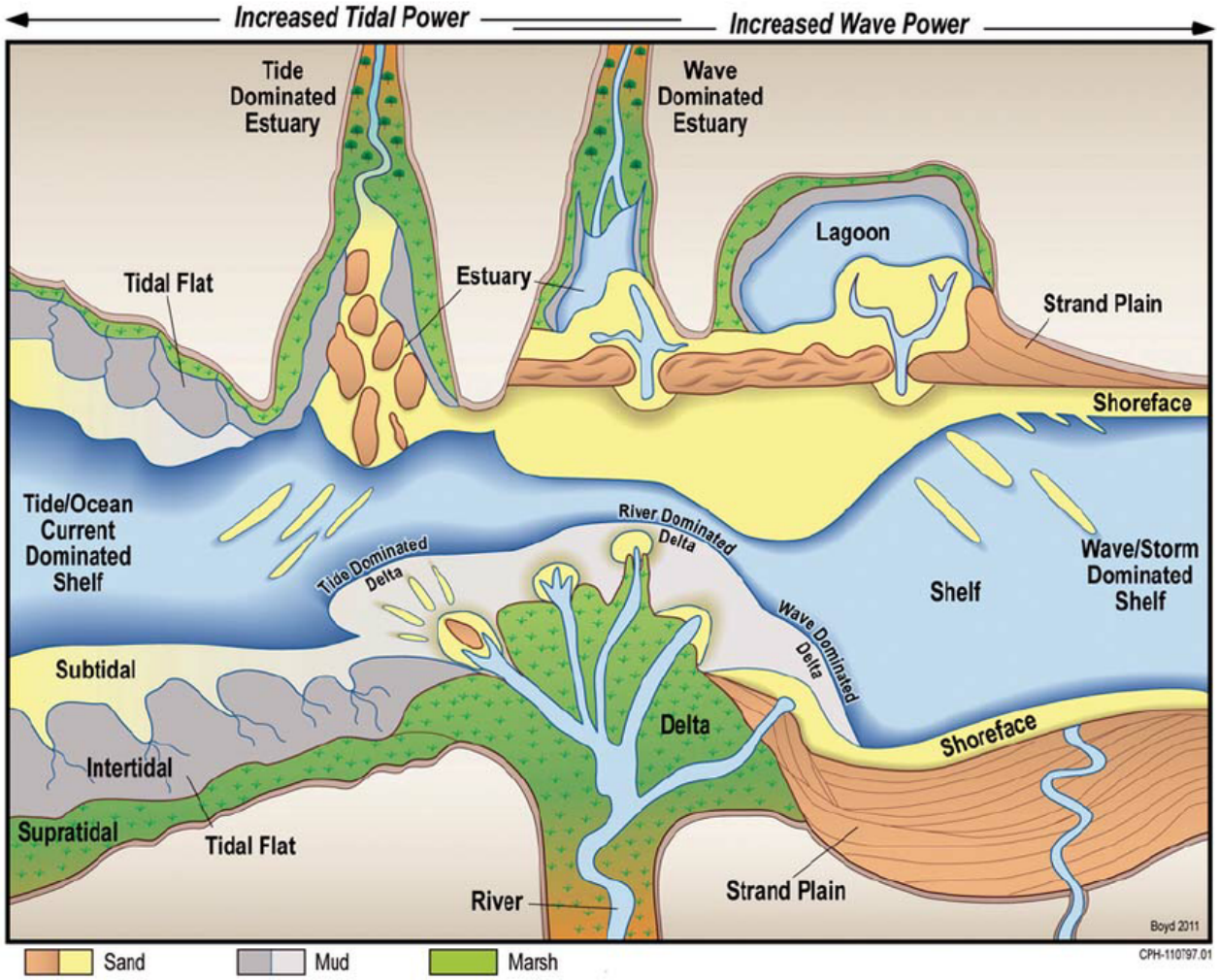

Fig. 1 The diagram shows a variety of common coastal environmental systems ranging from tidally- to wave-dominated (Boyd et al. 1992, updated by James and Dalrymple 2010). The upper half of the diagram shows examples of environmental systems that may form on transgressive coasts (estuaries, lagoons and open coast tidal flats). The lower half of the diagram shows examples of environmental systems that form on regressive coasts (deltas, strand plains, open coast tidal flats).

Tidal flats act as a transition zone between the terrestrial and marine environment, and is often referred to as the fluvial-to-marine transition zone. Tidal flats are one of the most complicated environments on Earth because of the interaction of terrestrial and

marine processes. River currents, tidal currents and waves are the most significant, physical processes that influence the nature of tidal flat deposits. The relative importance of these processes varies in a systematic manner though the fluvial-to-marine transition zone (Dalrymple and Choi 2007).

The river current decreases in a seaward direction because of the decreasing physical and hydraulic gradient as the river enters the sea. Also contributing to this trend is that the river channels are splitting into more channels when the gradient physical gradient decreases (Dalrymple and Choi 2007).

The tidal currents increase as one goes landward from the sea, because of the incoming tidal wave is being compressed onto a smaller area, until the friction causes the current to decrease. This causes the maximum tidal current to occur within the middle to inner part of the delta plain, near the place where distributary channels are branching out (Dalrymple and Choi 2007).

The tidal limit is the maximum landward extent of tidal influence. This limit is better though of as a zone, as the limit moves upwards and downwards in the system following the tidal cycles (semi-diurnal, spring and neap, equinoxes) and variations in river discharge, due to seasonal changes and rain events. The river current generally vary slowly compared to the semi-diurnal variations in tidal current speed (Dalrymple and Choi 2007).

The first sign of tidal influence is variations in the river current speed, slowing down during flood tide and speeding up during ebb tide. Further seaward the river current will be stopped completely and, even further seaward the river current is reversed periodically. Salty ocean water brought in by the tidal current is mixed with fresh river water and which causes brackish water conditions. Periodic flow reversals happen to different extents until the tidal maximum limit. Fluvial processes dominate landward part of deltas and estuaries, and the seaward part is dominated by tidal processes (Dalrymple and Choi 2007).

The turbidity maximum zone (TMZ) is situated in the brackish-water to fresh water tradition where the main mud deposition is happening because of flocculation and destiny driven currents (La Croix and Dashtgard 2015, Dalrymple and Choi 2007). Deposits with tidal characteristics are more abundant here then anywhere else in the fluvial-to-marine transition zone (La Croix and Dashtgard 2015).

2.2.1 Sedimentological indicators of tidal influence

The sediment surface of tidal flats may show a wide range of features produced by tidal currents in semidiurnal/diurnal-, spring-neap- and annual cycles.

Desiccation cracks are features that form in clay-rich sediments. When subaerially exposed, the cohesive properties of these types of sediment lead to the formation of cracks. They typically form a polygonal pattern, and the surface between each mudcrack is slightly concave upward. They are easily recognizable in both depositional surfaces and in bedding planes. Desiccation cracks can form in tidal flats, but also in various other environments, such as fluvial flood plains. They are not the result of tidal processes, but of alternating wet and dry conditions (Davies 2012).

Tidal cycles produce currents of varying velocities and a spectrum of bedforms with varying geometries and scales. Some bedforms are linear and some are three-dimensional, and they are commonly preserved in the ancient record and are displayed in bedding planes and depositional surfaces. However, these bedforms may also be formed under non-tidal conditions, especially in fluvial environments. But together they serve as strong indicators of tidal influence (Davies 2012).

Migrating bedforms produce cross-stratification and cross-lamination, in a scale of the height of the bedform that produced it. Tidal fluxes may produce cross-strata with tidal signatures such as flaser, wavy and lenticular lamination, herringbone cross-stratification and reactivation surfaces. Bedforms such as ripples and dunes may accumulate clay and silt in their troughs as a result of sediment settling from suspension during high tide or low tide, slack water conditions. Here, a combination of relatively high-energy conditions exists as flood and ebb producing currents that move sediment, and low-energy conditions during slack tide when fine sediment can settle into bedform troughs. The mud-drapes will be incorporated as the sediment accumulates which produces flaser, wavy or lenticular lamination, depending of the amount of mud versus sand (Reineck and Wunderlich 1968) (Fig. 2). Sediments that consist of an alternation of relatively coarse grained and fine-grained lamina or layers are called heterolithic, and are very common in intertidal environments (Davies 2012).

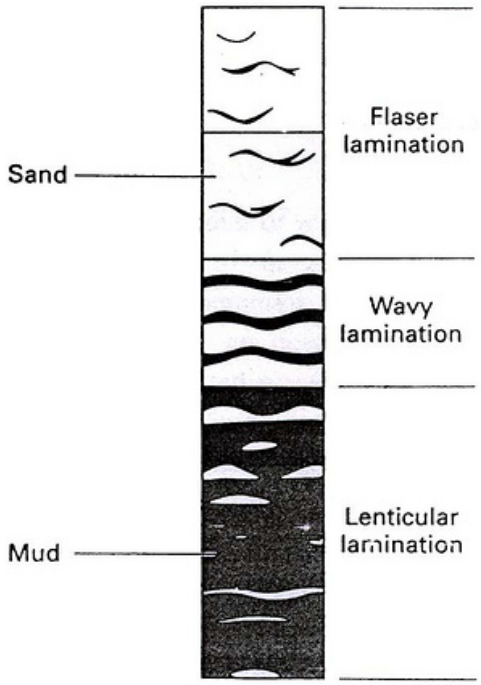

Fig. 2 Lenticular, wavy and flaser lamination (Reineck and Singh 1973).

Flood and ebb current are typically oriented in opposite directions. As bedforms migrate with flood and ebb currents, the direction of the cross-strata will reflect the change in current direction. This result in stacking of cross-sets dipping in opposite direction may form and is known as herringbone cross-stratification. The formation of herringbone

cross-stratification depends sediment supply, but also a near equal flood and ebb tidal current conditions at a given location. This is not common, as tidal channels typically are either flood-or ebb-dominated (Davies 2012). In a tidal cycle at a specific location one current, either flood - or ebb-current will be dominant, while the other will be subordinate. The dominant current moves bedforms and produce cross-stratification. When the subordinate current is not strong enough to reverse the direction of the ripple migration, it might only scour the upper part of the bedform (Davis 2012). This produces an erosional surface, called reactivation surface, that will be separating the next, overlying set of ripples formed by the dominant current (Klein 1970).

Tidal processes may also form planar, horizontal lamination, which reflect flood, slack, ebb, and slack conditions of the tidal cycle. During flood and ebb currents, relatively coarse material, typically sand will be moved and deposited. During high and low slack water conditions, fine suspended sediments such as clay and silt settling to the bottom, which results in heterolithic deposits (Davies 2012).

Tidal bundles are special a type of cross-strata structure ranging generally from 10-50 cm in thickness. Each bundle is a couplet consisting of typically heterolithic cross-strata, but may also be monolithic. They develop by the migration of small dunes (mega-ripples) and do therefore require relatively strong currents. As the small dunes migrate with the tidal current there is variation in the current velocity though the spring-neap cycle, which leads to differences from day to day, in the distance the bedform migrate. This produces differences in the individual bundle thickness from spring to neap, with the thickest bundles during spring tide, and the thinnest during neap tide (Davies 2012).

2.2.3 Sedimentology and geomorphology on tidal flats

Mud-, mixed- and sand flats

According to Dalrymple (1992, 2010), tidal flats shows a general pattern along a transect from the supratidal, though the intertidal and to the subtidal zone going from salt marches, mud flats, mixed sand-mud flats to sand flats (Fig. 3). This pattern is caused by the landward decrease of tidal current speed on tidal flats due to friction against the bed (Dalrymple and Choi 2007).

Salt marches are found in the supratidal zone, but may extend from into the upper zone of the mudflat, causing bioturbation in the mud flat sediment (Nichols 2012[2]). The mudflats area is often located in the upper part of the intertidal zone, between high tide levels on spring and neap tides (Dalrymple 1992, 2010). The sedimentation here mainly happens through settling of suspended mud during high slack tide conditions, and because of the tidal current speed variations though tidal cycles, alteration of clayey and silt laminations are produced. Some very fine sand will typically be present in thin layers and lenses, which creates a deposit with lenticular lamination (Gao 1995). Desiccation cracks are very common in this zone, due to that this zone experiences several days of subaerial exposure after each inundation, which leads desiccation to take place (Davies 2012).

The mixed sand and mud flats lie seaward of the mudflat. Mixed flats are affected by slightly higher tidal current speeds than mudflats. This causes a gradual transition from lenticular lamination to wavy lamination, as the ration of sand to mud increases. Burrowing organisms may produce a variety of *Skolithos* icnhofacies traces and

horizontal burrows of the *Cruziana* ichnofacies (Dalrymple 1992, 2010). Heterolithic current ripple-, wave ripple- and planar laminations are commonly found here. Reworking of deposited sediments are more common here and therefore also reactivation surfaces (Gao 1995).

Sand flats form the lowest portion of the tidal flats and intertidal zone and are transitional into the adjacent tidal channel and tidal bar environments. This area experiences high tidal current speeds and therefore abundant supply of sand. At slack tides, deposition of thick mud drapes can occur, producing deposits with flaser lamination (Gao 1995). Sand flats are often subject to tidal current and waves, resulting in a large variety of sedimentary structures, such as dune cross bedding, tidal bundles and current-ripple lamination. Planar lamination may also occur it the current velocities are exceptionally strong (Dalrymple 1992, 2010).

The progradation of tidal flats typically produce a fining- and shallowing-upward succession. A complete succession may consist of cross-bedded channel fill overlain by sand flat deposits (flaser lamination) that grades upward into mixed flat deposits (wavy lamination) and then mud flat deposits (lenticular lamination) (Fig. 3) (Dalrymple 1992, 2010).

On tidal flats, geomorphological elements such as tidal channels, rill channels, tidal bars and cheniers might be present.

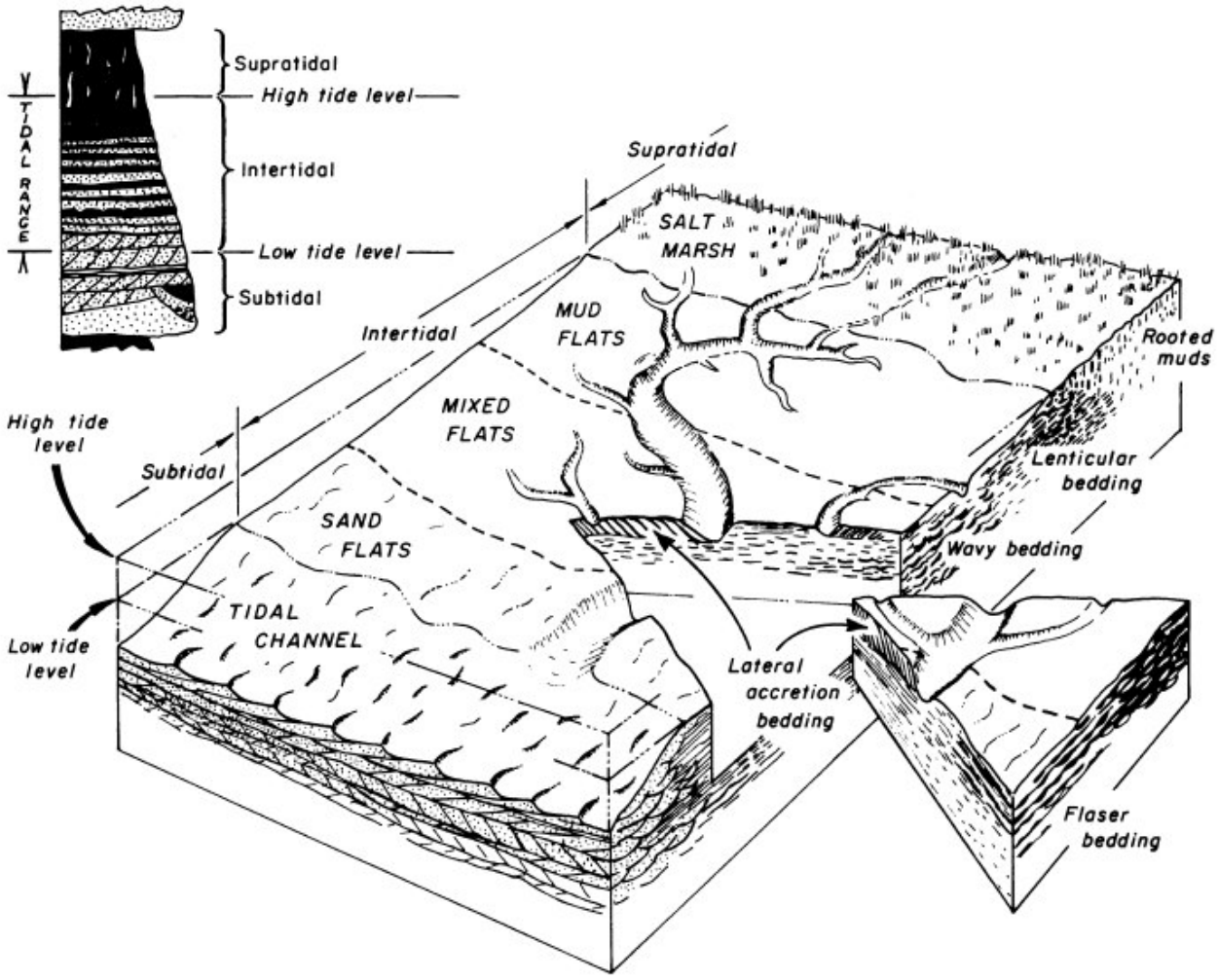

Fig. 3 Facies model for tidal flats showing geomorphological elements (tidal channel, rill channel and tidal flat) and a the general division of the tidal flat into salt march, mud flat, mixed flat and sand flat producing a variety of heterolithic deposits (lenticular, wavy and flaser lamination) (Dalrymple 1992).

Tidal channels

Tidal channels form major drainage systems on tidal flats that are responsible for transport of large amounts of sediment, both in seaward and landward directions (Choi and Jo 2015).

The width and depths of tidal channels vary according to the tidal cycle, but they are typically quite shallow (<1 m) on tidal flats. Because the tidal current in the channels decreased landward due to friction with the bed, tidal channels widen seaward, and are often called funnel-or trumpet-shaped (Dalrymple 1992, 2010).

Tidal channel systems can both be meandering, braided, anastomosing or something in-between like purely fluvial systems. Meandering tidal channels migrate laterally by lateral accretion on point bars and lateral erosion on cut banks (Choi and Jo 2015). In braided tidal channels, channel change is driven by sediment transport (Bierman *et al.* 2014). In anastomosing tidal channels, channels are more stationary but abandon and form new channels by avulsion (Makaske 2000).

In some settings, brackish salinities make the suspended mud particles flocculate, which can result in the formation of dense fluid mud on the bottom of the channels. Deposition

of these fluid muds can produce an unusual combination of mudstone with cross-bedded gravelly or shelly sands (Dalrymple 1992, 2010). A coarse channel-lag deposit of gravely material and shells typically forms at the base of channels due to current speeds occurring here. Sand moving though the channel bottom as bedload may form dunes, which produces dune cross-bedding in a variety of forms (Dalrymple 1992, 2010). Tidal bundles, herringbone cross-stratification, reactivation surfaces and flaser, wavy and lenticular lamination may form in this type of deposit (Davies 2012).

Rill channels
Rill channels, also known as rill marks, are dendritic erosional structures that form due to the concentration of a thin layer of running water. They can form on tidal flats, but also in sediments and soils that are exposed to sheet flow under non-tidal conditions. On tidal flats, rill channel erosion happens either during falling stage (ebb tide) (Das 2017) or due to heavy rain events, especially during low tide (Choi and Jo 2015).

Tidal bars
Tidal bars, typically elongated, form normal to the coast (Dalrymple and Choi 2007), either as point-bars, on the inside of meander bends in the same way as purely meandering river systems (Nichols 2012[2]), or as mid-channel bars as in braided river systems (Dalrymple 1992, 2010).

Inclined heterolithic stratification (interbedded sand and mud with depositional dip; IHS) is a large-scale sedimentary structure that is formed by the lateral accretion in point-bars (Thomas *et al.* 1987; Choi 2010; Sisulak and Dashtgard 2012; Choi *et al.* 2013; Johnson and Dashtgard 2014; Choi and Jo 2015). The current speed decreases upward along both point-bars and mid-channel bars. This typically produces an upward-fining deposit with dune-cross bedding in the lower part of the bar and current-ripple cross lamination higher up on the bar (Dalrymple 1992, 2010). Tidal bundles may form at the base of tidal bars, while planar, flaser, wavy and lenticular laminations are common in upper parts. Reactivation surfaces are also common, and herringbone cross stratification may form if the current conditions are right (Davis 2012).

Cheniers
Cheniers are shelly, sandy and/or gravely barrier islands and beach spits that form on tidal flats. Not much research is done on cheniers and their formations is still poorly understood. There are a few theories on how they may form. Dougherty and Dickson (2012) explain that the development is mainly controlled by storm waves. Another study by Morales *et al.* (2014) suggest that cheniers develop mainly during spring high tide, and that they migrate over the tidal flat in the same way classical beach ridges migrate onto the shorelines.

2.3 Cold region tidal flats
Modern tidal flats in cold regions are in many ways different from those in warm and temperate regions, because they are influenced by shore ice and frost processes. Because of this, cold region tidal flats display numerous distinctive sedimentary features (Dionne 1988).

2.3.1 Shore ice

Shore ice is both responsible for protection, erosion, transportation and sedimentation of sediments on tidal flats in cold regions. Shore ice offers significant protection against tidal current and wave action during the winter, a period with typically frequent storms and increased erosion in most temperate regions. The shore ice is not frozen to the tidal flat, and during flood tide water penetrates under the ice and lifts it up. Suspended sediments that are brought in with rising tides settle rapid under the ice cover, and therefor many cm of mud can be deposited every winter (Dionne 1988).

Despite the ice covering the tidal flat, the tidal flat is to some degree exposed to tidal currents and wave action. This causes sediments to be re-suspended and removed. Shore ice is both responsible for eroding, scouring and deforming the sediment in tidal flats, and this leads to a wide variety of sedimentary structures (Dionne 1988, 1997). The sedimentary structures can be divided into two categories: erosional and deformational structures (Dionne 1997).

Erosional structures

Sediment freezes to the base of the ice cover, and when it breaks up due to tidal currents and wave action, the sediment is transported away with ice cakes (pieces of ice less than 20 m across). This creates erosional scars in the form of shallow depressions (5-10 cm deep) (Dionne 1988).

Tidal and wave motion makes the ice sheet, ice cakes and ice floes (pieces of ice larger than 20 m across) scour and distribute the sediment on the tidal flat. This forms micro-relief consisting of circular depressions of various sizes and forms, typically around 30-100 cm across. The depressions are typically around 20-40 cm deep. They may have frontal and lateral push ridges, up to 40-45 cm high (Dionne 1997). The frontal ridges are always larger than the lateral ridges. The formation of these depressions is disturbing the deposits of the tidal flats greatly, for example by mixing heterolithic laminations. During the ice-free season, erosion by tidal current and waves occur on the ridges, while deposition occurs in the depression, filling them with sediments. The micro-relief will commonly not be entirely reworked by tidal currents and waves during the ice-free season and therefor possible to observe the whole ice-free season (Dionne 1988). In cross section these structures are bowl-shaped and resemble ball-and-pillow structures (Dionne 1997).

Furrows and groves are elongated, erosional features that are produced by the pointy bottom of ice cakes or ice floes with dragged along the bottom by tidal currents (Dionne 1969, 1971). These features are oriented in the direction of the ebb current. They are typically 1-2 km long and around 50-75 cm wide and 10-30 cm deep. The furrows often have small lateral ridges and a larger frontal ridge formed by sediments removed from the furrow. Ribbed groves are series of small holes that form when the keel of ice cakes only touching the bottom at regular intervals. Polished and striated surfaces result from ice cakes with flat bottoms that are being dragged along the tidal flat by ebb currents (Dionne 1988).

Deformational structures

In cold region tidal flats, physical deformation structures of various types are produced by ice-pushing and ice-scouring (Reineck 1976, Dionne 1985, Dashtgard *et al.* 2014).

Relatively large, single ice-push ridges without depressions may form by the scraping the soft sediment surface over long distances. These ridges have horns pointing landward and indicate a landward movement of ice cakes or ice floes. They are typically up to 30-40 cm long, 2 m wide and up to 60 cm high (Dionne 1988). Deformation structures such as folds, convolutions, contorted bedding and micro-faults are typically found in ice push ridges (Dionne 1988, 1997 and Dashtgard *et al.* 2014). Folds are the most common feature and are generally a few decimetres to a few meters in width (Dionne 1997).

Desiccation cracks may develop on the surface of ice push ridges on the lower tidal flat (Dionne 1974), in the mixed flat and sand flat zone. The slight height difference of the ice push ridges and the surrounding areas caused the ridges to be subaerially exposed for longer periods, allowing desiccation to take place (Dionne 1988).

Parker (1963) described a special type of deformation structure that he called "inverted mud cracks". This structure is often arranged in a polygonal pattern. This feature develops right before the breakup of the ice cover, when small cracks in the ice cover are present. During low tide, when the ice sheet or ice floes are resting on the tidal flat, the weight of the ice pressure on the soft sediment and forces the mud into the cracks. If the ice cakes are removed at breakup without scouring the surface, this polygonal pattern of "inverted mud cracks" might be preserved (Dionne 1971).

Sometimes small pieces of ice, remaining form the ice cover, get buried in the sediment. When these ice pieces melts, they produce small kettle holes, which are eventually filled by sediments (Dionne 1988).

Transport and deposition of ice-rafted debris
Shore ice has the capacity of transporting sediments of all grain sizes several kilometres. As mentioned earlier, sediments can refreeze to the base of the ice cover. Sediment may also get incorporate in the ice cover in other ways. During freeze-up and breakup, when turbid water running though the numerous cracks in the ice cover, large volumes of mud and fine sand can get spread over the ice surface. The seawater may also submerge a complete ice cover during the spring high tide, which also results in the deposition of suspended mud on top of the ice cover. This sediment gets incorporated into the ice cover by freezing of meltwater and snow. Of all the sediments that are that is incorporated in the shore ice, it is believed that only a small part returns to the intertidal zone during melting and breakup.

A major difference between tidal flats in cold and temperate regions is the occurrence of coarse debris, such as gravel and boulders together with sand and mud. Gravel and boulder might be ice-rafted onto the tidal flat and dumped, causing gravel and boulder strewn tidal flats. This is more likely to happen in areas where coarse debris is easily accessible (Dionne 1988).

2.3.2 Frost action

In high latitude regions, annual frost and permafrost are important for the development of tidal flats. One effect of permafrost on tidal flats is the rising of the surface due to the formation of segregated ice in the substrate. On salt mashes, on the upper part of the tidal flats, segregated ice may form small frost mounds. The increased elevation of these

areas leads to less influence by tidal current, and therefor also less erosion and sedimentation in these area. However, as the segregated ice melts in the substrate, thermokarst depressions are formed (Dionne 1988). Permafrost is also believed to influence the development of tidal flats by increasing the input of sediments originating from slumping and slides (Forbes and Frobel 1985).

Annual frost is believed to produce several features on tidal flats. One of them in frost heaving of ice-drifted boulders incorporated in the fine-grained sediments. Miniature mud volcanoes are also known to form due to hydrological pressure when ice melts in the substrate. Brecciated structures may form when a superficial frost crust of the sediments breaks into pieces (Dionne 1988, 1997). The role of frost action on tidal flat development is still poorly documented.

2.3.3 Bioturbation

Cold region tidal flats generally have little bioturbation. Due to the shore ice and frost action, buried fauna is normally poorly developed. Several species of birds and mammals find food in the tidal zone in cold regions, and traces from these animals are therefor typically present (Dionne 1988). On a tidal flat in Chignecto Bay in Canada, the shore ice caused a rhythmic interbedding of undisturbed laminated beds and bioturbated beds. Laminated sediments are deposited during the winter when the buried fauna is at the minimum. During the summer, when the infaunal biomass is at a maximum, the sediments get completely bioturbated (Dashtgard *et al.* 2014).

2.4 Coastal environments in Svalbard

Some research has been done on costal environments in Svalbard, but only a few have focused on the sedimentology on tidal flats (Boròwka 1989, Eriksen 2013, Jensen *et al.* 2014, and Zajaczkowski and Wlodarska-Kowalczuk 2007).

Boròwka (1989) examined the surface and subsurface of the Petuniabukta tidal flat. The study found surface features indicating that a lowering of the relative sea level had occurred. Under the silty deposits on the tidal flat, a gravel-clay series was found. These sediments are interpreted to be glacial.

Jensen *et al.* (2014) examined modern processes and resulting sedimentary deposits at a tidal flat in Braganzavågen, Svea. The study found that sedimentation on the tidal flat in Braganzavågen is controlled by the interplay between fluvial and tidal processes, with coarse clastic fluvial systems and colluvial sediment supply playing an important role. Eriksen (2013) also examines the sedimentology on the tidal flat in Braganzavågen.

Wlodarska-Kowalczuk *et al.* (2007) studied the transport patterns, settling and deposition of sediments in a glacier-fed river estuary in Adventdalen. The study shows among other tings that the tidal flat sediments are rhythmically laminated due to the influence of tides and occasionally eroded by catastrophic events such as intense storms and/or winter ice cover scouring. The number of individuals and species of meio-and macrobenthic fauna are very low on the tidal flats. And they are sensitive to sediment instabilities and disturbances caused by high sedimentation rate and frequent sediment gravity flows.

Kowalska and Sroka (2008) examined the sedimentary environment of the Nottinghambukta delta, in SW Svalbard. The delta plain shows a lobate, but asymmetric form and it is almost completely submerged during high tide, and river channels become tidal channels. The sediment consists mainly of gravel, sand and silt.

Szcucinski and Zajaczkowski (2012) studied the factors controlling downward fluxes of sediment in a glacier-contact and a non-glacier contact setting in Billefjorden, central Spitsbergen. They found that the major factors controlling sediment flux are the positions of freshwater inlets, meltwater discharge, local wind and tidal range.

Zajaczkowski *et al.* (2004) examined the resent sediment accumulation rates in Adventfjorden by using ^{210}Pb and ^{137}Cs dating. They found that modern rates in the central basin decrease downfjord from 1,87 to 0,87 cm/y. Comparison of old and new values reveals a noticeable increase in sedimentation accumulation rates in the last ten years, which corresponds well with the recent climate change (warming and increase in precipitation).

Szczuciński *et al.* (2009) reconstructed the Little Ice Age and 20th century sediment accumulation rates in Billefjorden using ^{210}Pb, ^{137}Cs and ^{14}C dating. The modern sedimentation rate in the fjord was 0,39 cm/y at the fjord head and 0,08 cm/y further out in the fjord. They link the increasing sedimentation accumulation rate to the post Little Ice Age glaciers retreating glaciers and a warming climate.

Majewski *et al.* (2009) examined the interaction of Arctic and Atlantic water-masses and the environmental change during the last millennium in Hornsund. Among other things, the study concludes with that the major climate changes in SW Spitsbergen correlate with the interaction between inflow of cold Arctic water and warm Atlantic water. And also that tidewater glacier was present in SW Spitsbergen throughout the last thousand years.

Rachlewicz *et al.* (2007) examined the post little ice age development of glaciers around Billefjorden in central Spitsbergen. The study was based on aerial photographs, maps, satellite photos and observation from 2000-2005. They concluded with that the glaciers had been retreating since the Little Ice Age. The surging tidewater glaciers had retreated in average 220 m/year, non-surging tidewater glaciers 15-70 m/year, land-terminating glaciers 10-20 m/year and small and cold glacier (cirque and valley) had retreated below 10 m/year.

Rachlewicz and Szczuciński (2008) studied changes in thermal structure of permafrost active layer in Petuniabukta in central Svalbard. They measured air temperature, air humidity, wind direction and velocity, precipitation, cloudiness, thickness of the permafrost active layer and ground temperature. The study found that inter annual variations were mainly due to changes in summer temperatures and to the length of period with snow cover in spring, which limited the beginning of thawing.

3. Setting

3.1 Svalbard

3.1.2 Physical geography and climate

The archipelago of Svalbard is located in the northwestern Barents Sea and includes all islands between 74 and 81 degrees north and 10 and 35 degrees east (Fig. 4). Svalbard has a total land area of 62 160 km^2. The West Spitsbergen Current, which is the northernmost branch of the North Atlantic Current (Fig. 4), reaches the west coast of Svalbard, keeping water open most of the year. The present climate of Svalbard is Arctic, and the mean annual temperatures in central Spitsbergen is -4,6 °C (Førland et al 2011).

Annual precipitation in central Spitsbergen is only about 200 mm water equivalent (w.e.), and 60 % occurs as snow (Eckerstrofer and Christiansen 2011). The area can be defined as a polar desert (Humlum 2003, 2007). Along the western and eastern coast of the island the precipitation is higher, about 400-600 mm w.e. (Humlum 2003, 2007).

According to Hagen *et al.* (1993) over 60 % of Svalbard is covered by glaciers, which constitutes 36600 km^2. The total volume is estimated to be c. 7000 km^3, and most of it is contained in ice caps and highland ice fields on Spitsbergen and Nordaustlandet (Hagen *et al*. 1993). Large valley glaciers and cirque glaciers are common along the western and eastern coast of Spitsbergen (Ingólfsson 2011). The glaciation in Svalbard is connected with the precipitation rates (Humlum 2002), and the glaciation in the central parts of Spitsbergen is therefore less extensive. Here small valley glaciers and cirque glaciers dominate. Many of Svalbard glaciers are polythermal, and of them many are of the surging type (Ingólfsson 2011).

At least 90 % of Svalbard's land surface not covered by glaciers is underlain by lateral continuous permafrost (Humlum *et al.* 2003; Christiansen *et al.* 2010). A seasonally unfrozen layer called the active layer overlies the permafrost. The active layer in Adventfjorden, central Spitsbergen is about 0,8 to 1,2 m thick (Christiansen *et al.* 2010).

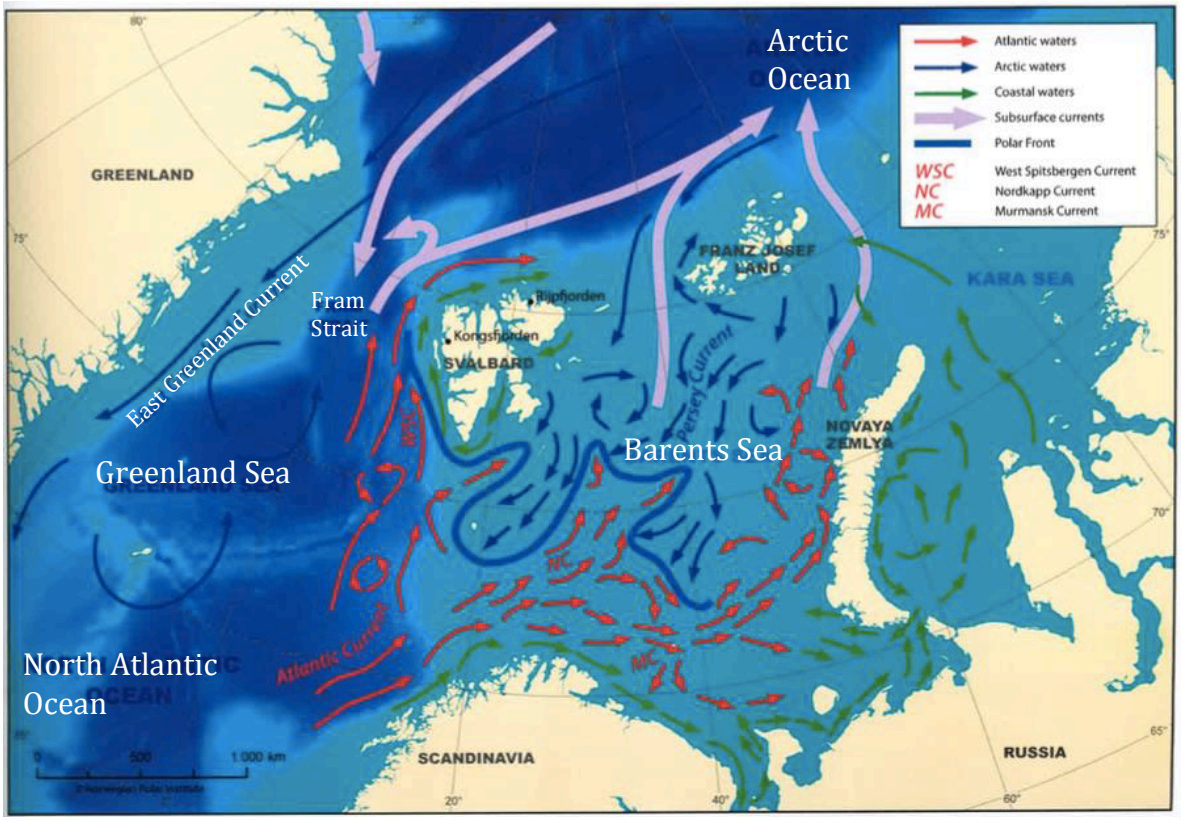

Fig. 4 Location of the Svalbard archipelago in the northwestern Barents Sea with the ocean currents surrounding it. The West Spitsbergen Current (WSC) supplies warm water up to the west coast (Modified from Dallmann 2015).

3.1.3 Glaciations and sea level

Svalbard has been glaciated several times during the late Quaternary (Manglerud *et al.* 1998; Ingólfsson and Landvik 2013). At the last glacial maximum (LGM), about 20 ka BP, a thick ice-sheet was covering the Svalbard-Barents Sea region (Landvik *et al.* 2005). This ice drained through valleys and fjords and removed most of the sedimentary record of previous glaciation-deglaciation cycles (Elverhøi *et al.* 1995). The transition into an inter-glacial mode happened relatively rapid, and shelf areas west of Spitsbergen were ice-free by about 15 ka BP (Landvik 1998). At about 11,5 ka BP, the central Isfjorden was deglaciated (Forwick and Vorren 2009). The inner tributary fjords of Isfjorden were deglaciated by about 10 ka BP (Svendsen and Mangerud 1997; Lønne and Lyså 2005). Between the 1400s and the 1900s, the Little Ice Age occurred in Svalbard, and most glaciers in this area are believed to have had a significant advance during this period (Martín-Moreno *et al*. 2017).

Eustatic sea level rise occurred in response to the deglaciation, but was surpassed by the rate of glacio-isostatic crustal rebound. This caused a forced regression to occur in Svalbard. Holocene, relative sea level curves from western Spitsbergen shows an exponentially declining fall (Forman *et al*. 2004). In the outer parts of Isfjorden, post-LGM raised beach ridges are found up to 48 m above sea level. In the inner parts, post-LGM raised beach ridges occur up to 90 m above sea level (Salvigsen 1984; Forman 1990). In Ny-Ålesund (north-west Spitsbergen), the uplift cause by changes in ice volume during the deglaciation has been predicted by models to be about 3,3 mm/ year the past ten years. The overall uplift measured however is 8,5 mm/year. This large uplift observed is believed to reflect both changes in ice volume during the last deglaciation,

the Little Ice Age and today (Tadahiro *et al.* 2006). It is a well-known fact that the global sea level is rise is increasing (Douglas 1991), but the isostatic uplift in Svalbard is believed to be higher that the sea level rise. Barentsburg (central, west Spitsbergen) has had an average relative sea level fall of 2,74 mm/year in the period of 1949-2015 (Norwegian Polar Institute 2018).

3.2 Study area: Dicksonfjorden

3.2.1 Physical geography and climate

Dicksonfjorden is a non-glaciated tributary fjord of Isfjorden, located on Svalbard's largest island, Spitsbergen (Fig. 5 A and B). The fjord is a part of the large geomorphic system of Isfjorden that drained the Svalbard-Barents Sea Ice-sheet to the shelf edge during the late Weichselian glaciation (Ingólfsson and Landvik 2013). The fjord is about 28 km long, 7 km wide and 123 m at the most (http://toposvalbard.npolar.no). The innermost part of Dicksonfjorden has a fjord-head delta with a tidal flat comprising mainly mud and very fine sand. Delta receives sediments from a glaciofluvial river system, the Dicksonelva that is running through the valley, Dicksondalen. It is not known how long the river is frozen during the year, but the river system Adventelva (central Spitsbergen) which is also situated in a fjord-valley and comprises relatively fine grained sediment, transports meltwater and sediments for about four moths a year. This period normally extends from late May/early June to late September/early October. The river is frozen during the rest of the year (Prior *et al.* 1981).

The tides in Dicksonfjorden are semi-diurnal and the range is microtidal (Tidevannstabeller 2018). Sea ice normally covers the fjord during the winter and spring months, but the sea-ice conditions in the recent years have been poor. As the other inner tributary fjords of Isfjorden, Dicksonfjorden was deglaciated by 10 ka PB (Svendsen and Manglerud 1997; Lønne and Lyså 2005). Small valley- and cirque glaciers cover substantial parts of the catchment area of Dicksonelva, and Batteybreen is the largest glacier in the catchment and is occupies the uppermost part of Dicksondalen (http://toposvalbard.npolar.no). Batteybreen is known to have surged due to a landforms such as crevasse squeeze ridges, eskers, looped moraines and push moraines found in the forefield of the glacier. The timing of the surge is unknown (Hagen *et al.* 1993).

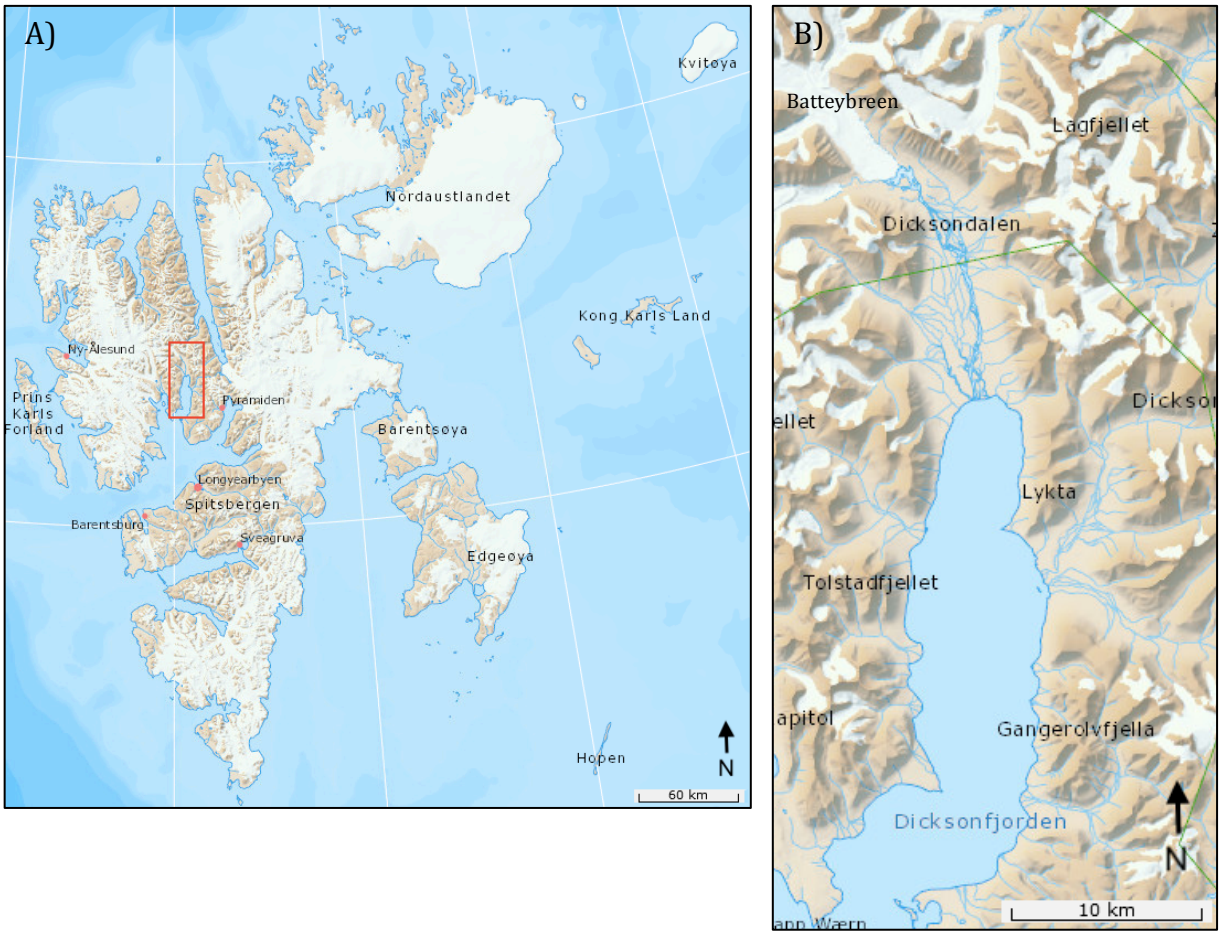

Fig. 5 Location of study area, Dicksonfjorden. A) Svalbard archipelago with the location of Dicksonfjorden marked with a red square. B) The study area, Dicksonfjorden. Source: TopoSvalbard, Norwegian Polar Institute (NPI), 2018 (http://toposvalbard.npolar.no).

3.2.2 Bedrock geology

The bedrock in the catchment area consists of the Early Devonian Wood Bay Formation of the Andreé Land Group and the Austfjorden Member of the Wood Bay Formation (Fig. 6). The Wood Bay Formation is exposed in central N Spitsbergen. The formation consists of iron oxidized clastic sedimentary rocks and underlying limestone. The Austfjorden Member consists of calcareous sandstone and pebble conglomerate (Dalmann 2015). The Wood Bay Formation represents continental terrestrial molasses deposition under arid to semi-arid conditions (Blomeier *et al.* 2003).

A small portion of the catchment area also consists of the overlying Wordiekammen Formation, from the Dickson Land Subgroup in the Gipsdalen Group. The Wordiekammen Formation consists of a platform succession of cyclic carbonates of Late Carboniferous-Early Permian age. The Wood Bay Formation and the Wordiekammen Formation are separated by an unconformity (Ahlborn and Stemmerik 2015).

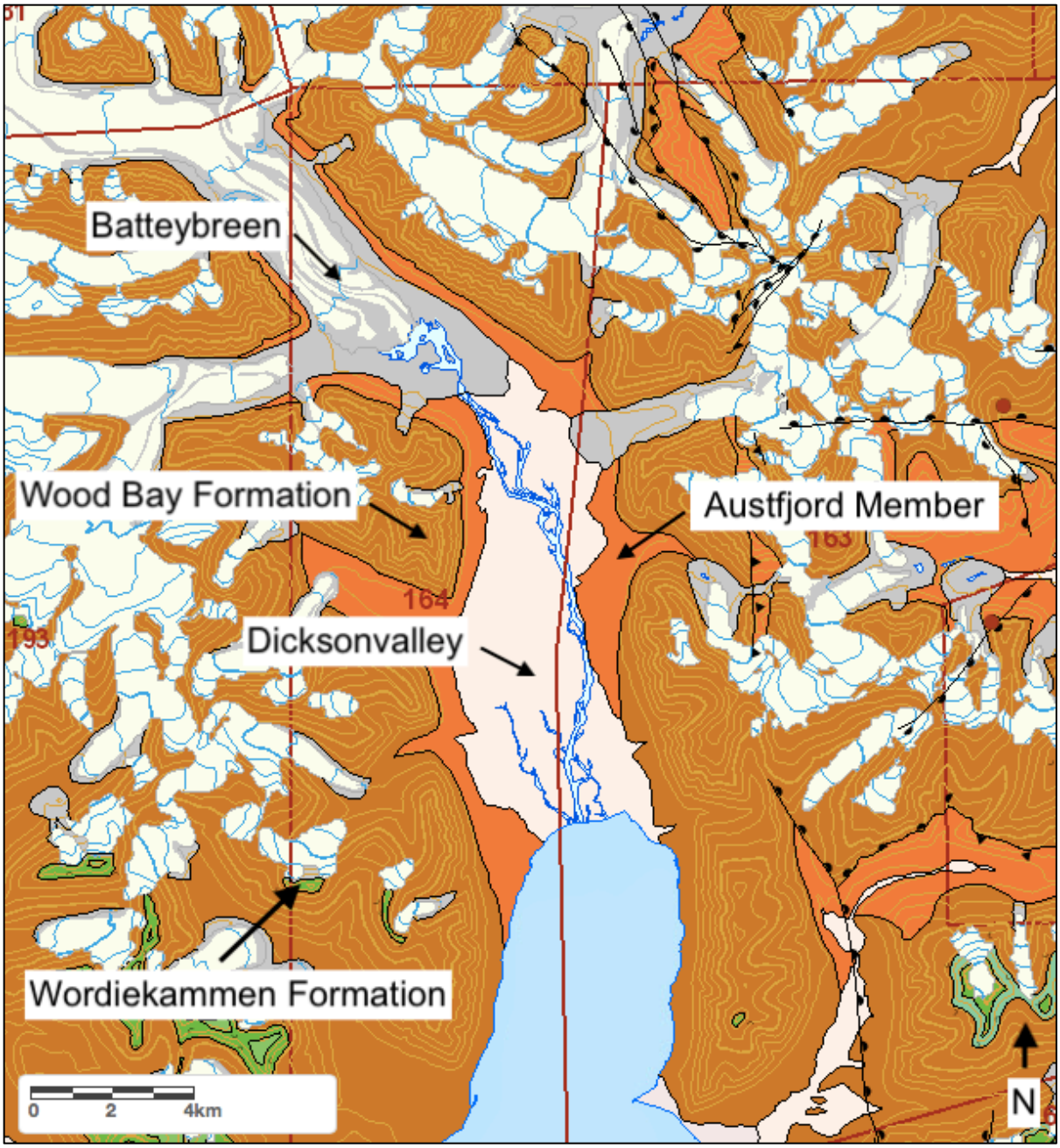

Fig. 6 Bedrock map of Dicksonfjorden. The Wordiekammen Formation, Wood Bay formation and the Austfjord Member of the Wood Bay Formation is marked. Source: Svalbardkartet, Norwegian Polar Institute (NPI), 2018 (http://svalbardkartet.npolar.no).

4. Materials and methods

4.1 Remote sensing and software

High-resolution aerial photos of Dicksonfjorden were acquired to be able to map geomorphological features, investigate the area prior to fieldwork and to study the development of the fjord-head delta (Fig. 7 A). The aerial photos (NP_Ortofoto_Svalbard_WMTS_25833) are provided by Norwegian Polar Institute (npolar.no)/ USGS Landsat and licenced under the Creative Commons Attribution-NonCommercial 4.0 International (CC BY-NC 4.0) license. Most of the photo that makes the basis for the geomorphological map was taken in 2011 on the 5th, around 12 AM (UTC), but a small part in the SW corner of the image was taken 17th of August, around 9 AM (UTC). Three oblique, grey-scaled photos taken during NPIs flight campaign in 1938 (Fig. 69), was used to describe the development of the delta front. Analysis of an aerial photo from 2011 was conducted with ESRI ArcGIS 10.4 and 10.3 to produce a geomorphological map of the delta covering an area of ~ 40 km^2 in total. The zoom level while mapping was set to 1:2000. The geomorphological map was produced in a scale of 1:40 000. A grain-size map was produced in a scale of 1:12 000.

4.2 Logistics

Fieldwork took place during a period of about four weeks from the 10.08.16 - 22.08.16 and 21.07.17 - 04.08.17. The fieldwork was organized by the research project «Sediment flux from source to sink - the coastal link», financed by the Svalbard Science Forum. The University Centre in Svalbard (UNIS) provided field equipment. UNIS provided also the transport of equipment and people between Longyearbyen and Dicksonfjorden.

4.3 Fieldwork

In order to examine the processes and deposits on the delta and to ground verify the morphological map, sediments and landforms were described and sampled. Two core-transects with in total 19 sediment cores were collected from the delta during fieldwork in August 2016 (Fig. 8). The cores were collected by hammering or pushing plastic tubes with a diameter of 5 cm down in the sediment. Then, the area around the core was excavated with a shovel, and the core was extracted. The cores where all taken from the tidal flat and spaces approximately 10 m apart. This was done to make a representative transect. During the fieldwork in 2017 in total 8 cores were collected with plastic tubes with a diameter of 7,5 cm. They were collected several hundred meters apart from each other to be able to capture variations between different geomorphological elements identified from the aerial photos (Fig. 7 B). Three of the cores were collected from the tidal flat, and the remaining 5 were acquired from active point bars. Information about the 27 cores that were collected in 2016 and 2017 is shown in Table 1. In 2016, 22 bulk samples were collected from the uppermost cm of the tidal flat, spaced several hundred meters apart (Table 2). During the fieldwork in 2017 only one bulk sample was collected from the upper cm of a point bar. Surface features were documented by descriptions and photographs both during the fieldwork in 2016 and 2017. The focus was on morphological elements in the intertidal and supratidal zone such as tidal channels, rill channels, tidal bars, tidal flat and cheniers (beach spits). The surface sediments where described in respect to grain-size, amount, lithology and roundness. A handheld Garmin

GPS 64s was used for acquiring locations and tracks. When needed, a Panasonic CF-19 Toughbook was used in field to map directly.

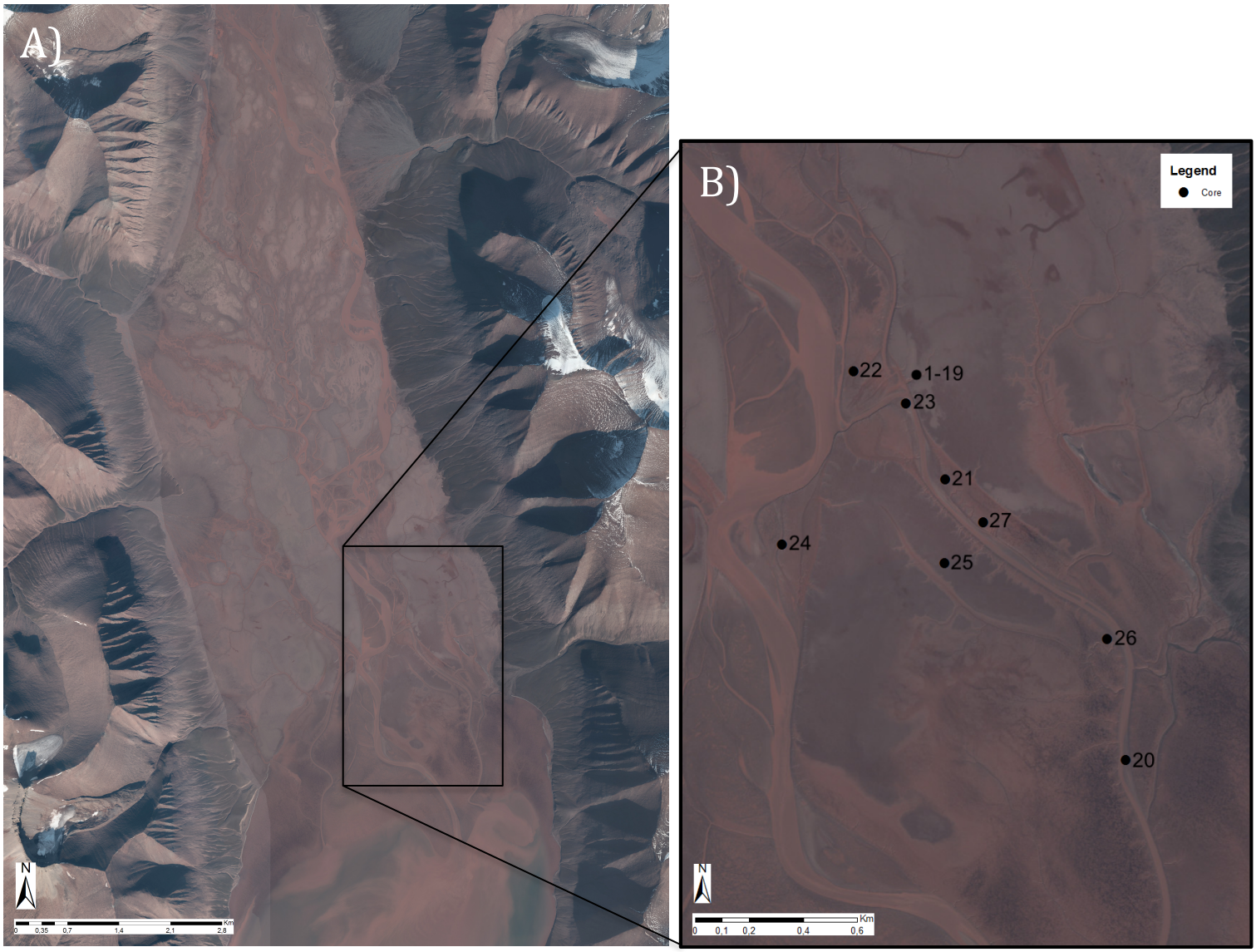

Fig. 7 A) Aerial photos from the Norwegian Polar Institute (NPI) (2011) of the fjord-head delta in Dicksonfjorden. Black square marks the area where the sediment cores where obtained. The aerial photos were used to produce the geomorphological map of the area. B) Location of sediment cores obtained in 2016 and 2017.

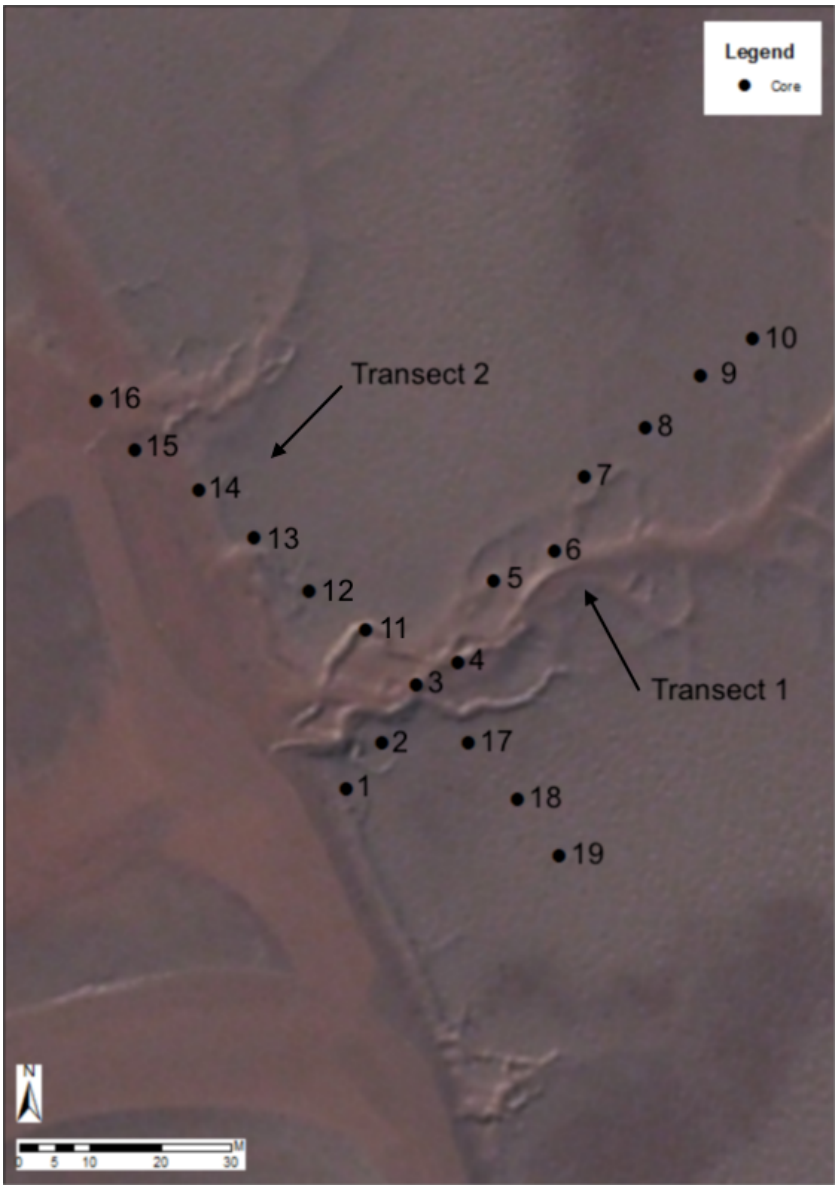

Fig. 8 Location of core-transect 1 and 2.

***Table 1**. Description of the sediment cores*

Core	Date	Length (cm)	Geomorphological element	Coordinates (UTM 33X)
1	15.07.2016	28	tidal flat	E507704/N8752542
2	15.07.2016	37	tidal flat	E507704/N8752543
3	15.07.2016	39,5	rill channel	E507704/N8752544
4	15.07.2016	29,5	rill channel	E507704/N8752545
5	15.07.2016	36	tidal flat	E507728/N8752572
6	15.07.2016	19,5	tidal flat	E507736/N8752579
7	15.07.2016	33	tidal flat	E507744/N8752587
8	15.07.2016	36	tidal flat	E507696/N8752549
9	15.07.2016	40	tidal flat	E507696/N8752550
10	15.07.2016	37,5	tidal flat	E507688/N8752556
11	16.07.2016	40	rill channel	E507681/N8752563
12	16.07.2016	39	tidal flat	E507673/N8752571
13	16.07.2016	31,5	tidal flat	E507664/N8752576
14	16.07.2016	32,5	channel	E507658/N8752583
15	16.07.2016	37	channel	E507711/N8752534
16	16.07.2016	14	channel	E507718/N8752526
17	16.07.2016	37,5	tidal flat	E507724/N8752518
18	16.07.2016	43,5	tidal flat	E508555/N8752074
19	16.07.2016	37,5	tidal flat	E507724/N8752518
20	24.07.2017	20	point bar	E508498/N8751140
21	26.07.2017	27	point bar	E507831/N8752178
22	26.07.2017	41	mid-channel bar	E507491/N8752578
23	29.07.2017	34,5	point bar	E507686/N8752460
24	29.07.2017	36	point bar proximal tidal flat	E507228/N8751938
25	31.07.2017	30	tidal flat	E507829/N8751870
26	31.07.2017	33	tidal flat	E508428/N8751588
27	06.08.2017	39	point bar proximal tidal flat	E507970/N8752020

Table 2. *Description of the bulk samples*

Bulk sample	Date	Mean grain-size	Geomorphological element	Coordinates (UTM 33X)
1	21.07.2016	Coarse silt	channel	E508785/N8752985
2	21.07.2016	Coarse silt	point bar	E508629/N8752926
3	21.07.2016	Coarse silt	channel	E508236/N8752716
4	21.07.2016	Coarse silt	tidal flat	E509080/N8751496
5	21.07.2016	Medium silt	tidal flat	E508931/N8751490
6	21.07.2016	Medium silt	tidal flat	E508752/N8751470
7	21.07.2016	Medium silt	tidal flat	E508722/N8751360
8	21.07.2016	Medium silt	channel	E508710/N8751053
9	21.07.2016	Medium silt	channel	E508616/N8751048
10	21.07.2016	Medium silt	channel	E508689/N8751347
11	21.07.2016	Coarse silt	point bar	E508652/N8751601
12	20.07.2016	Medium silt	channel	E507659/N8752576
13	20.07.2016	Medium silt	tidal flat	E507638/N8752779
14	20.07.2016	Medium silt	tidal flat	E507774/N8752412
15	20.07.2016	Coarse silt	tidal flat	E507984/N8752457
16	20.07.2016	Medium silt	tidal flat	E508379/N8752497
17	20.07.2016	Medium silt	tidal flat	E508546/N8752438
18	20.07.2016	Coarse silt	tidal flat	E508866/N8752251
19	20.07.2016	Very fine sand	channel	E508802/N8752536
20	20.07.2016	Very fine sand	point bar	E508700/N8752442
21	20.07.2016	Coarse silt	channel	E508567/N8752357
22	31.07.2017	Very fine sand	point bar	E508502/N8751480

4.3 Laboratory analysis

All laboratory analysis was performed at the laboratory of the Department of Geosciences at the UiT - The Arctic University in Norway. The sediments cores and bulk samples where transported from UNIS to the University in Tromsø - The Arctic University in Norway by airplane. The cores where split lengthwise and cleaned up with a plastic card.

4.3.2 X-ray scanning
Whole and half cores where imaged using the Geotek MSCL-XCT X-ray imaging machine. This was done in order to get information about sedimentary structures, bioturbation, clasts and shells that might not be visible when studying the core-halves with the naked eye. When the X-ray travels though the material, the attenuation depends on the density of the material. Materials with high density like clasts and shells will appear white, while mud, which has a low density, will appear darker.

4.3.3 Colour images
Colour images were taken of the half cores using the Jai L-107CC 3 CCD RBG Line Scan Camera, which is installed in the Avaatech XRF core scanner. Some hours prior to the scanning the core were taken out of the cold room and the protective plastic cover was removed. This makes the surface water evaporate and reduces reflections on the image. Also, the surface of the core was gently smoothened using a plastic card in order to make sedimentary structures more visible.

4.3.4 XRF core scanning
The Avaatech XRF core scanner was used for qualitative element-geochemical measurements of the half cores. 24 hours before the scanning, the cores were taken out of the cold room so that the surface water could evaporate, and the surface was smoothened with a plastic card. An uneven surface or a thin water film on the surface would reduce the measured amount of light geochemical elements (Forwick 2013). Last, a 4 mμ thin plastic film was put on the surface of the cores to avoid pollution.

Measurements every 10 mm where done with different currents, voltages, and filters applied for the various runs. Filter is normally used for measurements of heavier minerals in order to avoid noise form lighter elements (Forwick 2013).

The measurements were carried out in three runs:
1. 10 kV, 1000 μA, no filter, to measure light elements from Mg to Ca.
2. 30 kV, 2000 μA, Pd-thick filter, to measure medium-heavy elements from Ni to approximately Mo.
3. 50 kV, 2000 μA, Cu-filter, to measure heavy elements from approximately Mo to U.

XRF core scanners have been used for over a decade and have become very important in palaeo environment research using marine and lacustrine cores (Croudace and Rotwell 2015). Only a few studies have been done on fluvial environments (Turner *et al.* 2015). Jones *et al.* 2010, Tjallingii *et al.* 2010 and Wang *et al*. 2011 are some of them. It is more challenging to study fluvial cores because of the heterogeneous and discontinuous nature of the sediment. Due to winnowing, reworking and erosion, fluvial sediments have low preservation potential (Lewin and Macklin 2003; Croudace and Rotwell 2015). However, floodplains can be excellent archives recording flood events (Baker *et al.* 1983).

The Zr/Rb ratio has been used as a sediment grain-size proxy in lacustrine (Kylander *at al.* 2011), marine (Dybvik and Harris 2001), subaqueous deltaic sediments (Wang *et al.* 2011) and in loess (Chen *et al*. 2006). Zr tends to become concentrated grain-sizes from coarse silt to fine sand. High Rb amounts is typically found in clay an the finest silt

fraction (Veldkamp and Kroonenberg 1993; Dypvik and Harris 2001; Oldfield *et al.* 2003. This means that when the Zr/Rb ratio increase, the grain-size is increasing as well (Croudace and Rothwell 2015).

The bedrock in the catchment area for the Dicksonelva River consist almost exclusively of the Devonian Wood Bay Formation of the Andre Land Group (Blomeier *et al.* 2003), and because of this it not possible to make a provenance study from the geochemical element data.

4.3.5 ^{210}Pb and ^{137}Cs dating

Four cores were dated at the Adam Mickiewicz University in Poznan in Poland in 2016 and 2017 using the ^{210}Pb dating method. Lead-210 (^{210}Pb) is a naturally occurring radioactive isotope that is a part of the Uranium-238 (^{238}U) radioactive decay series (Flett (n.d.)). The time required for the levels excess ^{210}Pb to decline below the limits of what the detector can measure is normally around 100 years (Muhammed *et al.* 2008). Cesium-137 (^{137}Cs) is also a radioactive isotope and a marker of post 1952. ^{137}Cs marker is used to provide an age at a certain point in cores to validate the ^{210}Pb chronology (Flett (n.d.)).

The calculations for the ^{137}Cs dating was done by dividing the number of cm with ^{137}Cs present in the core, with 65 or 64 years, depending of the core was obtained in 2017 or 2016. This provides a maximum yearly sediment accumulation rate since 1952. Determining the excess ^{210}Pb was done by subtracting the supported ^{210}Pb from the total amount of ^{210}Pb measured in the cores. To calculate the sediment accumulation rates from the excess ^{210}Pb measurements, the number of cm with excess ^{210}Pb present in the cores is divided with 100 years, as this is the amount of time excess ^{210}Pb needs to decay. This will provide a minimum yearly sediment accumulation rate for the last century.

The four cores (2, 20, 24 and 26) (Table 3) were chosen for dating because they were taken from different geomorphological features and have different sedimentological properties. Core 2 and 26 was taken from the tidal flat, while core 20 was taken from a point bar. Core 24 was taken from a point bar proximal tidal flat. Core 2 was sampled in thicker intervals because of that the diameter of this core is smaller then the three others. Pure sand layers should be avoided sampled, because the presence of silt or clay is important for the ^{210}Pb dating process. Core 2 has a sand-rich layer from 16,5-17 cm, and the sampling interval had therefor to be changed from 15-17 cm to 14-16 cm. The upper 5 cm of core 24 was destroyed during opening of the core and is therefor missing. The sediment samples were extracted by using a knife and small spoon. The samples were dried at 40 degrees and grounded and homogenized before they were packed in labelled plastic bags. After drying the samples weighed about 20 g each. The ^{210}Pb and ^{137}Cs dating was performed by Witold Szczuciński at the Adam Mickiewicz University in Poland. The measurements were supported by the Polish National Science Centre grant no 2013/10/E/ST10/00166.

Table 3. *Information about 210Pb dating sampling intervals*

Core	Sampling interval (cm)
2	0-2, 5-7, 10-12, 14-16, 20-22, 25-27, 30-32, 35-37
20	0-1, 5-6, 10-11, 15-16, 19-20
24	5-6, 10-11, 15-16, 20-21, 25-26, 30-31, 35-36
26	0-1, 5-6, 10-11, 15-16, 20-21, 25-26, 30-31

4.3.6 Laser diffraction particle size analysis

A laser diffraction particle size analyser (Beckman Coulter LS 13320) was used to determine the particle distribution of the bulk samples. The laser diffraction particle size analyser measures particles in the area between 0,04µm and 2mm. Grain-size was classified according to the Udden-Wentworth scale (Fig. 9).

Before analysis, the following preparations were done. For each of the 22 samples, approximately > 2 g of dry sample was taken out and put into labelled PIDS tubes, and treated with ca. 40 mL of 20% hydrochloric acid (HCl) to remove calcareous residues (foraminifera etc.). The tubes was left inside a fume hood for 24 hours before they were centrifuged for 4 minutes at 4000 rpm and washed with distilled water. The centrifuging and washing was repeated three times. Afterwards, the samples were treated with 20% hydrogen peroxide (H2O2) to remove organic material. The tubes were covered with aluminium foil and then put in a water bath (80°C) for two hours. During the first 15 min the tubes needed constant monitoring in order for the samples not to boil over and loose sediments if the reactions were strong. If the reaction was strong the sample needed to be takes out of the bath to calm down before it was put back again. All the samples had a strong reaction, but only some boiled over. After two hours, the samples were again centrifuged and washed three times with distilled water. The clean samples were transferred into plastic cups and set to dry in a laboratory fume hood.

Once dry, about 0,5 g of dry sample was poured into plastic cups together with 2 ml of water. Then the plastic cups where placed on a shaker machine to mix for minimum 24 hours. Two drops of soap solution (Calgon) was added in the suspended samples before they were placed in an ultrasound bath for five minutes. The soap was added to prevent flocculation of the sediments. The samples were then ready to be poured into the laser diffraction particle size analyser.

4.4 Sedimentary logging

Sedimentary logs of the 27 cores were drawn by hand in the scale of 1:2. Grain-size and sedimentary structures were illustrated on the logs. Grain-size was classified according to the Udden-Wentworth scale (Fig. 9). Patterns and symbols for sedimentary structures are based on the symbols used by Nichols (2012[5]). Silt and clay are described together as mud, as high-resolution grain size samples in mm-scale were not a priority. The logs were drawn in a realistic way, to capture as many details as possible from the sedimentary structures observed in the cores. However, some standardize symbols was used to make the logs easier to read.

It is worth noting that in some of the cores containing laminations, it was difficult to observe the changes in the mud vs. sand content. It was therefor not possible to draw every single lamination, and the respective content of mud vs. sand. In these cases a symbol for horizontal lamination was used instead to indicate the presence of laminations.

Also, the cores only provide a small window into the sediments, which makes it impossible to capture large scale or even medium scale sedimentary structures such as dunes.

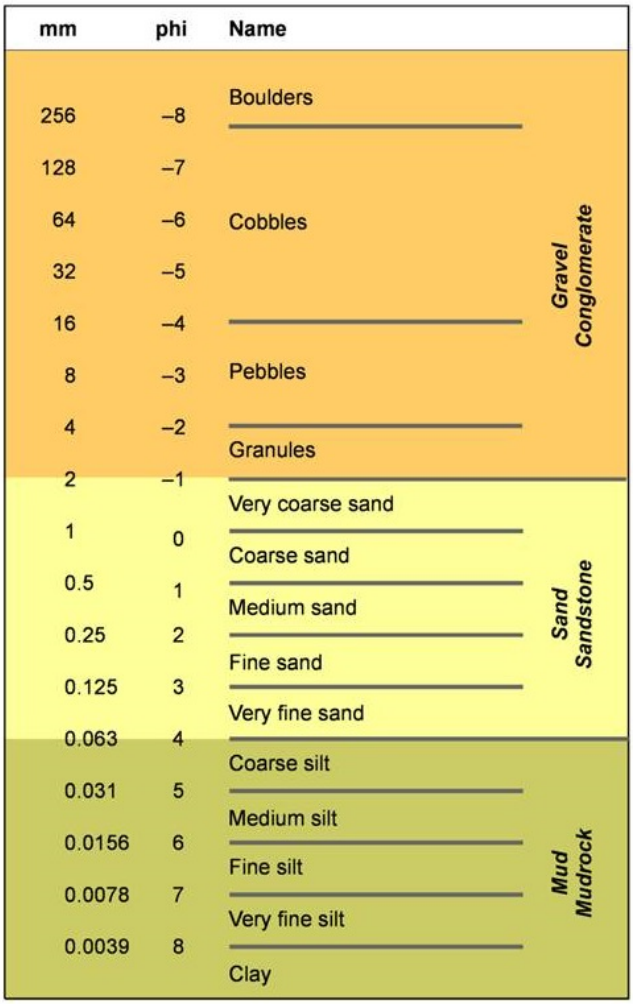

Fig. 9 The Udden-Wentworth grain size scale (Nichols 2012[5])

4.5 Facies analysis

7 facies have been described based on the logs from the 27 cores from the fjord-head delta in Dicksonfjorden. The depositional processes and environments of the facies have been discussed and interpreted. A summary of the facies is given in table X.

The concept of facies was first introduced into the geological discipline by Nicolas Steno in 1669, however, the modern use of the term is usually attributed Gressly (1838). Description of the physical and chemical characteristics of a rock or sediment is referred to as lithofacies and is used to determine the transport and depositional processes of the

sediment. Biofacies and ichnofacies give information about the paleoecology during and after deposition of the sediment. Through facies analysis past sedimentary environments can be reconstructed. Facies associations are groups of facies that are formed by processes occurring the same environments (Nichols 2012). This thesis only deals with lithofacies, and the term "facies" is therefor used instead of lithofacies.

The facies was divided into one of the following sedimentary deposits; tidal flat deposits and tidal bar deposits. This was done order describe the deposits and processes occurring in these two distinct sedimentary environments.

4.6 Software and statistics

Microsoft Excel was used to create line charts to display quantitative geochemical element ratios. It is an advantage to plot the element ratios (e.g. Zr/Br) instead of a single element vs. core depth. Element ratios provide information of changes in the total amount of the selected element that is plotted against the sum of the other elements. When using element ratios one reduces the possibility for misinterpretation as well as the matrix effects (uneven surfaces, porous sediments and thin water film) (Tjallingii *et al.* 2007; Weltje and Tjallingii 2008). Weltje and Tjallingii (2008) concluded that element compositions are best expressed as logarithms of element ratios (log-ratios). This way, the element compositions become mostly normally distributed and subject to multivariate statistics, which makes them more robust record of chemical changes and reduces the risk of wrong interpretation. Elements that should not be used are; Rh: because the anode of the X-ray source is made of Rh and Ag: because parts of the detector are made of Ag (Forwick 2013). Cl is not used because the evaporation of water as well as the crystallization of NaCl in the sediment might be effected by grain-size. Therefor, changes in the detected Cl in the cores might only be due to grain-size changes (Hennekam 2015).

Microsoft Excel was also used in order to view the grain-size data from the bulk samples and calculate median values for each sample. The median is the middle core for a set of data that has been arranged in order of magnitude. The mean is equal to the sum of all the values in the data set divided by the number of values in the data set. The median is less affected by outliers and skewed data, than the mean (A guidebook to particle size analysis (n.d.)).

Later, the coordinated of the bulk samples were plotted on a zoom in version of the geomorphological map using ESRI ArcGIS 10.4. The mean grain-size of the samples where illustrated with color-coding.

Geotek Quick View was used to adjust the black/white contrast of the X-ray images so that sedimentary structures and clasts would become more visible.

CorelDRAW was used in order to digitalize the sedimentary logs in scale of 1:4 and to make figures.

5. Facies analysis

5.1 Facies A - Current ripple cross-laminated sand

Description

Facies A includes very fine to medium sand with asymmetrical ripples. Some beds also contain a small amount of mud. Both planar and trough cross-lamination seems to be occurring (Fig. 10 A and B). Sigmoidal cross-lamination and climbing ripples is present in core 23 (Fig. 10 A). The cross-lamination in Fig. 10 A) is dipping in the same direction and lay in the same plane, which forms planar cross-lamination. While the cross-lamination in Fig. 10 B) have are dipping in several directions, and are called trough cross-lamination.

Mud-drapes may be occurring between the cross-lamina. Cross-lamina thickness range from 1-3 mm, sets are 1-3 cm thick, while stacking of sets results in beds with a thickness up to 12 cm. The beds are often characterized by sharp bed boundaries, and reactivation surfaces are sometimes present. The ripples are commonly only visible on X-ray images and not with the naked eye.

The facies also includes lenses consisting of pure fine sand, generally 0,5-3 cm high and 1,5-2,5 cm wide. Current ripple cross-laminated sand is commonly found together with facies C (Structureless sand), but also together with facies F (Structureless mud) and D (Heterolithic mud and sand). Facies A is found in core 20, 21, 22, 23 and 24 which are all taken from point bars in tidal channels.

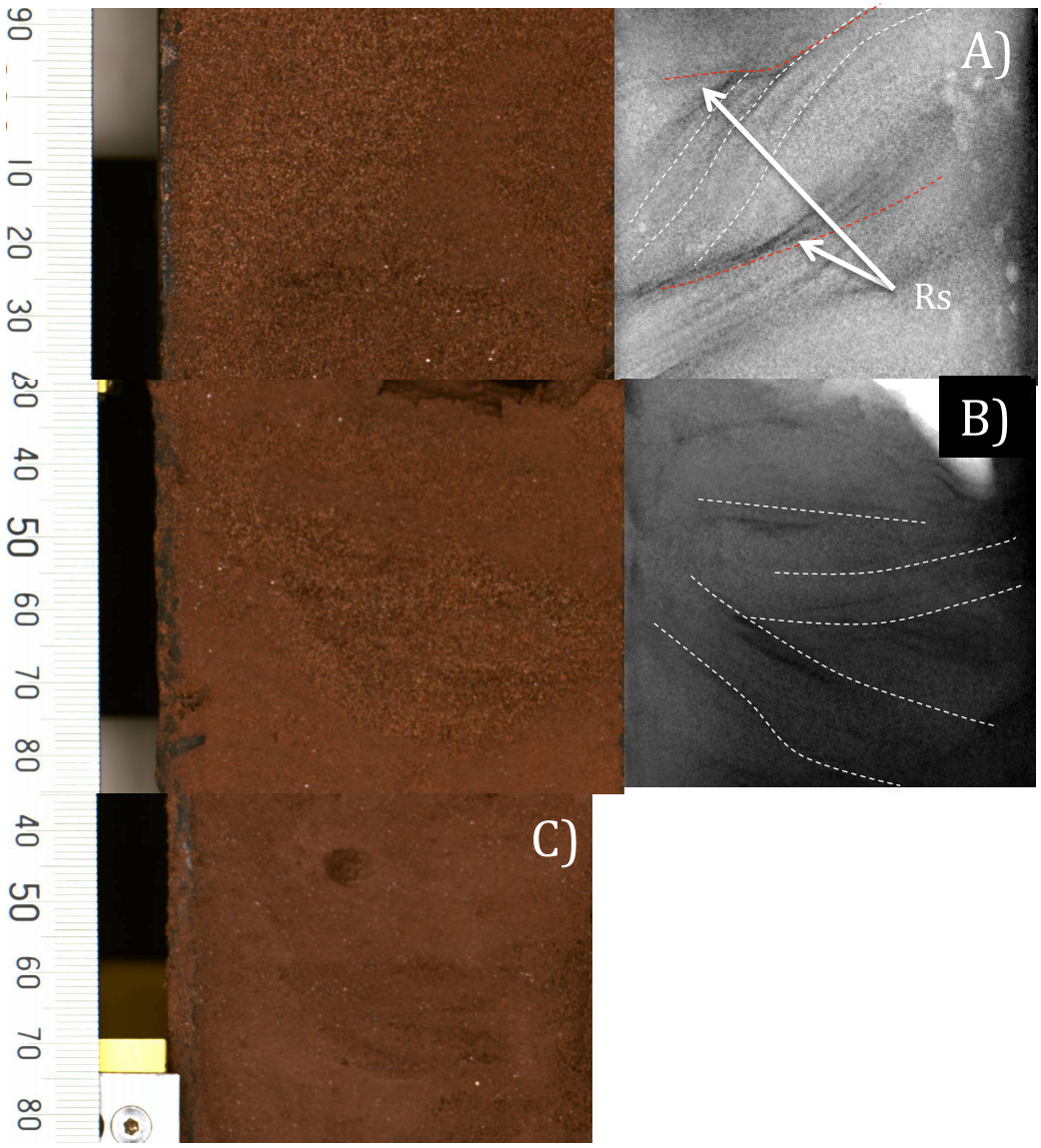

Fig. 10 *Facies A – Current ripple cross-laminated sand* A) Climbing planar cross-lamination from core 23 (point bar). Sigmoidal cross-lamination is occurring in the uppermost cross-lamina set. The cross-lamination is only visible on the X-ray image (right), not on the colour image (left). Cross-laminations are marked with white stippled lines. Reactivation surfaces (Rs) are marked with red stippled lines. B) Trough cross-lamination from core 24 (point bar). The cross-laminations are marked with white stippled lines. The cross-lamination is best visible on the X-ray image. C) Lenses of fine sand (white stippled lines) from core 21 (point bar).

Interpretation

Asymmetrical ripples are formed by unidirectional currents of the lower flow regime in shallow waters (Collins *et al.* 2006, Boggs 2011). The formation of current ripples requires moderate flow velocities over a hydrologically smooth bed (Nichols 2012[3]). Collinson *et al.* (2006) states that grain size is the dominant controlling factor on ripple size. Increasing flow velocity also tends to increase ripple size and complexity of ripple morphology (Boggs 2011). The planar and trough cross-lamination is formed by respectively straight and sinuous ripple migrations. The sinuous ripples are curved and the angle of the dipping cross-lamination will therefor be in several directions, not only to the angle of the flow (Nichols 2012[3]). Straight ripples tend to evolve into sinuous ripples though time and at higher current velocities (Baas 1994). Due to the typical lens

shape of the lenses, they are interpreted to have formed by infilling of fine sand in the troughs of current ripples. The mud-drapes on the ripples forms when mud settles from suspension during slack water conditions (Nichols 2012[3]).

According to the «Bedform stability diagram» (Nichols 2012[3], modified from Southard 1991 and Allen 1997), current ripples of fine and medium sand will only form in a flow velocity between 20-60 cm/s. This is only valid for water depth between 25 and 40 cm, and for clear water at a particular temperate (10 °C). During the deposition of the ripples, the water temperature might have been colder than 10 °C and the water might have contained suspended sediments, but this gives an indication of what the current velocity might have been.

Climbing ripples form when high sediment supply and rapid deposition leads to aggradation of ripples with downstream migration (Collins *et al.* 2006). Sigmoidal cross-lamination is an indication of variable flow conditions, where erosion of each lamina is taking place, shaping it into the sigmoidal form (Tinterri 2011).

Asymmetrical ripples with reactivation surfaces indicate the presence of one dominant current (either flood or ebb), with a subordinate current that is not strong enough to reverse the direction of the current ripples, but strong enough to scour the upper part of the ripple, forming a reactivation surface. Current ripples typically form on the upper part of tidal bars and produce current-ripple cross lamination (Dalrymple 1992, 2010).

5.2 Facies B - Current ripple cross-laminated mud

Description

Facies B includes mud with planar asymmetrical ripples. Cross-lamina thickness range from 0,5-1 mm and the set is about 1 cm thick. The upper and lower boundary of the bed is sharp (Fig. 11 A)). The ripples are only visible on X-ray image and not with the naked eye. Lenses of silt and clay can be found in this facies (Fig. 11 B)). Due to the typical lens shape of the lenses, they are believed to have formed by infilling in the troughs of ripples. Facies B is rare and only found in core 4 (tidal flat) and 24 (point bar). Current ripple cross-laminated mud is found together with facies D (Heterolithic mud and sand), facies E (Heterolithic clay and silt) and facies F (Structureless mud).

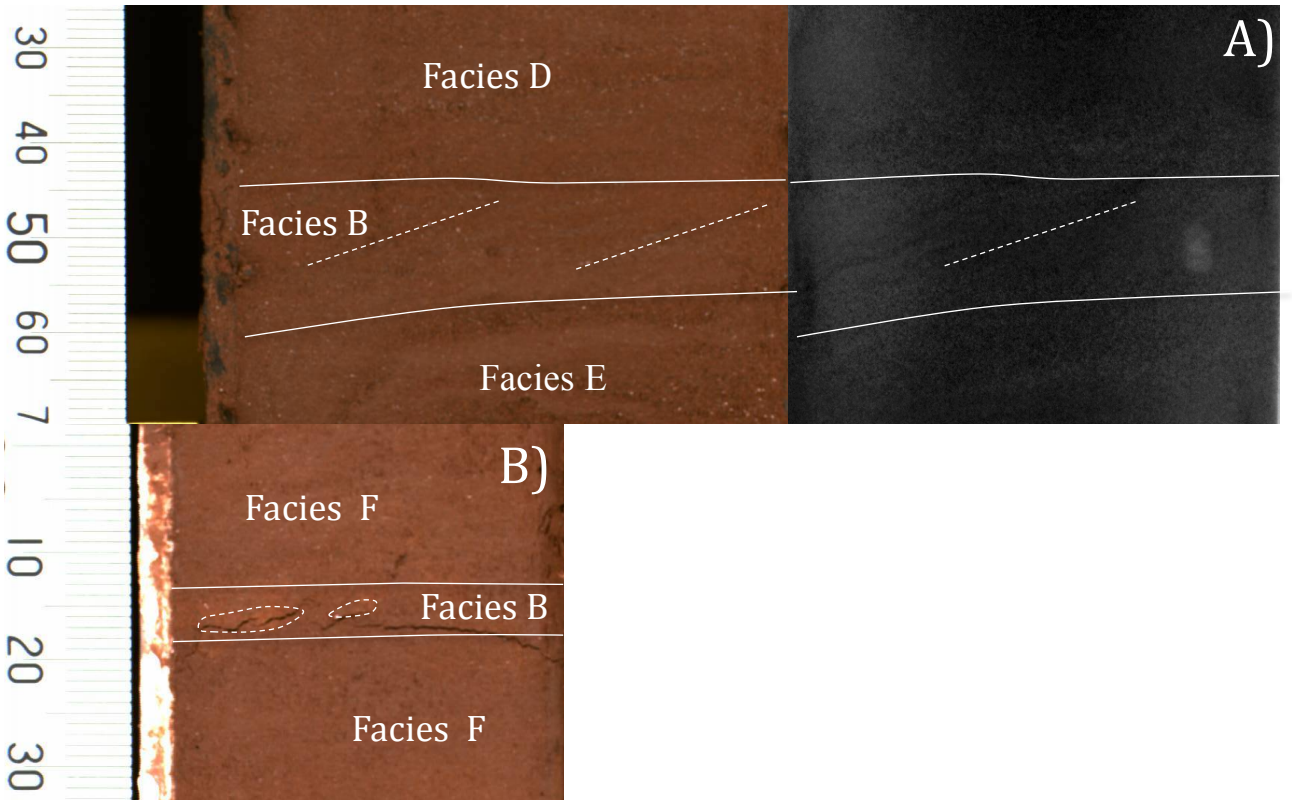

Fig. 11 *Facies B – Current ripple cross-laminated mud* A) Planar cross-lamination from core 24 (point bar). The cross-lamina is both visible by the naked eye and on X-ray images. B) Lenses of pure silt from core 4 (tidal flat).

Interpretation
As asymmetrical ripples formed in sand, asymmetrical mud ripples are formed by unidirectional currents of the lower flow regime in shallow waters (Collins *et al.* 2006, Boggs 2011). Planar cross-lamination is formed by the migration of straight crested current ripples. The formation requires moderate flow velocities over a hydrologically smooth bed (Nichols 2012[3]).

According to the «Bedform stability diagram» (Nichols 2012[3], modified from Southard 1991 and Allen 1997), ripples of silty material will only form with flow velocities between about 18-65 cm/s, which gives and indication of the current velocity during deposition. Schieber *et al.* (2007) argues that clay and silt particles can flocculate and because of this be transported and deposited at the same flow velocities as sand.

5.3 Facies C - Structureless sand

Description
Facies C consist of very fine and fine sand with no visible structures. Some of the beds also contain a small portion of mud. The bed thickness range from 2-13 cm. The beds are typically characterized by sharp boundaries, which sometimes are undulating. Lenses of mud or fine sand are sometimes present in this facies (Fig. 12). Facies C is found in core 20, 22, 23, 24 and 27 which was all was sampled from point bars on tidal channels, except core 27. Facies C is commonly found together with facies A (Current ripple cross-laminated sand), facies F (Structureless mud), and sometimes facies E (Heterolithic clay and silt) and facies D (Heterolithic mud and sand).

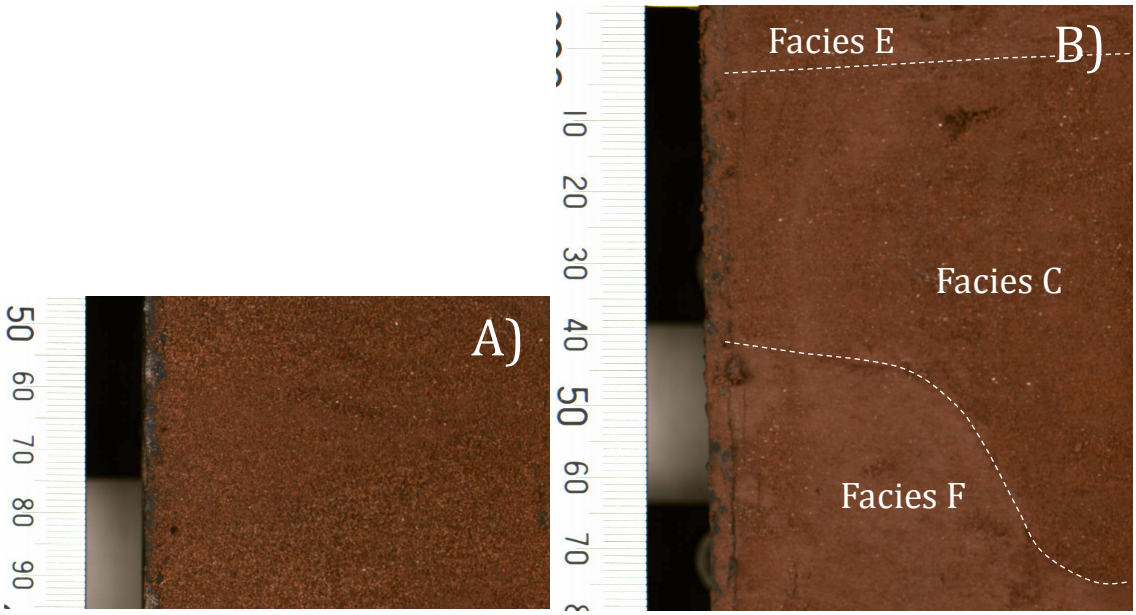

Fig. 12 *Facies C – Structureless sand* A) Structureless sand from core 23 (point bar). B) Structureless sand with a small portion of mud from core 24 (point bar).

Interpretation
Absence of laminations may reflect conditions of deposition or it may be the result of destruction of original lamination. A primary lack of lamination most commonly result from rapid deposition, most probably though the deceleration of a heavy sediment-laden current. Grains arrive at the bed so rapidly that they are buried before any bedload movement can occur (Collingson and Thompson 1987). Laminations can be destroyed due to bioturbation (Nichols 2012[1]), but some burrows would be likely to find in this case. Deformation due to liquefaction or shore ice pushing/souring are a more likely explanations (Dionne 1988, 1997, 2011; Nichols 2012[4]). The muddy and sandy lenses found in the facies may have been formed by the same deformational processes, with incorporation of underlying or overlying sediments into the structureless sand.

Facies C can have different origins, but medium or high flow velocities are required to transport the very fine and fine sand grains as bedload (saltation or rolling) (Nichols 2012[3]). The small portion on mud that occurs in some beds may be explained by flocculation of mud particles, which may lead them to fall out of suspension at higher flow velocities than single mud particles do (Schieber *et al.* 2007). Medium to high flow velocities typically occurs in channels and on the bars in the channels (Dalrymple 1992 and 2010).

5.4 Facies D - Heterolithic mud and sand

Description
Facies D consists of alternating muddy and sandy laminations (Fig. 13). This facies includes planar, horizontal and undulating laminations, ranging from well defined to weakly defined. The muddy and sandy laminations are classified based on the relative content of mud and sand in each lamination. The “muddy” laminations typically only consist of mud, sometimes a small portion of very fine sand. The “sandy” laminations commonly consist of 50-100% very fine, sometimes a little fine sand. Sometimes, the

"sandy" laminations only contain a small portion of sand, but then the "muddy" laminations contain only mud. Little variation in the content of the "muddy" and "sandy laminations are often seen as weakly defined laminations, while large variations are seen as well defined laminations. In some cores, the laminations are parallel but slightly dipping. The lamina thickness range from 2 mm – 1 cm and the bed thickness range from 1-40 cm. The beds are often characterized by gradational bed boundaries, but sharp contacts do also occur. A few coarse sand grains are sometimes present in this facies. Facies D is most common in the cores obtained from the tidal flat. Heterolithic mud and sand is commonly found together with facies E (Heterolithic clay and silt), facies F (Structureless mud), facies G (Deformed mud) and sometimes found together with facies B (Current ripple cross-laminated mud), facies C (Structureless mud) and facies A (Current ripple cross-laminated sand).

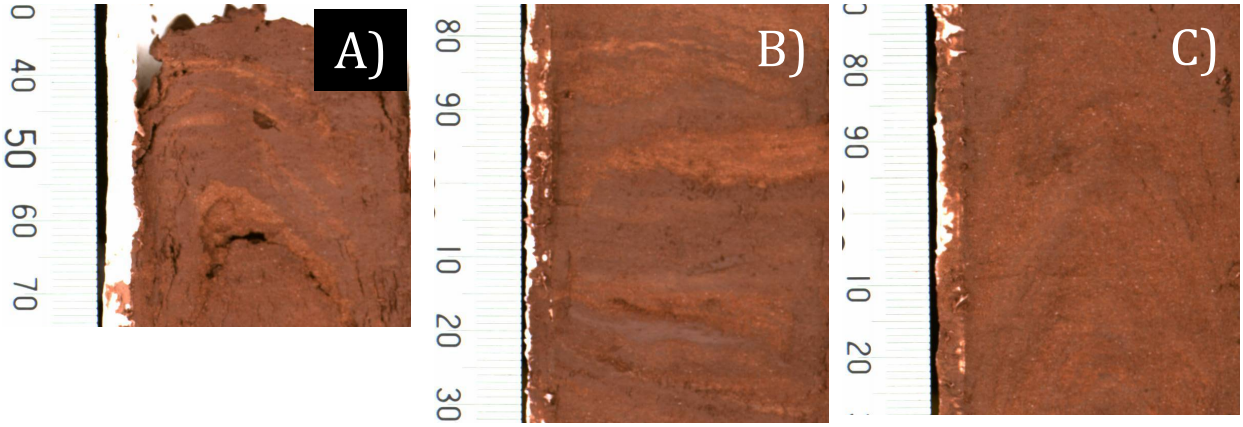

Fig. 13 *Facies D – Heterolithic mud and sand* A) Well defined heterolithic muddy and sandy laminations from core 7 (tidal flat). B) Well defined wavy heterolithic muddy and sandy laminations from core 18 (tidal flat). C) Weakly defined heterolithic muddy and sandy laminations from core 11 (tidal flat).

Interpretation

Planar, horizontal laminations of mud and sand are a result of alternating relatively high and relatively low current velocities. In tidally influenced environments this cyclic nature is common due to the flood, slack and ebb conditions of the tidal cycle. During flood and ebb currents, relatively coarse material, typically sand will be moved and deposited. During high and low slack water conditions, fine suspended sediments such as clay and silt settling to the bottom, which results in heterolithic deposits (Davies 2012). Such deposits are common for tidal flat deposits, and the sand to mud ration typically increases seaward, where tidal currents have more energy and can transport and deposit coarser materials (Dalrymple 1992, 2010).

The undulating and slightly dipping laminations may originally have been planar, horizontal laminations that have been deformed. The undulating lineations may have been formed due to ice-pushing from ice cakes which is a common process on tidal flats in cold regions (Reineck 1976, Dionne 1985, Dashtgard *et al.* 2014). Another way the lineation may have been formed is through the imprint of snow and ice, forming a crystalline surface pattern found on the tidal flat in Dicksonfjorden. The slightly dipping laminations are believed to be an artefact caused by tilting of the core during sampling.

5.5 Facies E - Heterolithic clay and silt

Description

Facies E consists of mud with laminations. This facies includes planar, horizontal and undulating laminations, ranging from well defined to weakly defined (Fig. 14 A and B). The facies generally consist of alternating clayey and silty laminations. In some cores, the laminations are parallel but slightly dipping. The lamina/layer thickness range from 2 mm - 2 cm. The bed thickness range from 1,5-28 cm. The beds are often characterized by gradational bed boundaries. Vertical structures resembling desiccation cracks (Dc) as seen in Fig. 14 B), occur in the facies. Single clasts of gravel are also sometimes present in this facies. Facies E is very common and is found in cores, which are mainly collected from tidal flats. Heterolithic clay and silt is commonly found together with facies G (Deformed mud), facies F (Structureless mud), facies D (Heterolithic mud and sand), and sometimes found together with facies C (Structureless sand) and facies B (Current ripple cross-laminated mud).

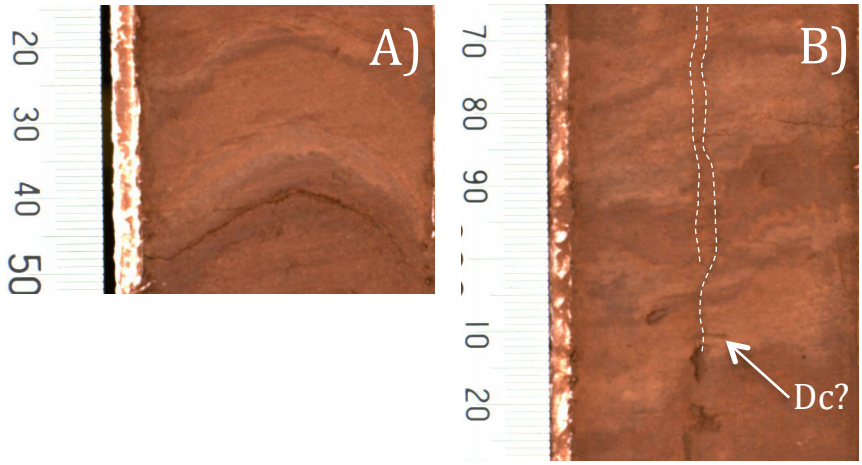

Fig. 14 *Facies E – Heterolithic clay and silt* A) Parallel, horizontal laminations from core 12 (tidal flat). B) Undulating parallel laminations from core 8 (tidal flat). Possible desiccation crack infill (Ds) is marked with a white stippled line.

Interpretation

Planar, horizontal laminations in mud are typically formed during low flow velocities and during slack water conditions, when clay and silt is settling from suspension (Collinson and Thompson 1987[1]). During the tidal cycle, current velocities vary during flood tide, slack water and ebb tide conditions. Mud is mainly being deposited during slack water conditions, while deposition of silty layers occur during weak flood and ebb tidal currents, that is not able to transport and deposit sand (Davies 2012). This results in the creation of a heterolithic deposit consisting of alternating clayey and silty laminations. Weak flood and ebb current velocities are commonly present on tidal flats (Dalrymple 1992, 2010). The current velocity decreases when moving landward due to friction against the bed (Dalrymple and Choi 2007).

The undulating and slightly dipping laminations may originally have been planar, horizontal laminations that have been deformed. The undulating lineations may have been formed due to ice-pushing from ice cakes which is a common process on tidal flats

in cold regions (Reineck 1976, Dionne 1985, Dashtgard *et al.* 2014). Another way the lineation may have been formed is through the imprint of ice, forming a crystalline surface pattern found on the tidal flat in Dicksonfjorden.

The slightly dipping laminations are believed to be an artefact caused by tilting of the core during sampling. Desiccation cracks are also very common on tidal flats due to the alternation of wet and dry contains (Davies 2012). The clasts of gravel are most likely dropstones transported by ice or kelp to the tidal flat. Both desiccation cracks (Fig. 62) and seaweed with gravel attached to it (Fig. 65) was observed during the field campaigns in 2016 and 2017.

5.6 Facies F - Structureless mud

Description

Facies F comprises mud with no visible structures (Fig. 15 A). Some beds consist of a small portion of very fine and fine sand (Fig. 15 B). Single clasts of very coarse sand are sometimes present in this facies. The bed thickness range from 1,5-22 cm. The beds are characterized with both gradational and sharp bed boundaries ranging from horizontal to undulating. Facies F is mainly found in cores taken from tidal flats. Structureless mud is commonly found together with facies E (Heterolithic clay and silt), facies D (Heterolithic mud and sand), facies G (Deformed mud), facies C (Structureless sand), and sometimes facies A (Current ripple-cross laminated sand) and facies B (Current ripples cross-laminated mud).

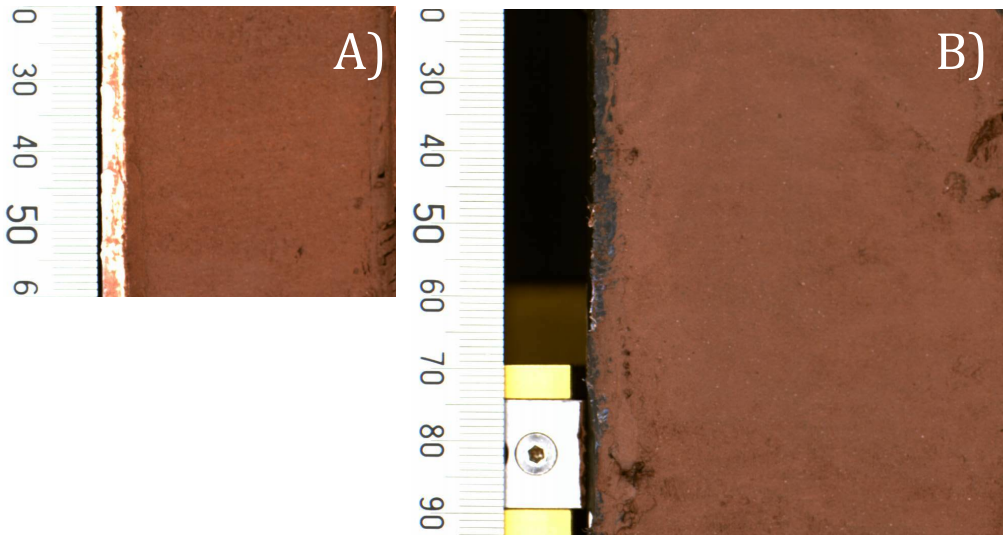

Fig. 15 *Facies F – Structureless mud* A) Structureless mud from core 7 (tidal flat). B) Structureless mud with a small portion of very fine and fine sand from core 3 (tidal flat).

Interpretation

The lack of structure in mud may reflect an original lack of depositional lamination or destruction of original laminations. Original lack of depositional lamination can be caused by a homogenous and/or a rapid depositional process. Destruction of original lamination may be destroyed later by a variety of processes, such as borrowing organisms and large-scale post-depositional processes (Collingson and Thompson 1987). Bioturbation is also not a likely way of formation as cold region tidal flats generally are sparsely bioturbated due to the shore ice and frost action (Dionne 1988). Also no observations of infaunal organisms were done during the field campaigns in

2016 and 2017. According to (Dionne 1988, 1997) deformation by ice-pushing and ice scouring are widely occurring in tidal flats in cold regions experiencing shore ice.

Mud is normally deposited during low flow velocities and during slack water conditions, when clay and silt is able to settle from suspension (Aplin and Macquaker 2011, Boggs 2011). The small content of very fine and fine sand that occurs in some beds indicates slightly higher flow velocities, as the sand grains are heavier and require slightly more energy to be transported (Nichols 2012[3]). These conditions commonly occur on tidal flats, which are flooded during high tide (Dalrymple 1992, 2010).

5.7 Facies G - Deformed mud

Description

Facies G mainly consist of mud with deformation structures (Fig 16 A, B, C, D and E). Some beds contain a small amount of very fine sand. The amount of deformation varies from light to heavy, but common for the facies is that no laminations are intact. Facies G includes lenses of fine sand (Fig. 16 C) or mud (Fig. 16 D). The bed thickness range from 2-22 cm. The beds are characterized by gradational boundaries. The facies is only found in cores obtained from the tidal flat (core 2, 8, 9, 10, 18 and 19). Facies G is commonly found together with facies E (Heterolithic clay and silt), D (Heterolithic mud and sand) and facies F (Structureless mud).

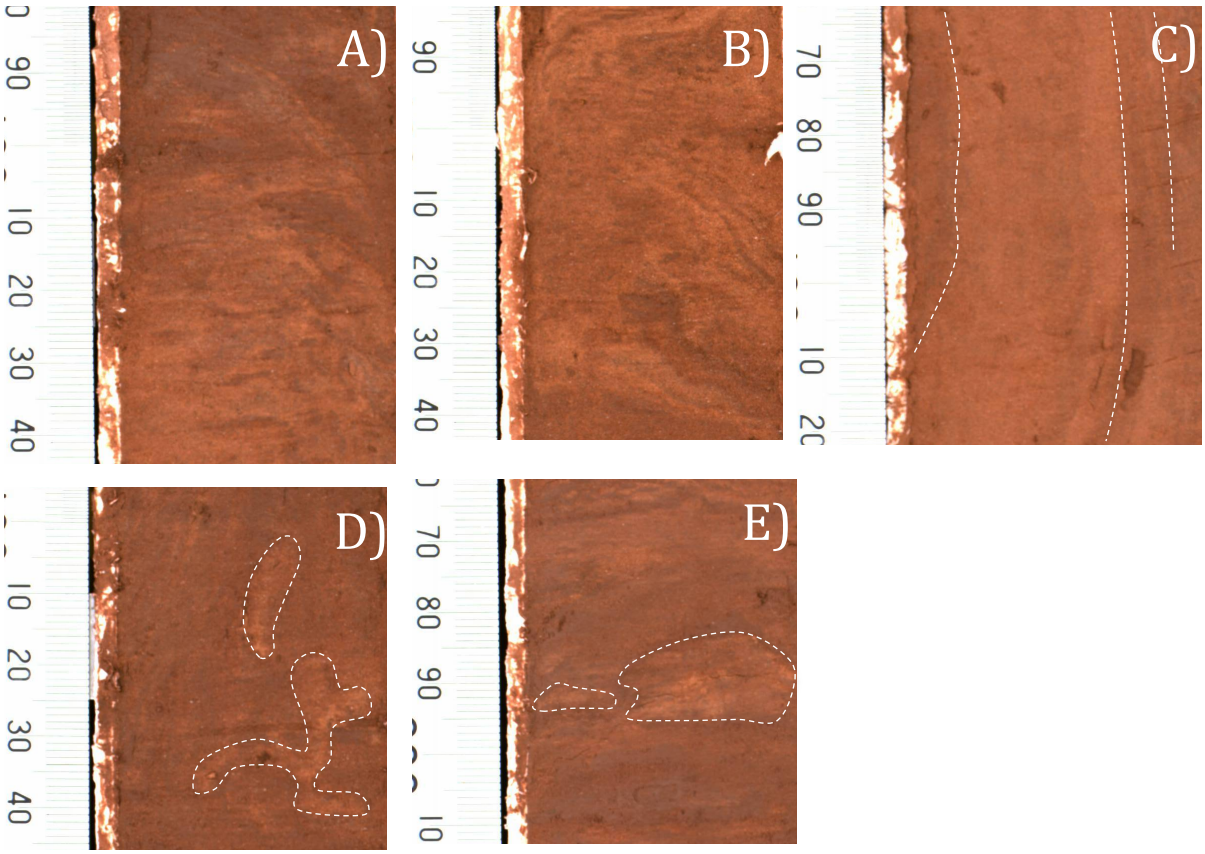

Fig. 16 *Facies G - Deformed mud* A) Deformed mud from core 10 (tidal flat). B) Deformed mud and small portion of very fine sand from core 2 (tidal flat). C) Deformed mud from core 8 (tidal flat). D) Lenses of fine sand from core 18 (tidal flat). E) Silty lenses from core 10 (tidal flat).

Interpretation
The deformed mud may originally have had planar, horizontal laminations (facies D or E), which have been destroyed through deformational processes. If the deformed mud originally was facies E (Heterolithic clay and silt) or facies D (Heterolithic mud and sand), typical depositional environments are tidal flats, where the alternation of relatively high and relatively weak current velocities is present (Davies 2012).

The deformational structures may have various origins, but it is unlikely that they are caused by bioturbation, as cold region tidal flats generally are sparsely bioturbated due to the shore ice and frost action (Dionne 1988). Also no observations of infaunal organisms were done during the field campaigns in 2016 and 2017.

During the fieldwork in 2016 and 2017 it was observed that the sediment close to the channels (including bars) and far out on the tidal flat (lower intertidal) contained a lot of water. Liquefaction of this type of sediment can occur and was in fact observed in field when taking core samples from the bars and adjacent to the channels. Deformational structures called convolute lamination can form as a result of this. Dewatering processes can also produce soft sediment deformational structures such as the "dash and pillar" (Nichols 2012[4]) and might be the origin of some of the deformational structures seen in the cores.

During fieldwork, it was also observed that the tidal flat sediment became drier moving away from the channels and into the upper intertidal zone. Cores taken from these dry areas also contain deformational structure, which are less likely to be due to liquefaction and dewatering processes. As known from other cold region tidal flats, ice pushing and ice-scouring may form deformational structures of various types (Dionne 1988, 1997 and Dashtgard *et al.* 2014). During the field campaign, circular depression of the surface of the tidal flat was observed (Fig. 57), which resemble those described by Dionne (1988, 1997). Core 18 (Fig. 37) was collected from an elevated "rigde" surrounding one of the circular depressions, and the core clearly shows deformation in the upper part of the core. This is a strong indication that shore ice scouring and deformation is causing deformation in the tidal flat deposits.

The sediment cores only provides a small and narrow "window" into the deposit, and it is important to stress that it is therefor not possible to capture large or even medium scale structures. A conclusion of which process has created the deformational structures in the mud is therefor not possible.

6. Log-transects and composite logs

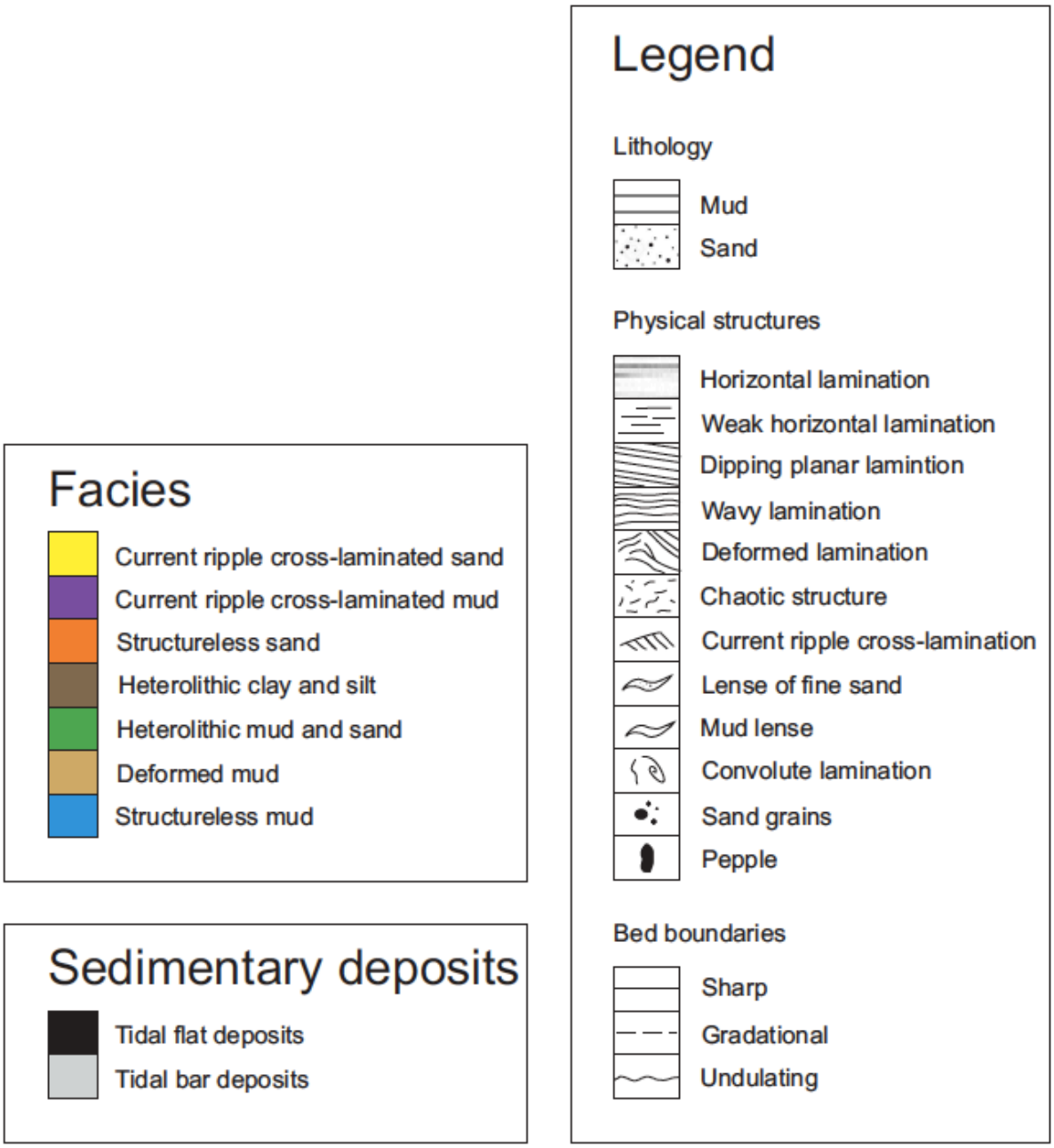

Fig. 17 Legend for the core-transects and composite logs.

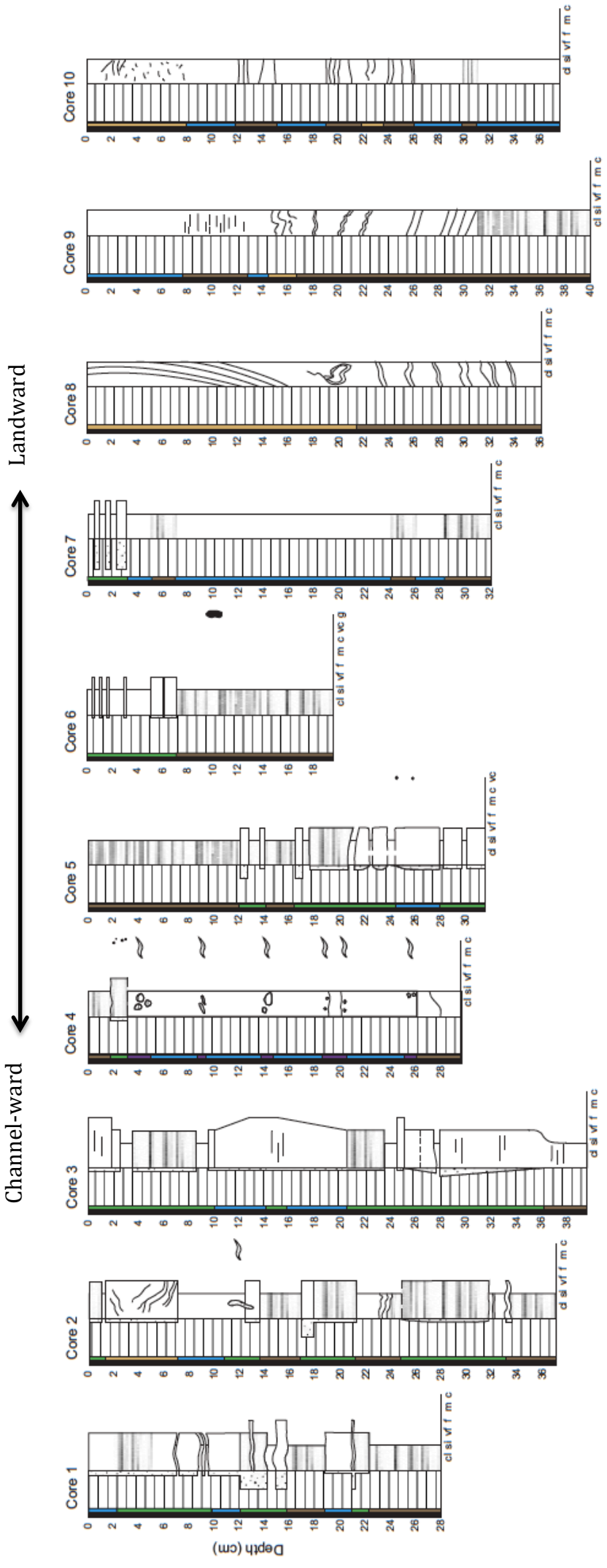

Fig. 18 Core-transect 1.

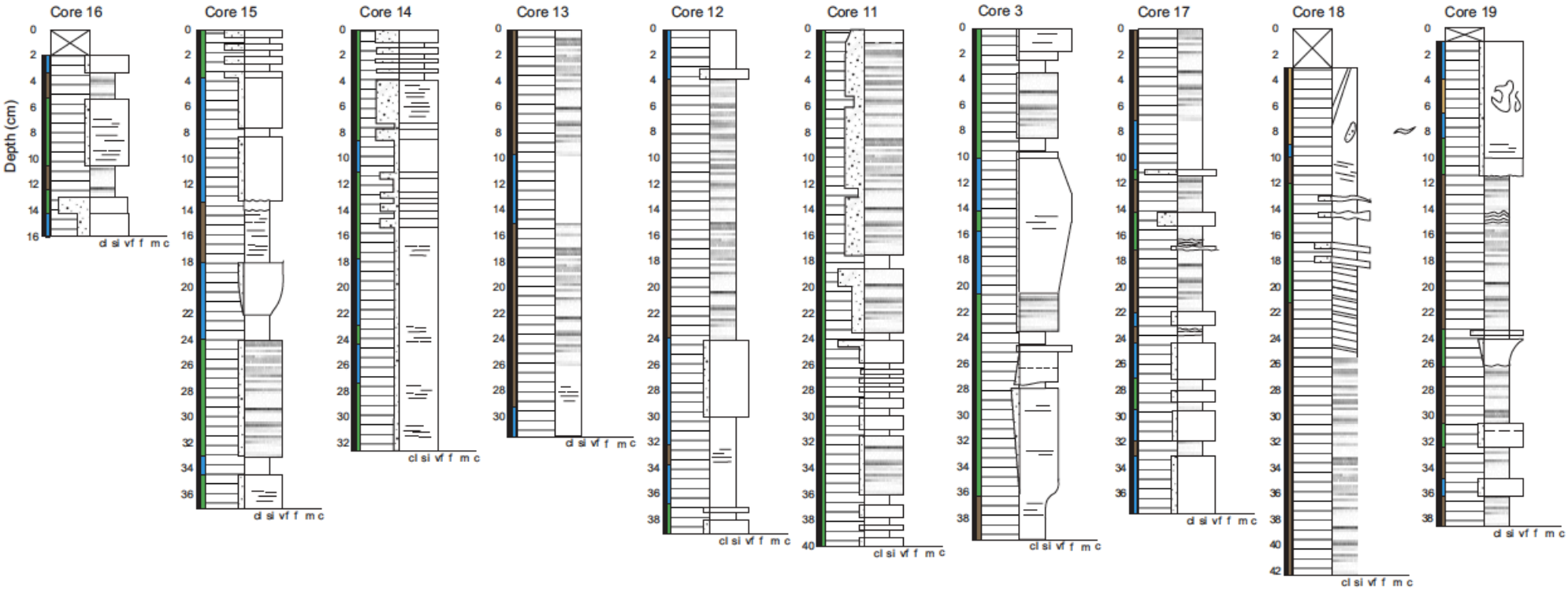

Fig. 19 Core-transect 2.

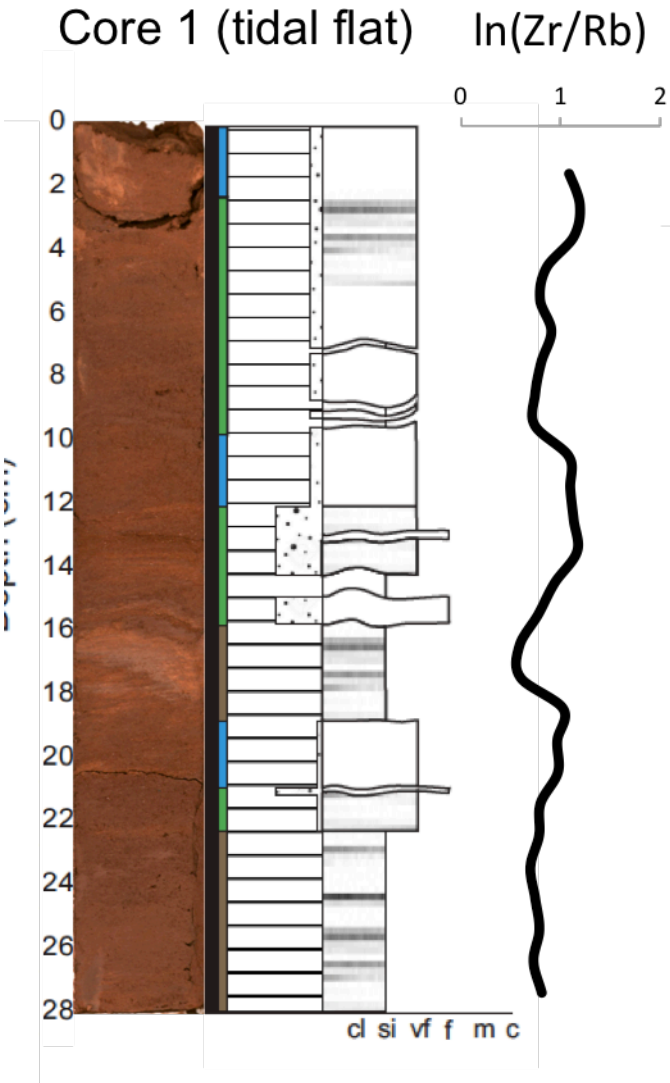

20 Composite log of core 1 obtained from the tidal flat.

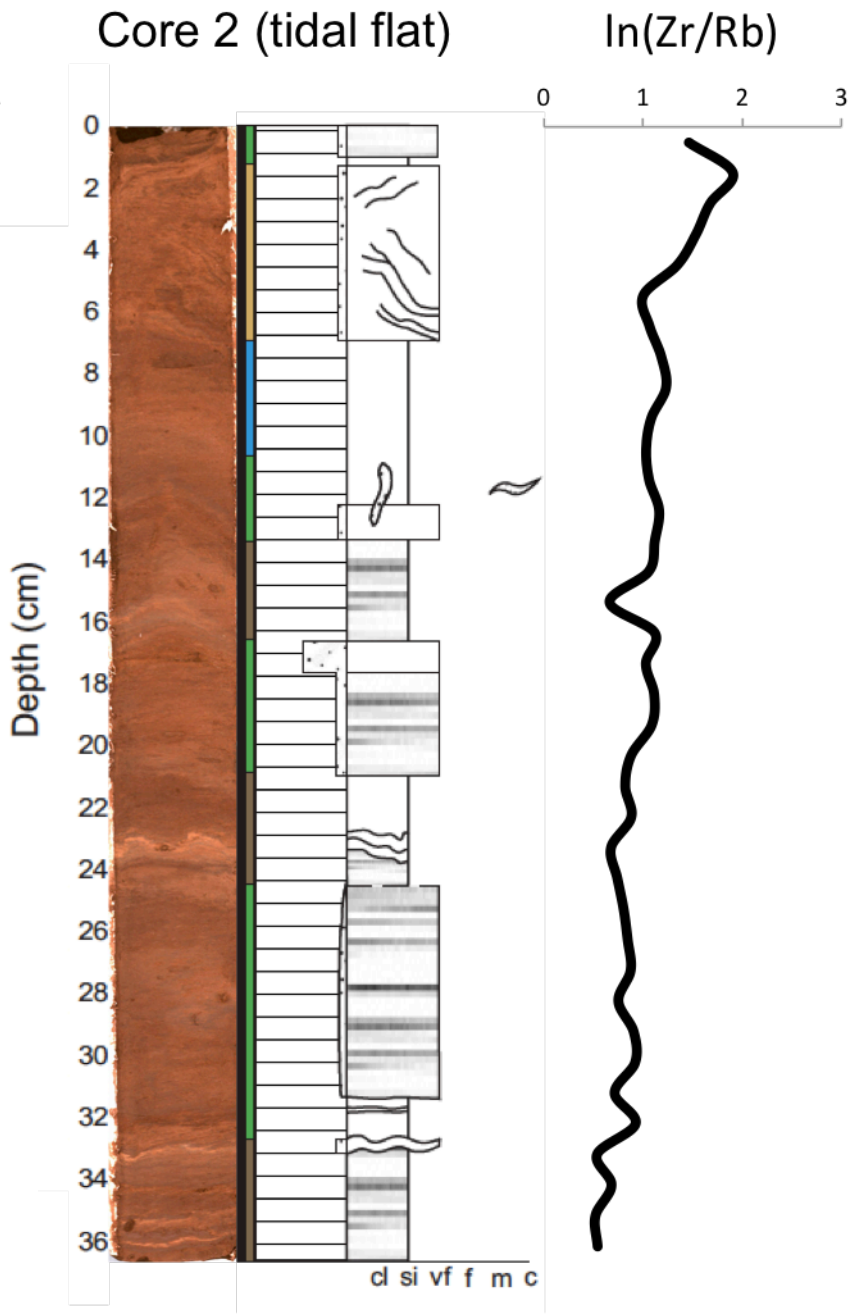

Fig. 21 Composite log of core 2 obtained from the tidal flat.

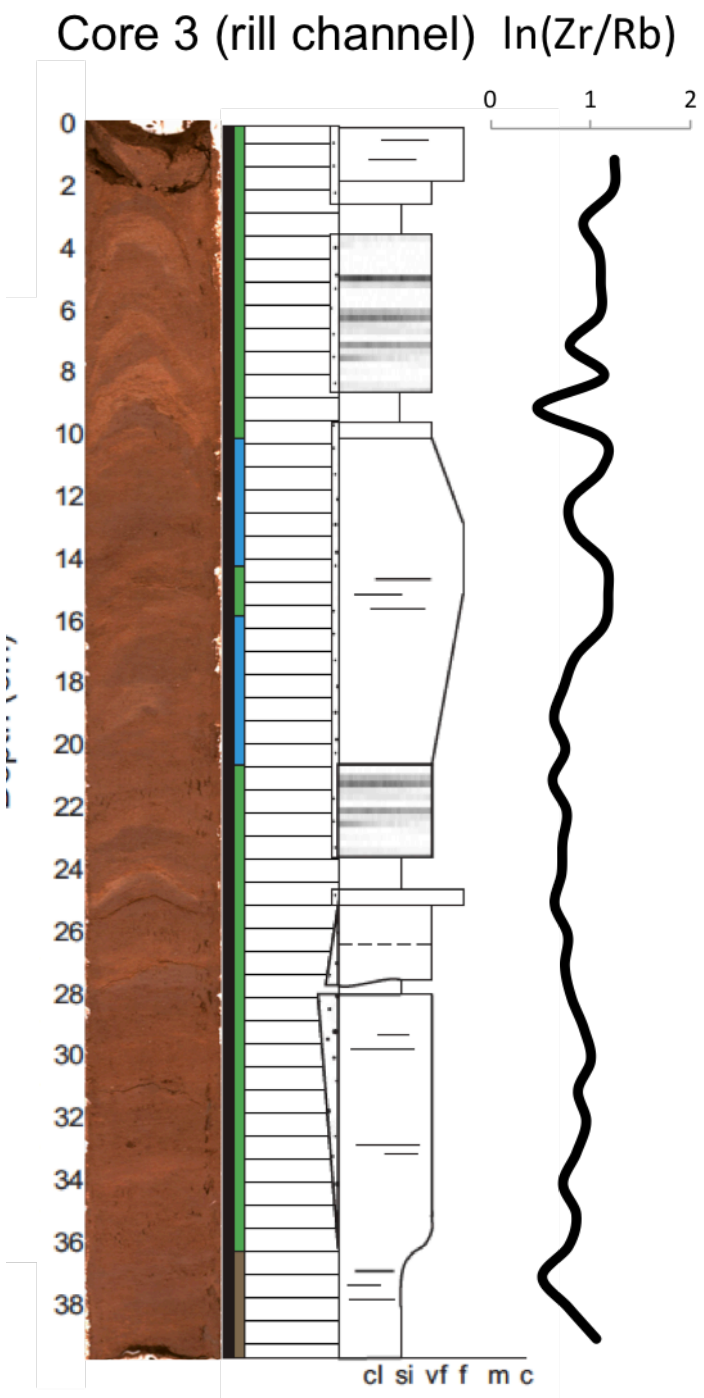

22 Composite log of core 3 obtained from a rill channel on the tidal

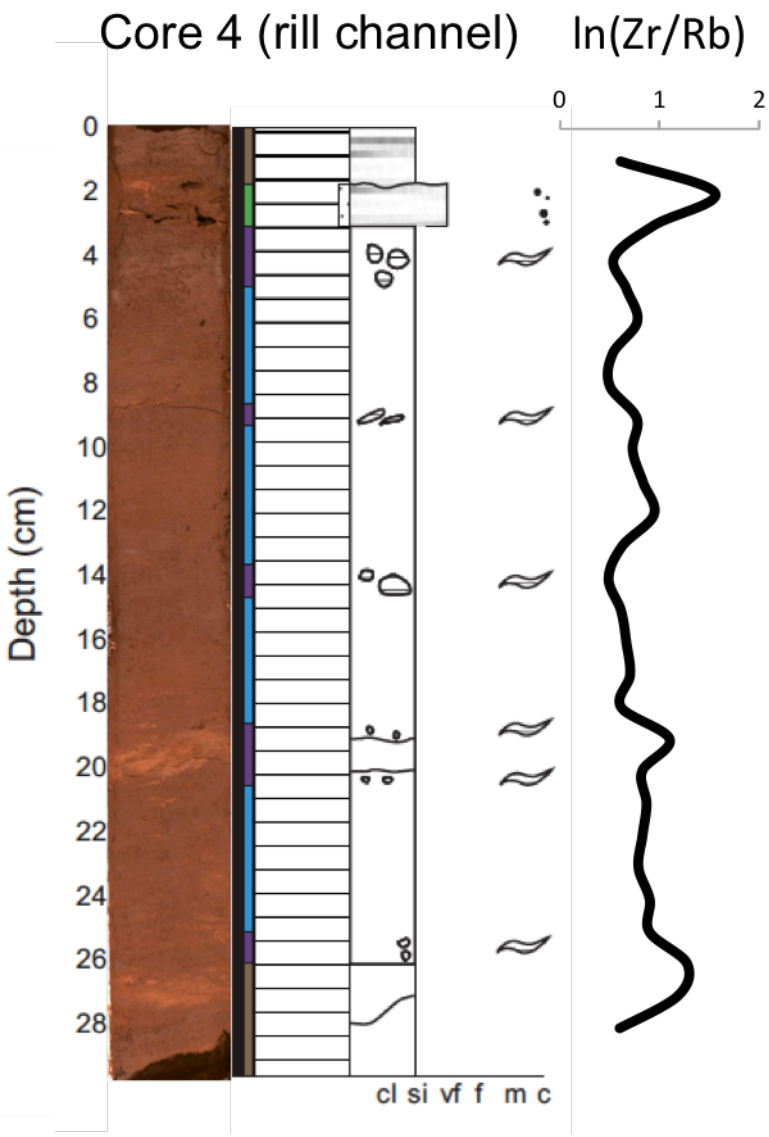

Fig. 23 Composite log of core 4 obtained from a rill channel on the tidal flat.

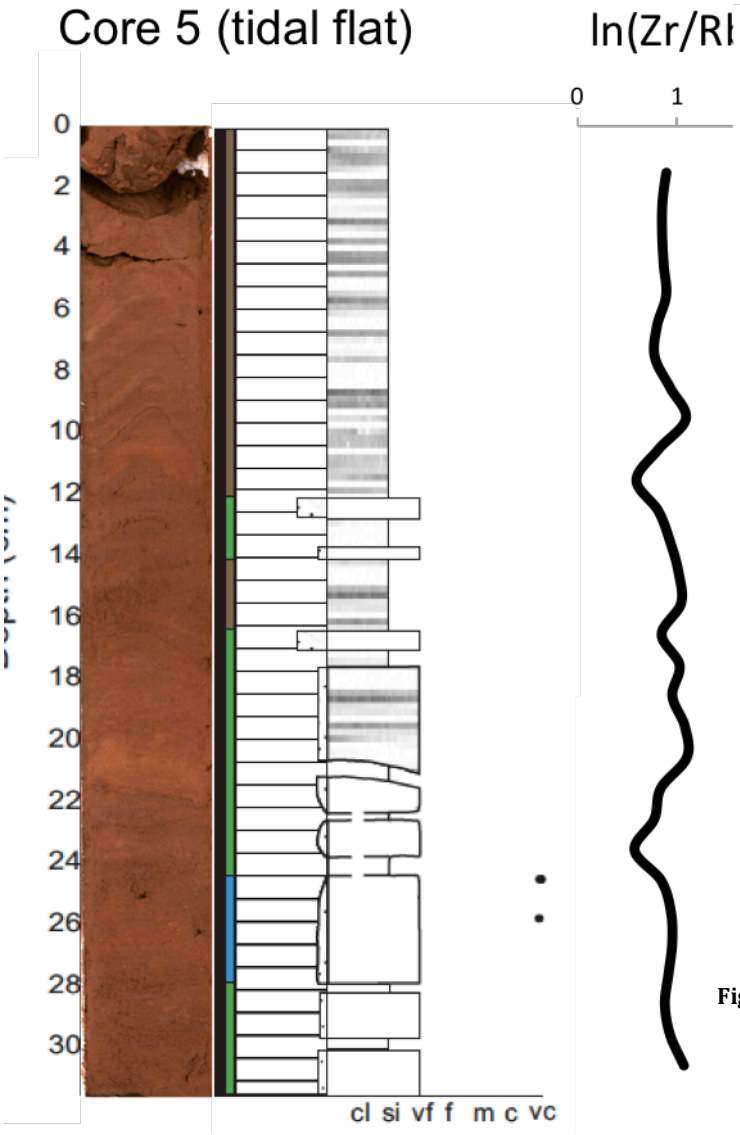

. 24 Composite log of core 5 obtained from the tidal flat.

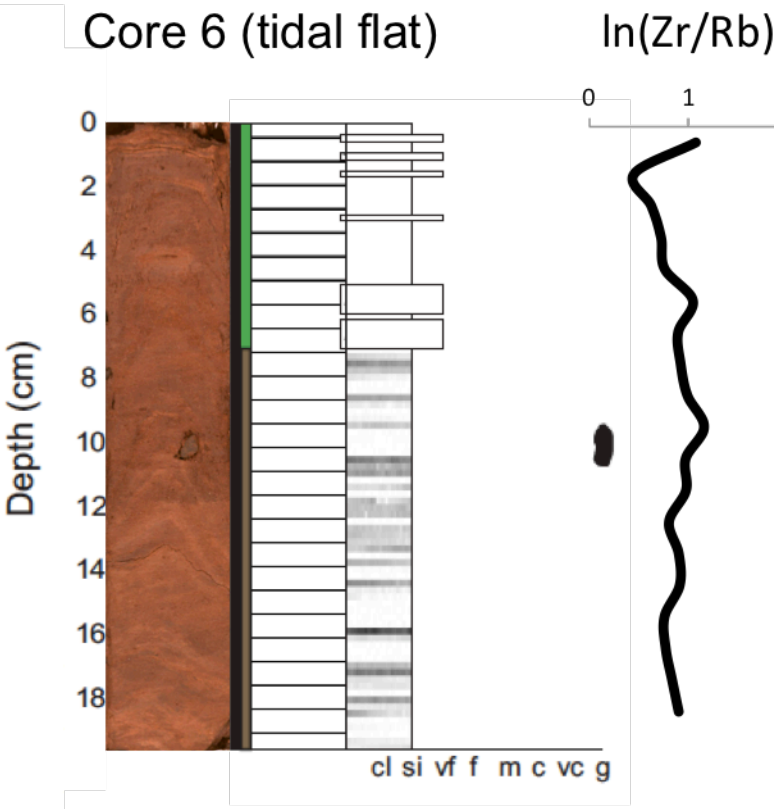

Fig. 25 Composite log of core 6 obtained from the tidal flat.

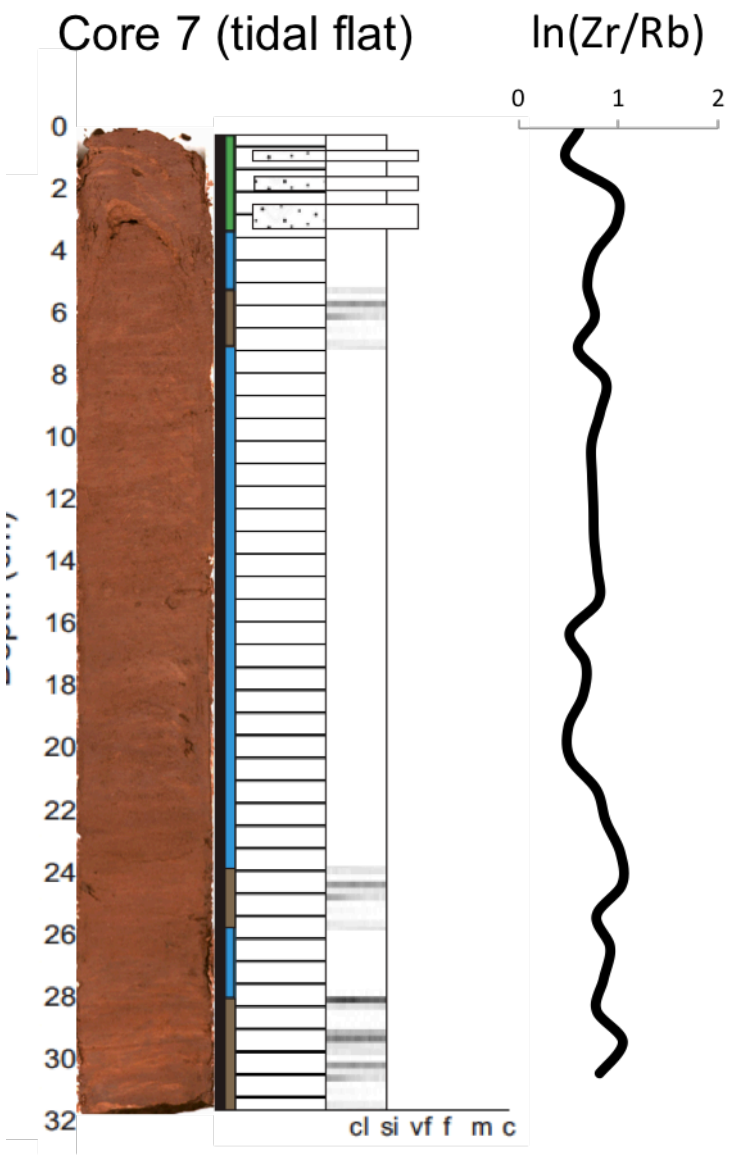

26 Composite log of core 7 obtained from the tidal flat.

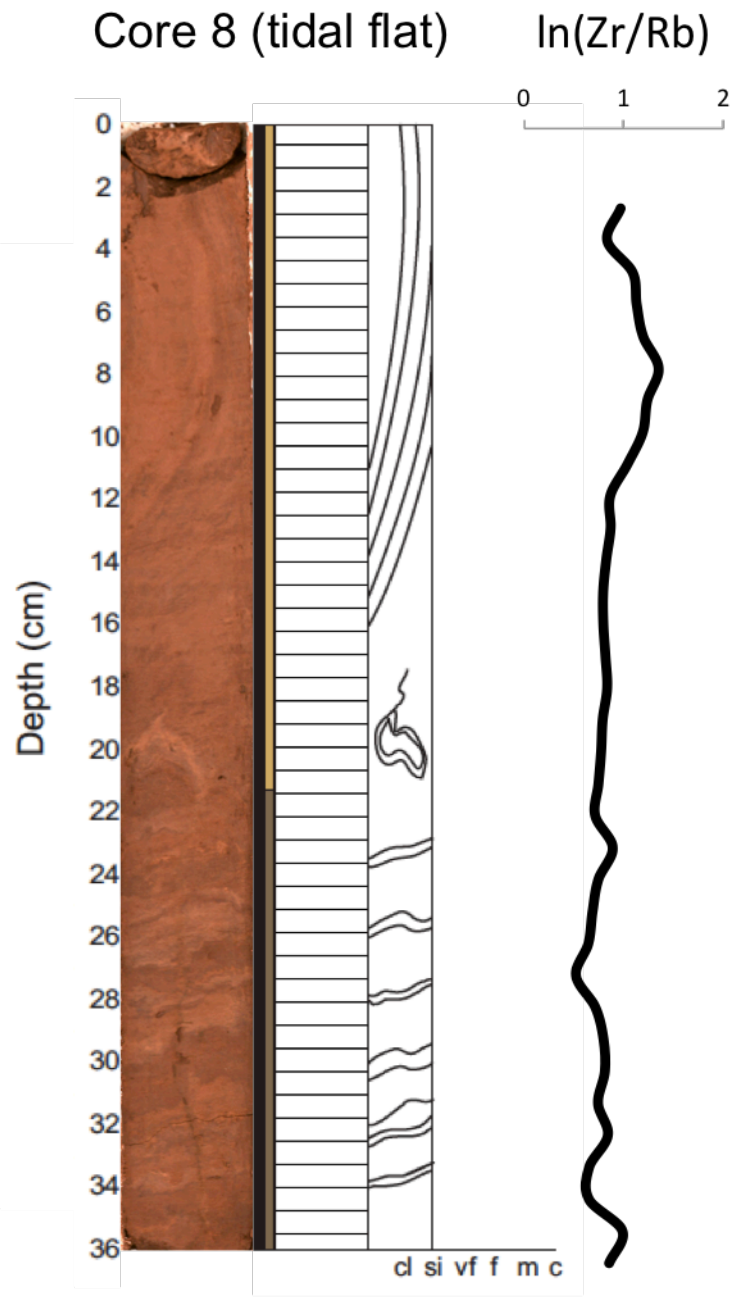

Fig. 27 Composite log of core 8 obtained from the tidal flat.

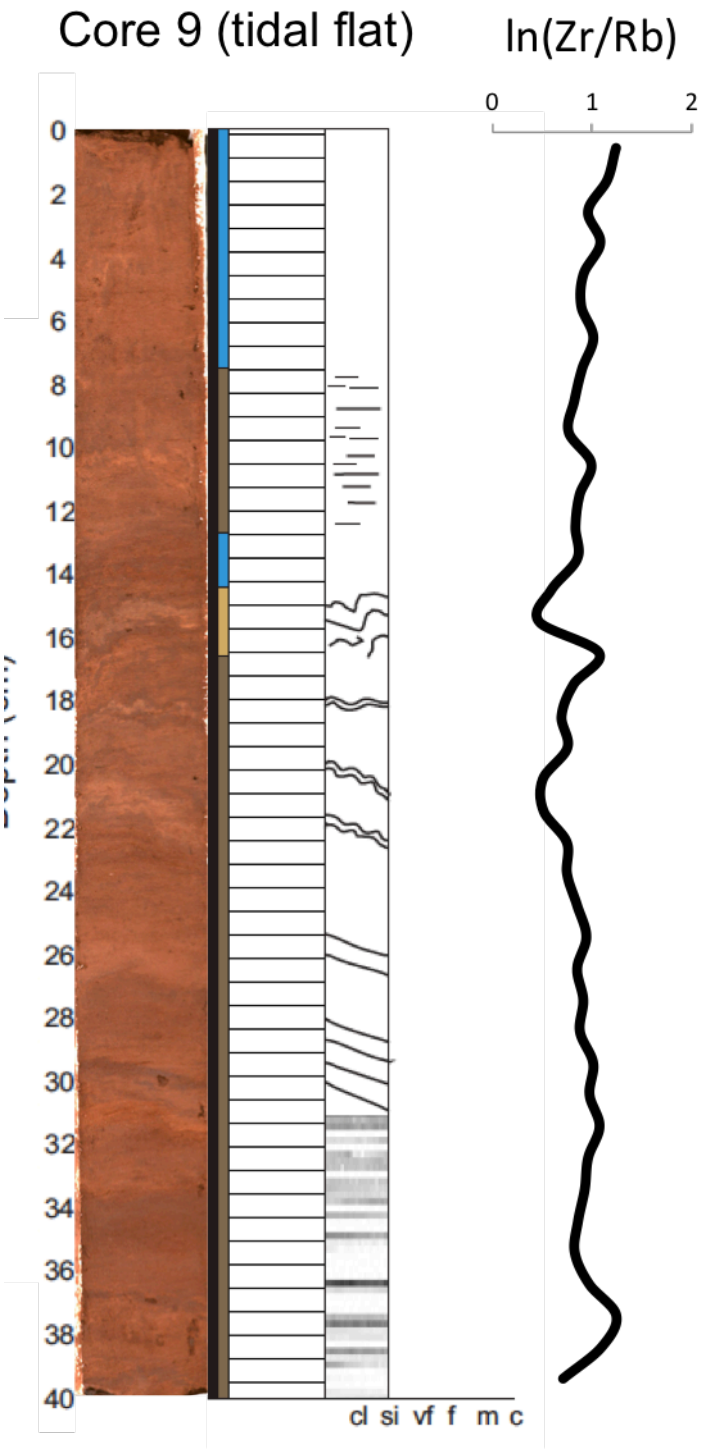

28 Composite log of core 9 obtained from the tidal flat.

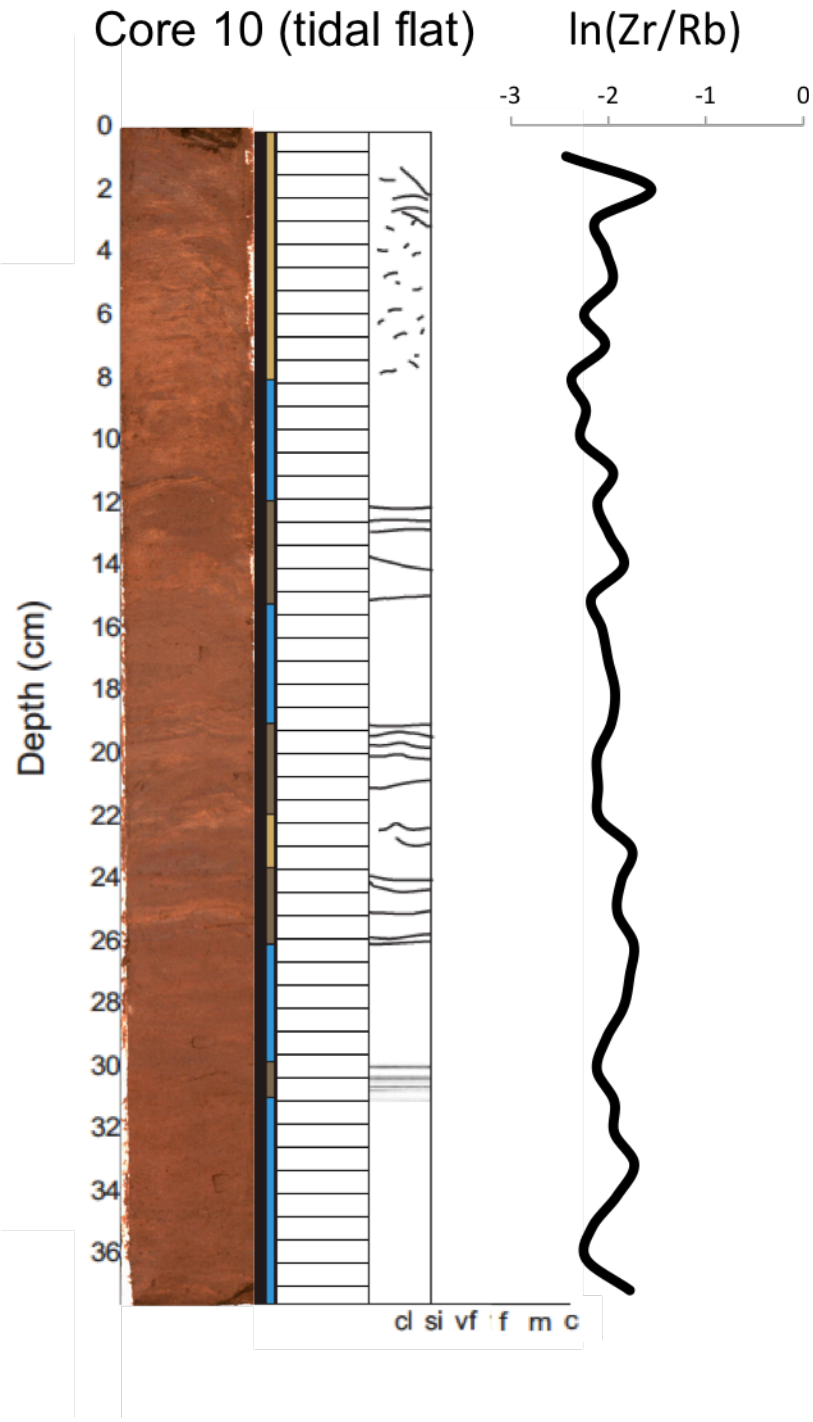

Fig. 29 Composite log of core 10 obtained from the tidal flat.

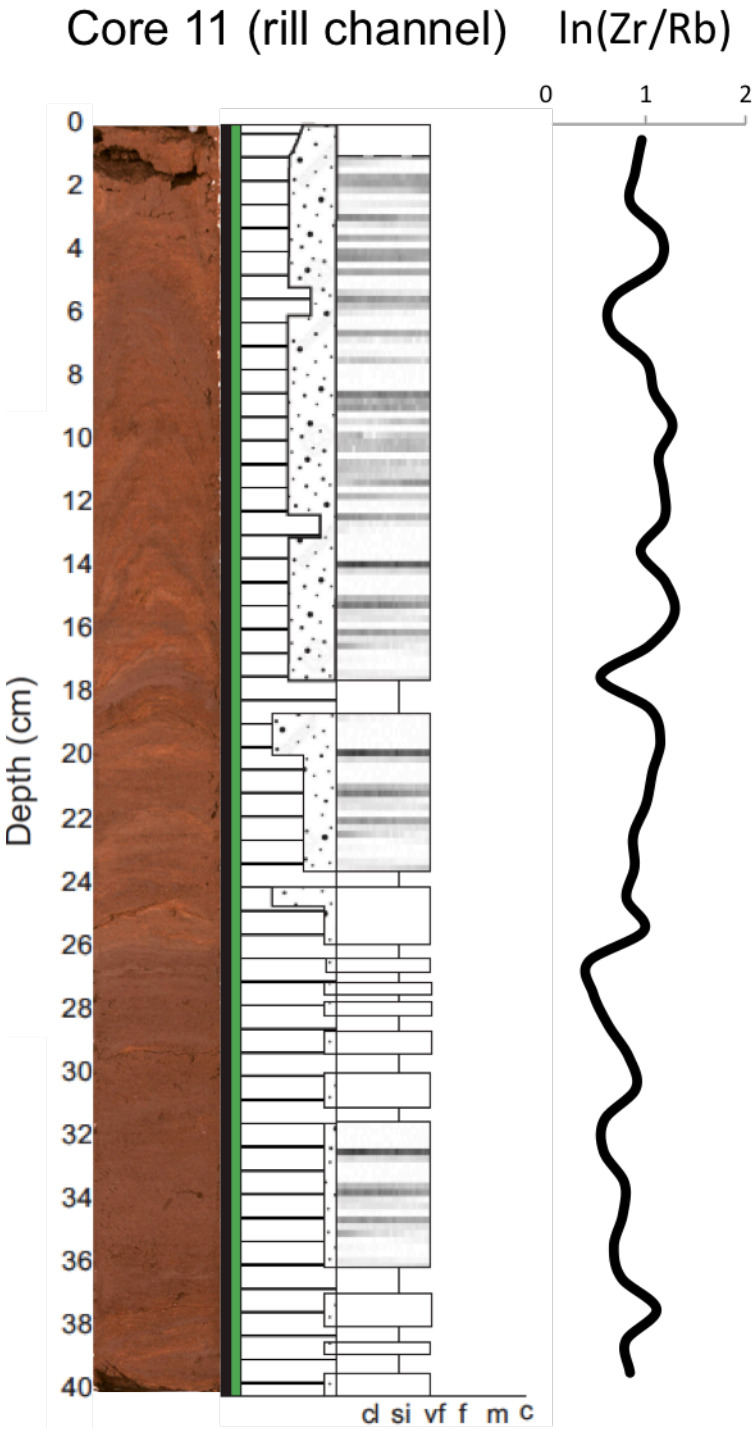

30 Composite log of core 11 obtained from the tidal flat.

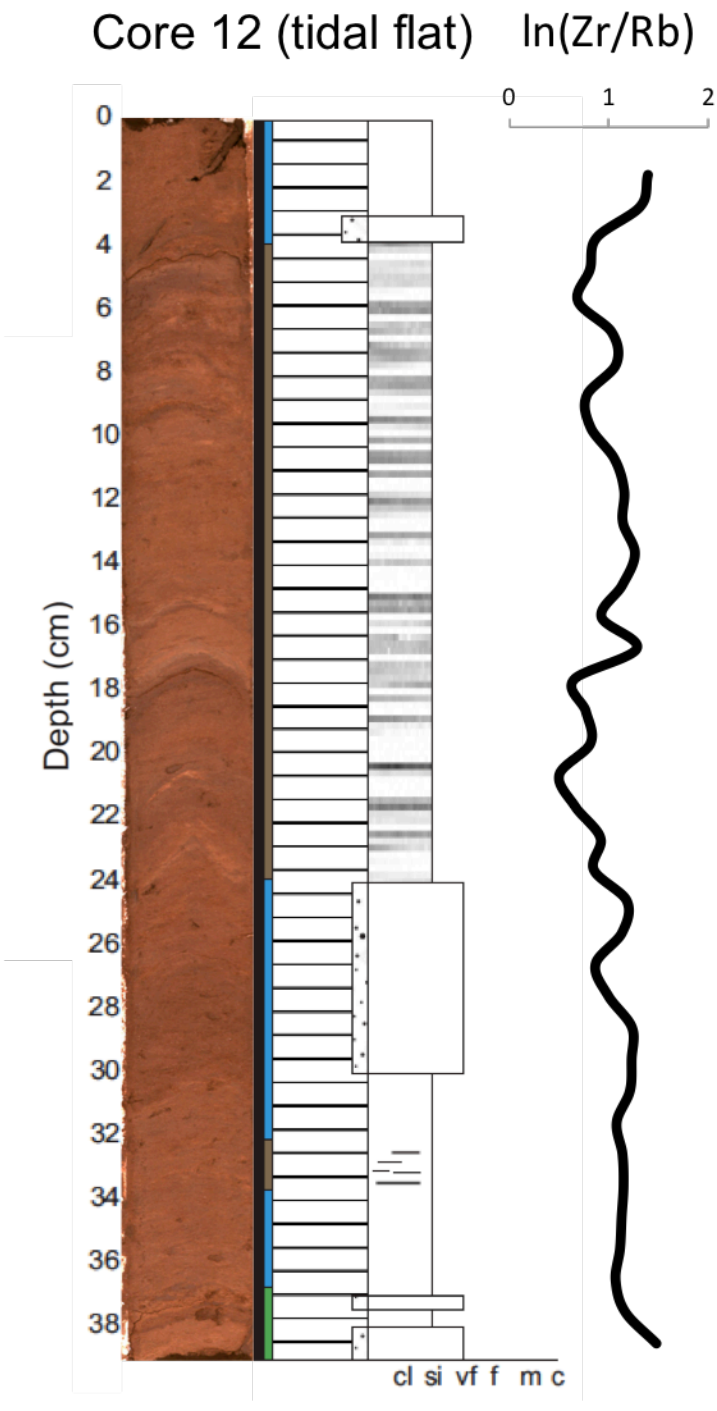

Fig. 31 Composite log of core 12 obtained from the tidal flat.

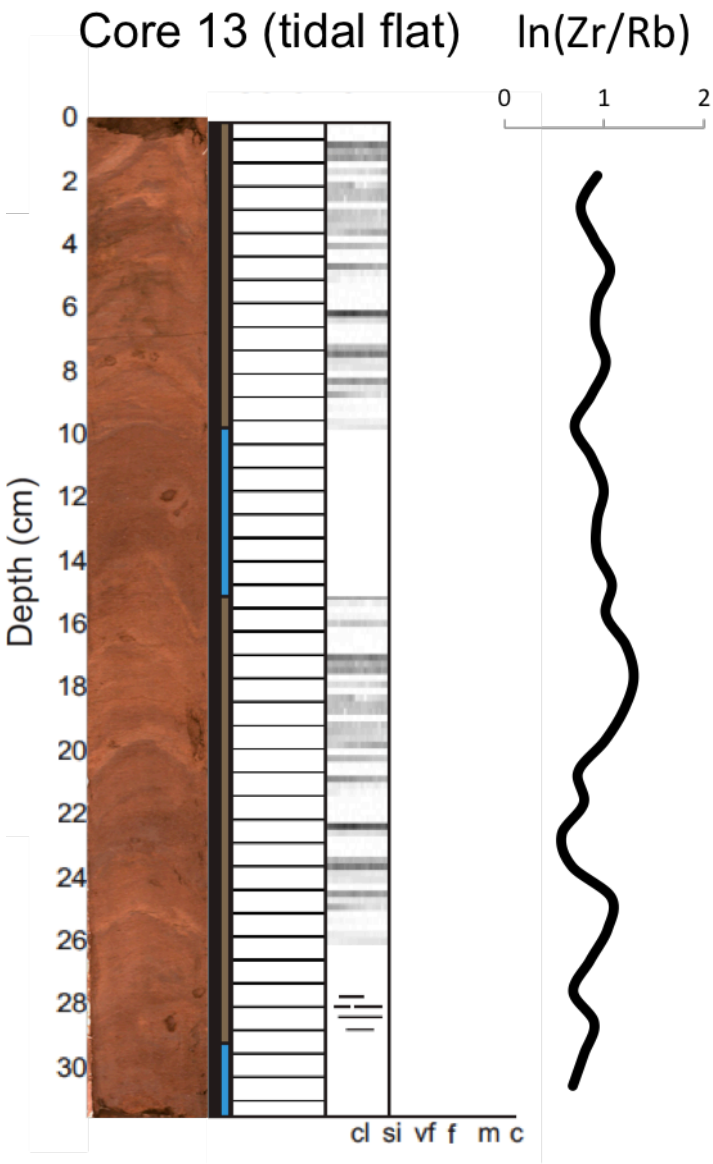

32 Composite log of core 13 obtained from the tidal flat.

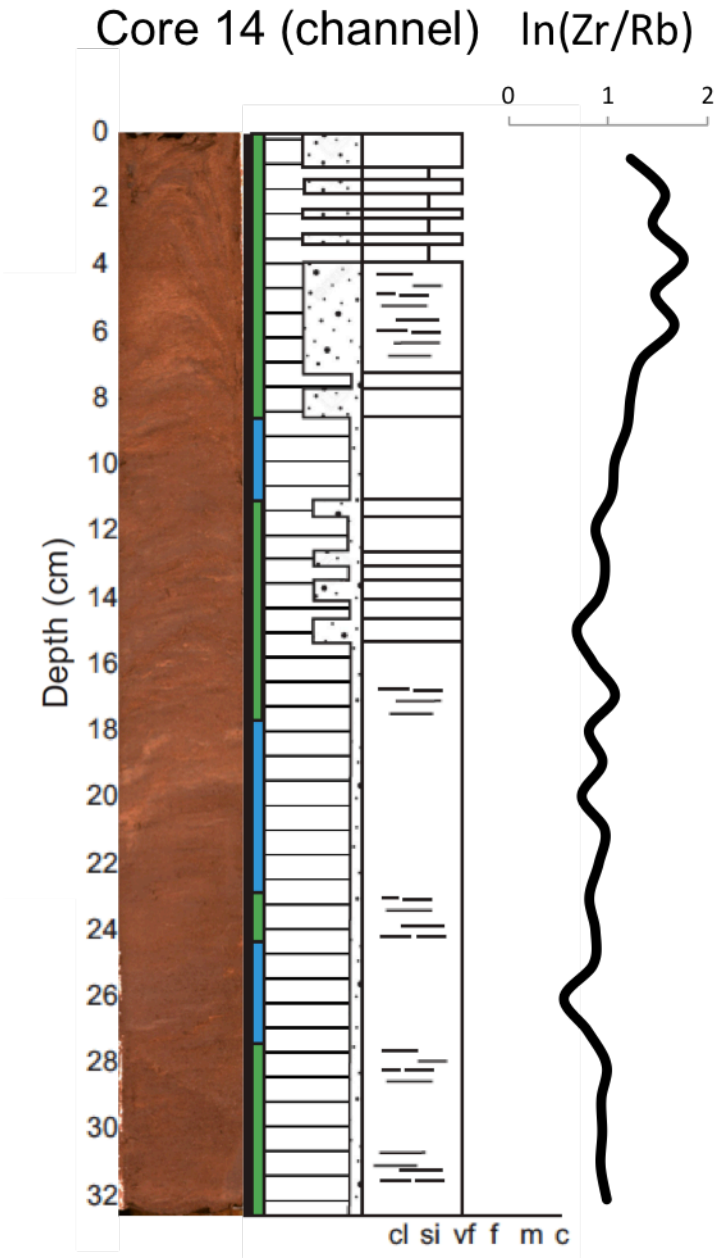

Fig. 33 Composite log of core 14 obtained from the tidal flat.

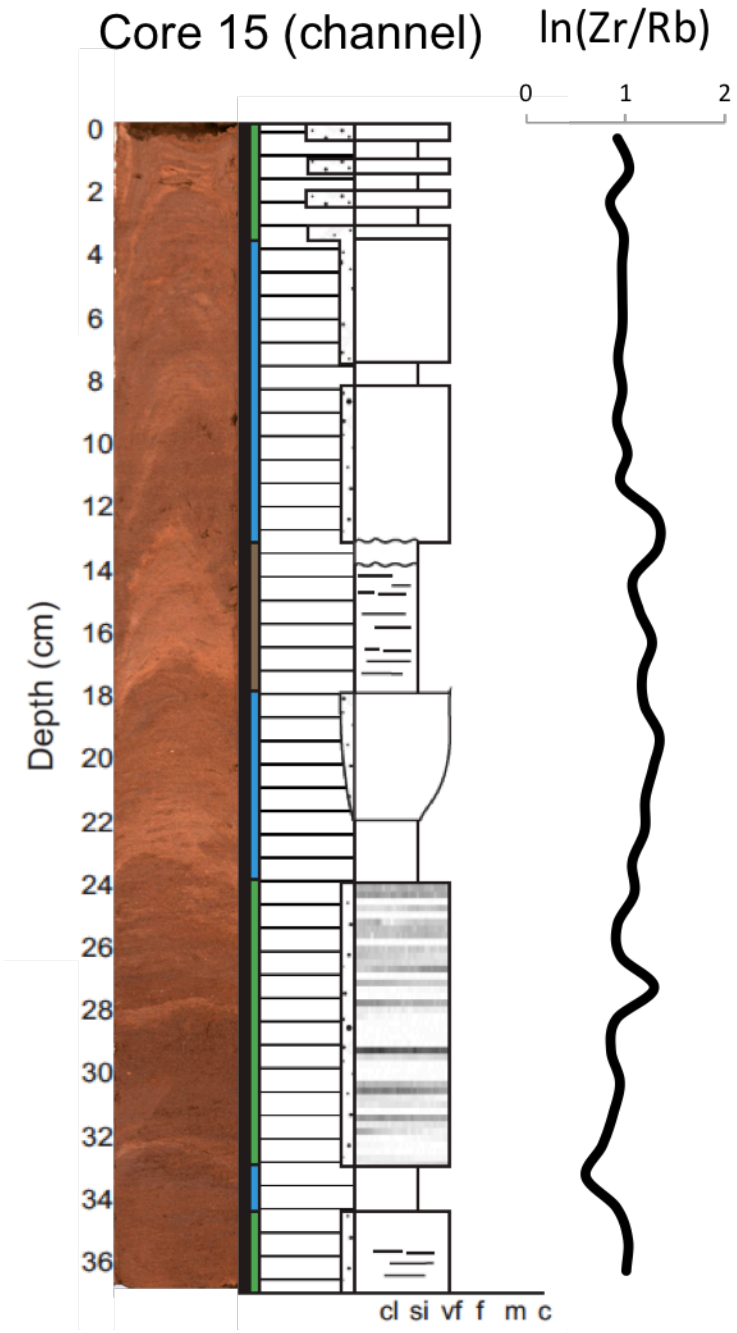

ig. 34 Composite log of core 15 obtained from a tidal channel on the tidal at.

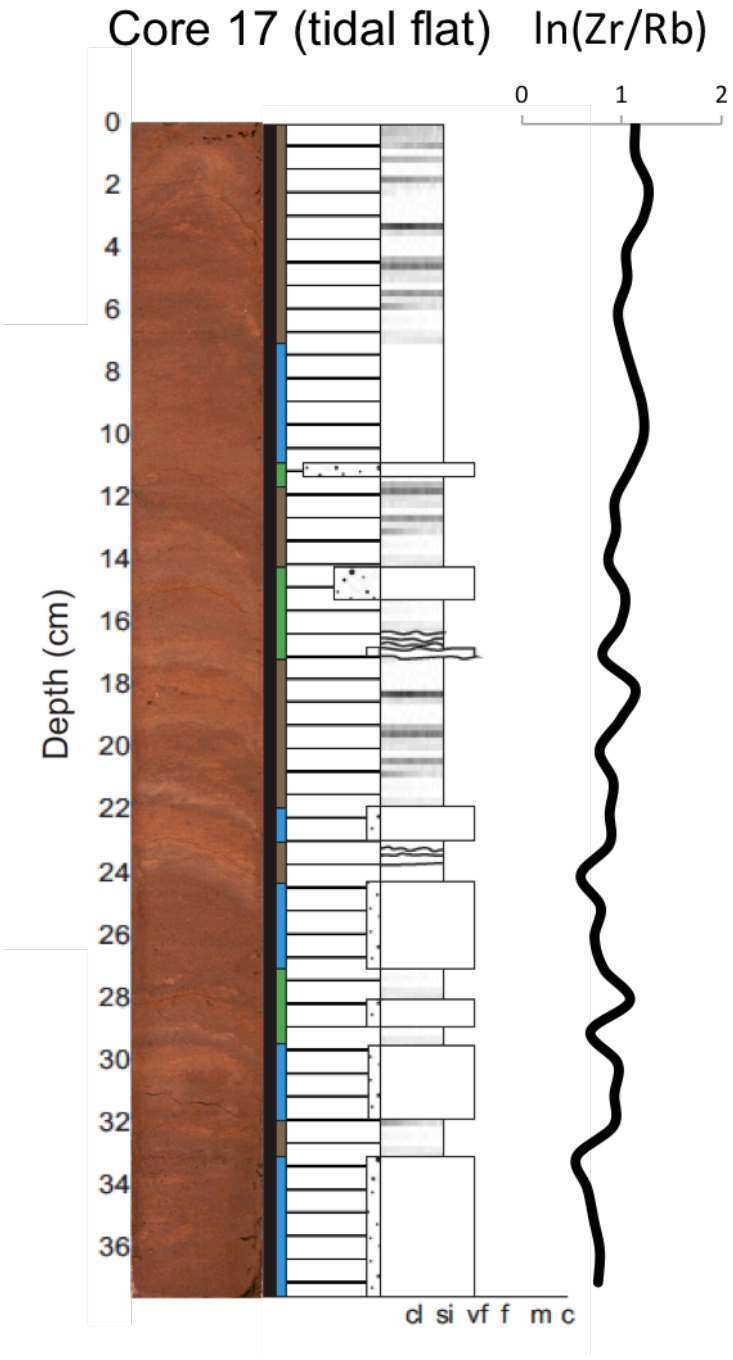

Fig. 35 Composite log of core 16 obtained from the tidal flat.

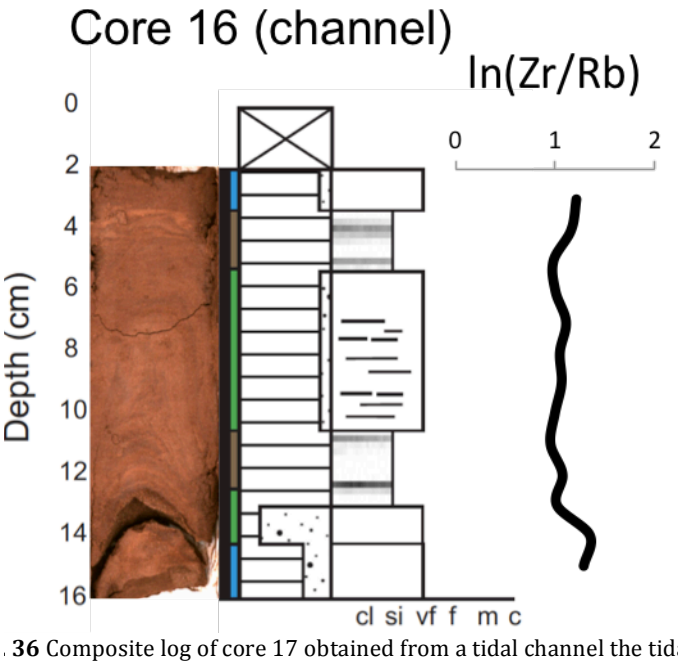

. 36 Composite log of core 17 obtained from a tidal channel the tidal

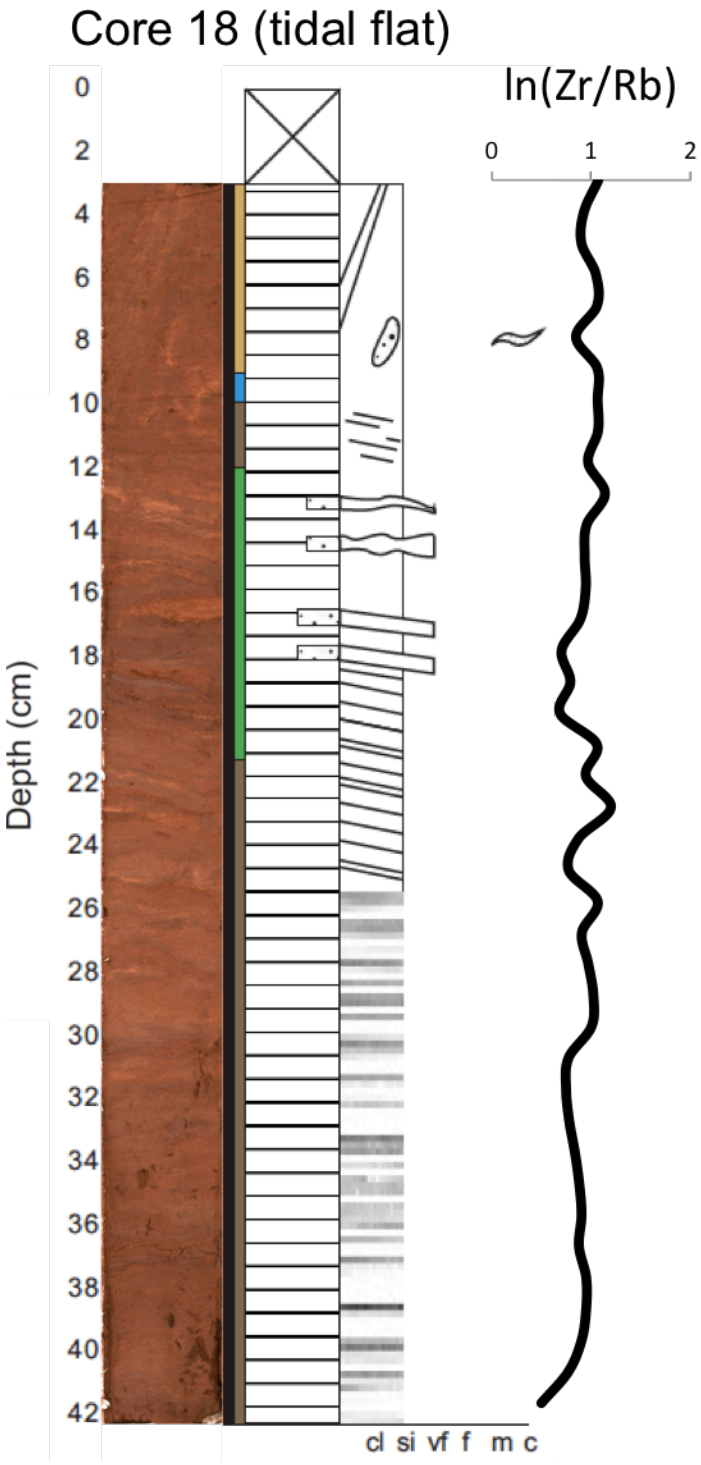

37 Composite log of core 18 obtained from the tidal flat.

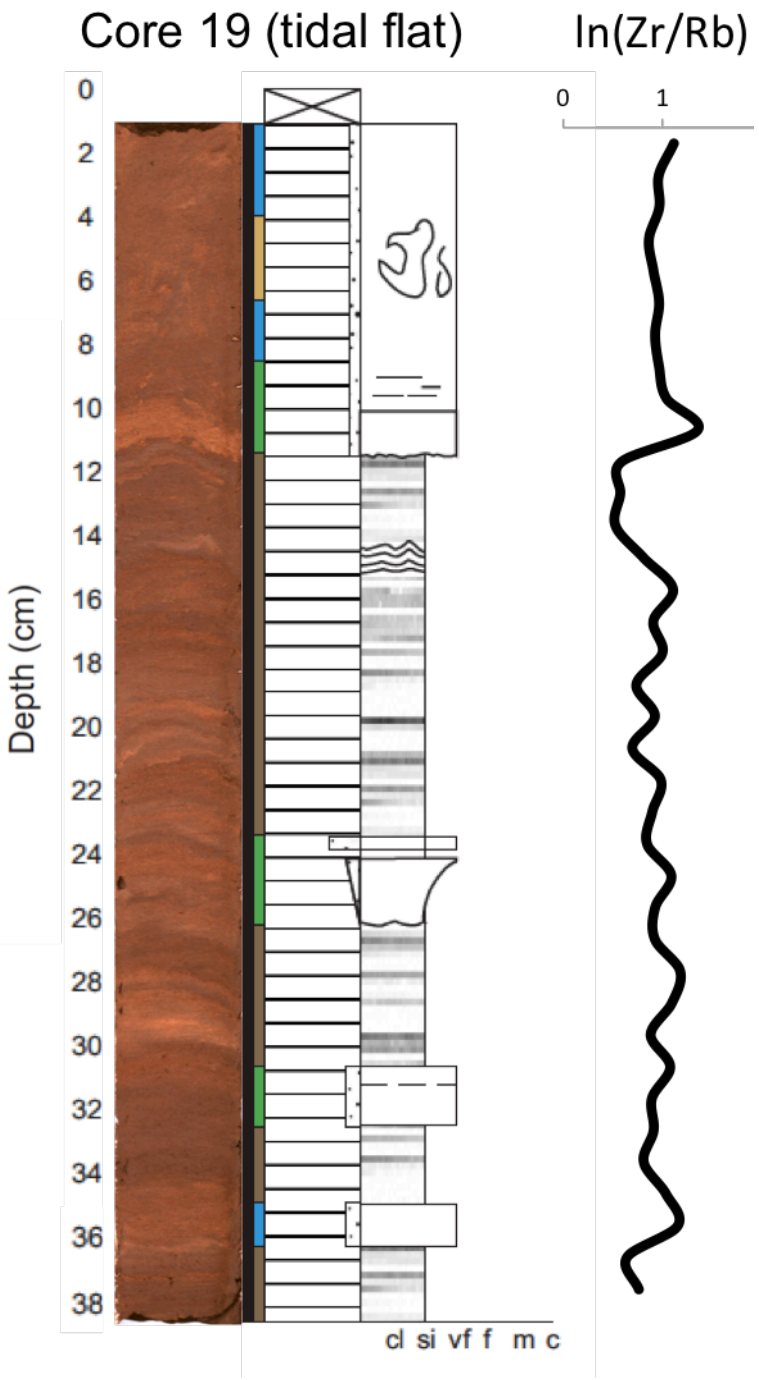

Fig. 38 Composite log of core 19 obtained from the tidal flat.

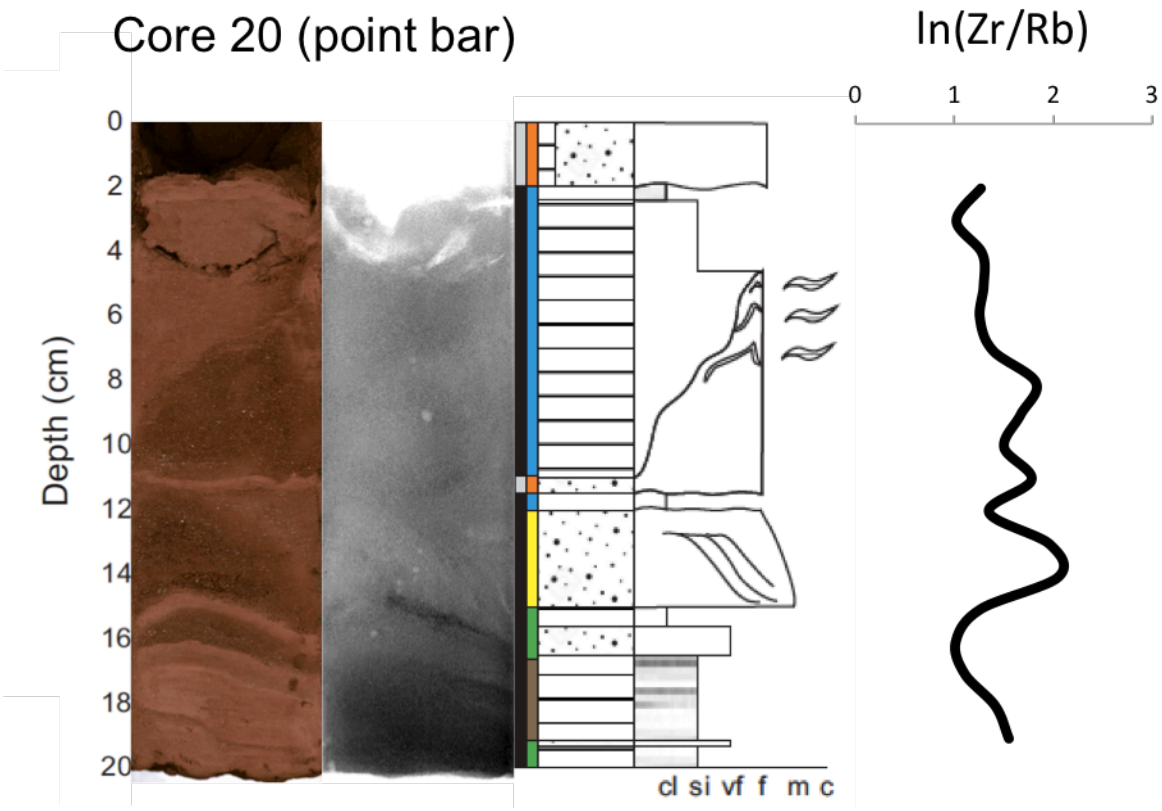

Fig. 39 Composite log of core 20 obtained from a point bar in a tidal channel.

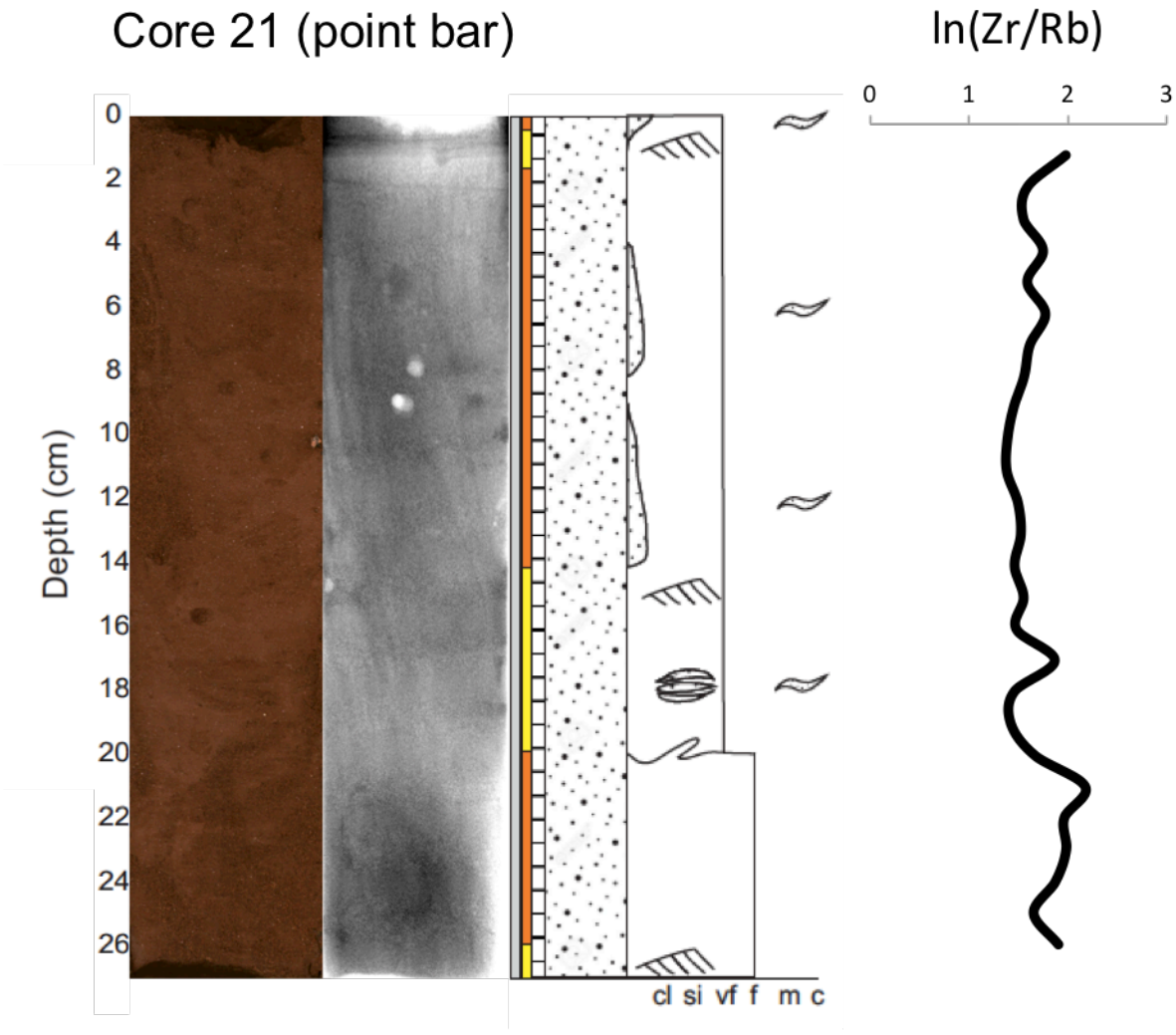

Fig. 40 Composite log of core 21 obtained from a point bar in a tidal channel.

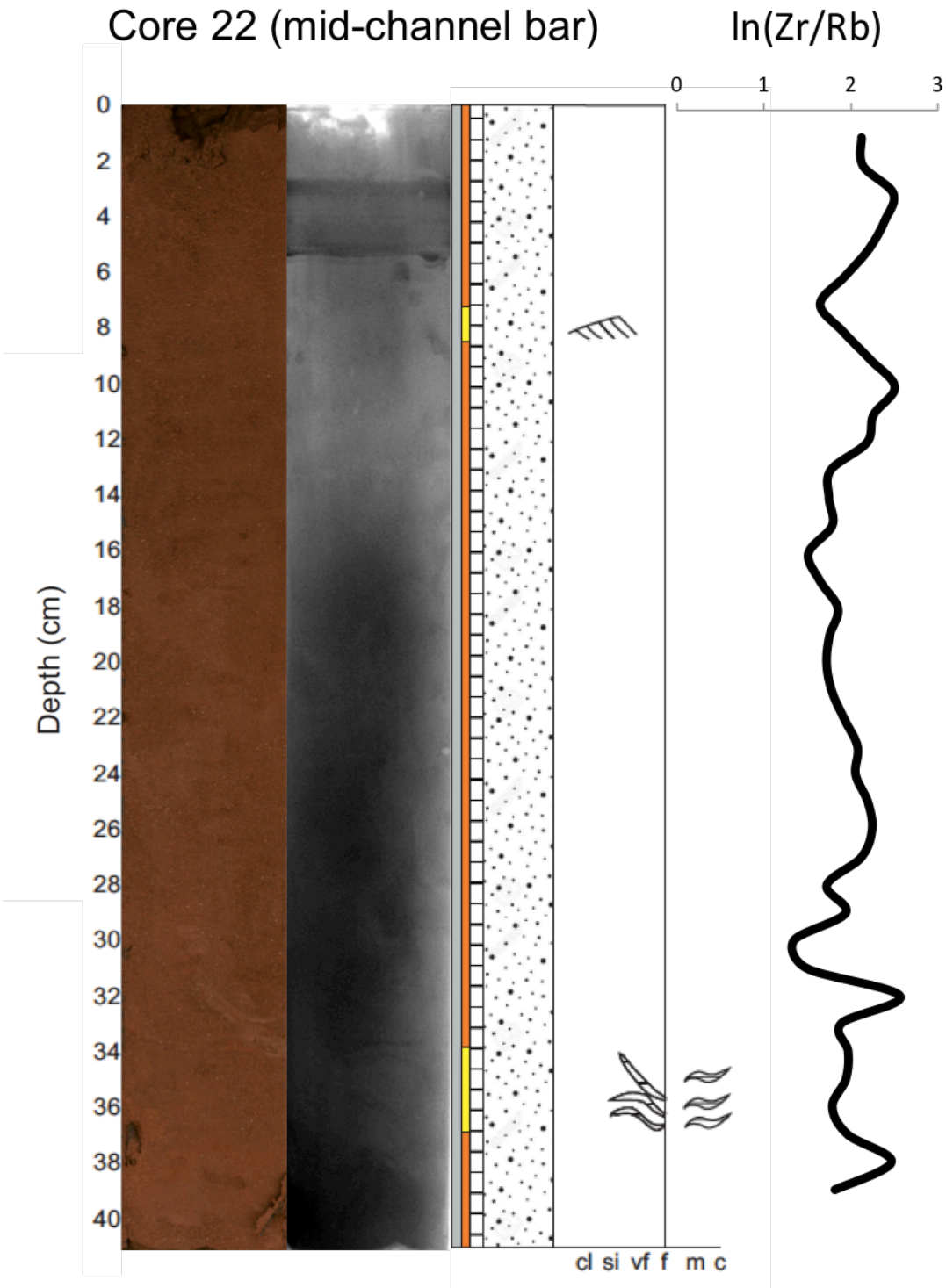

Fig. 41 Composite log of core 22 obtained from a mid-channel bar in a tidal channel.

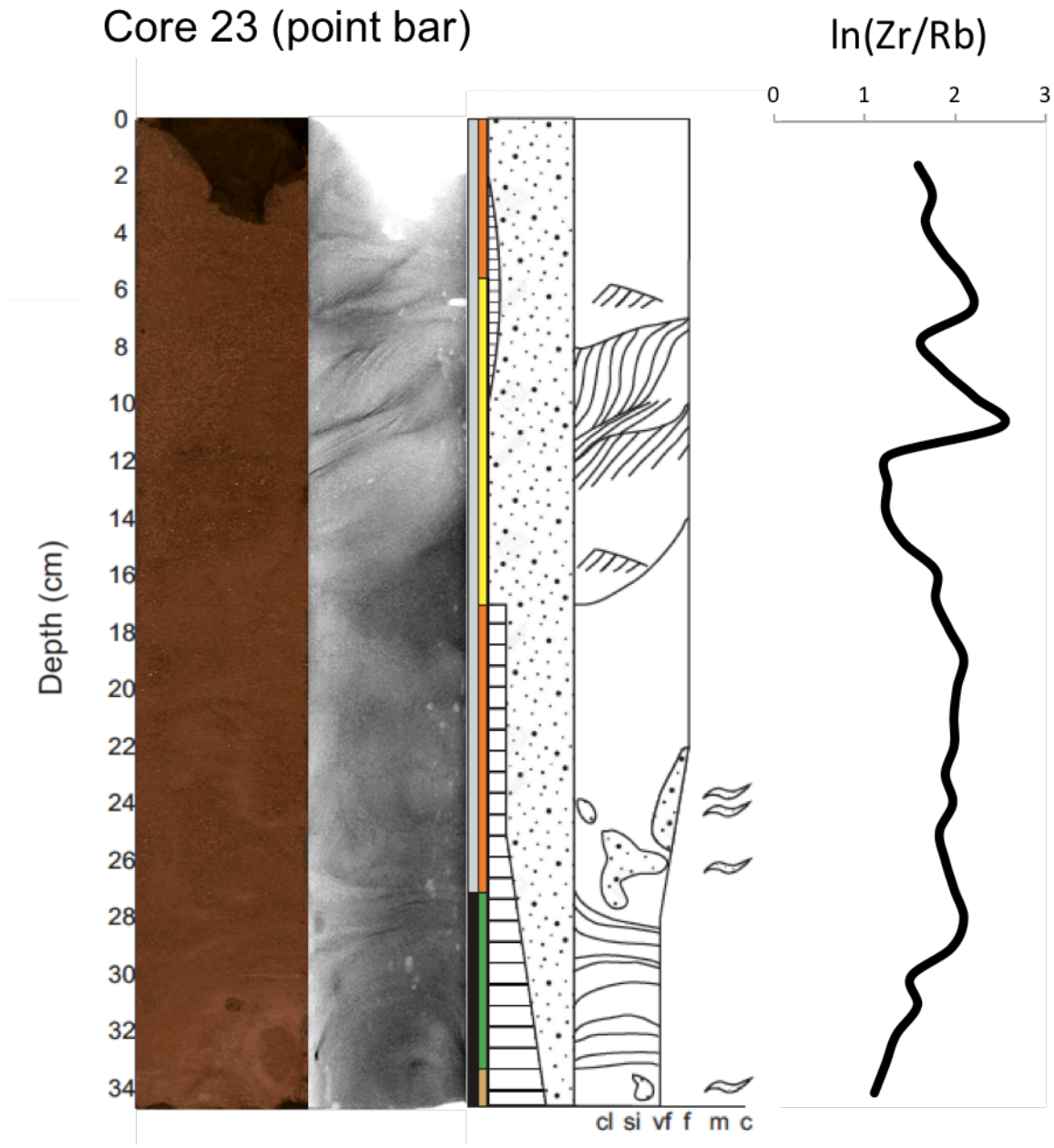

Fig. 42 Composite log of core 23 obtained from a point bar in a tidal channel.

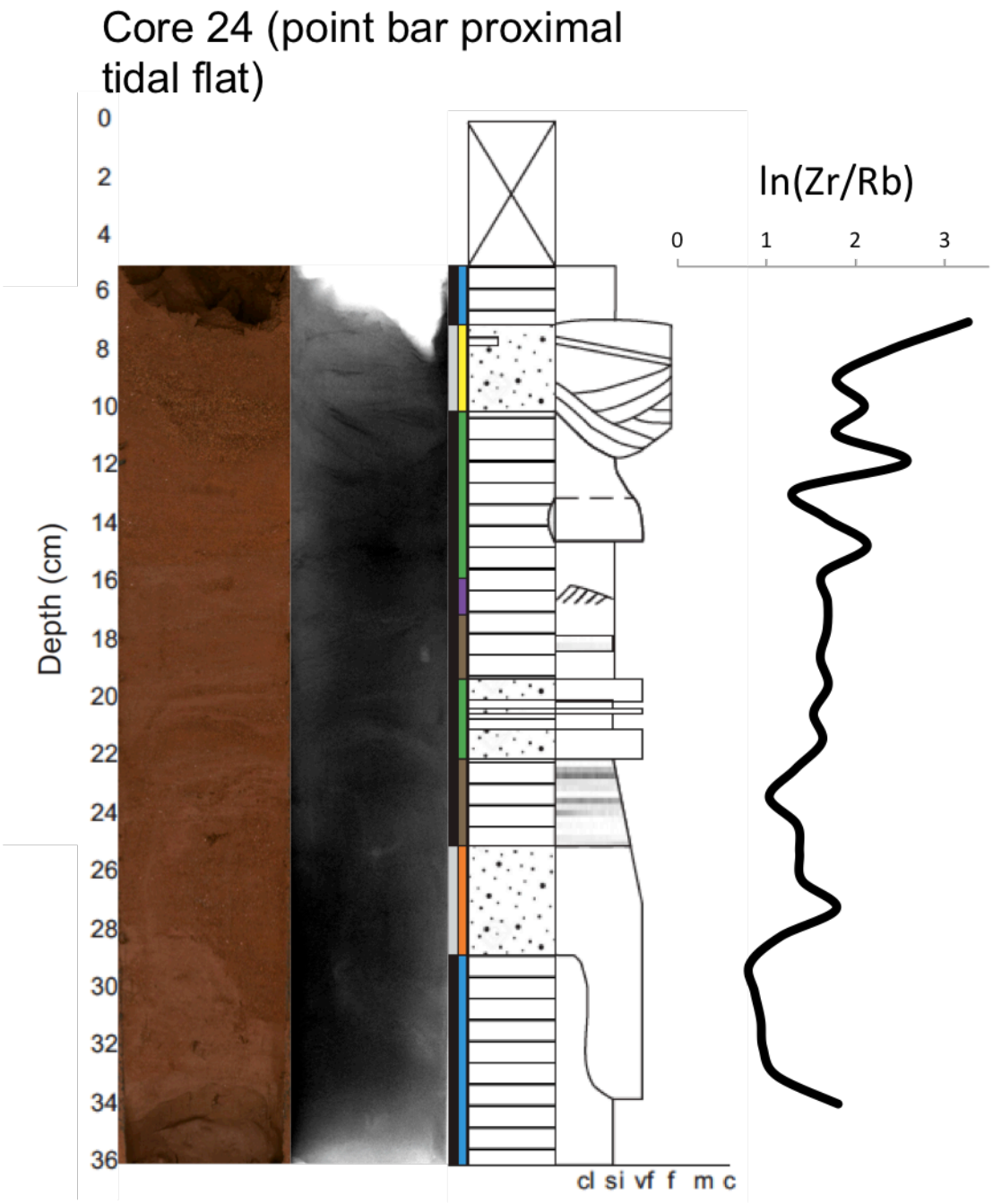

Fig. 43 Composite log of core 24 obtained from the boarder between the tidal flat and a point bar.

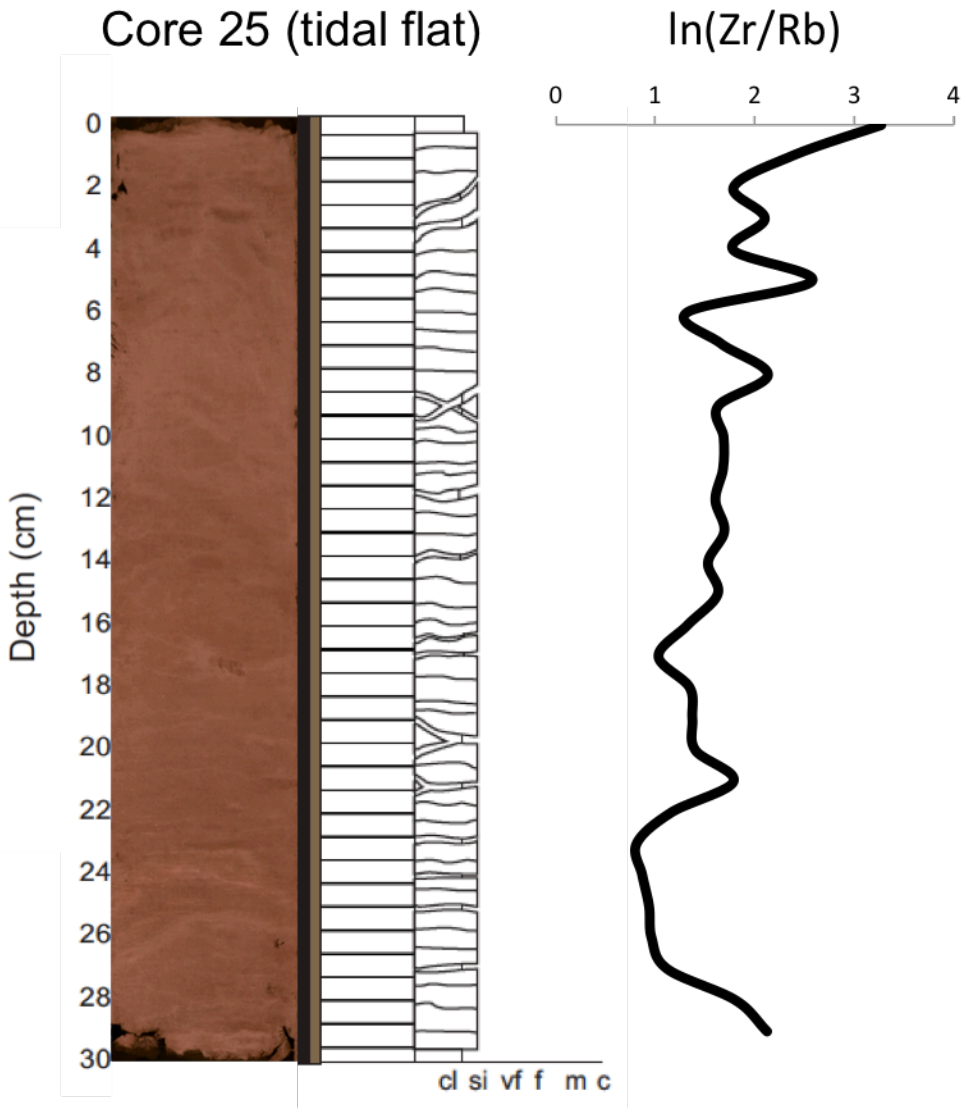

Fig. 44 Composite log of core 25 obtained from the tidal flat.

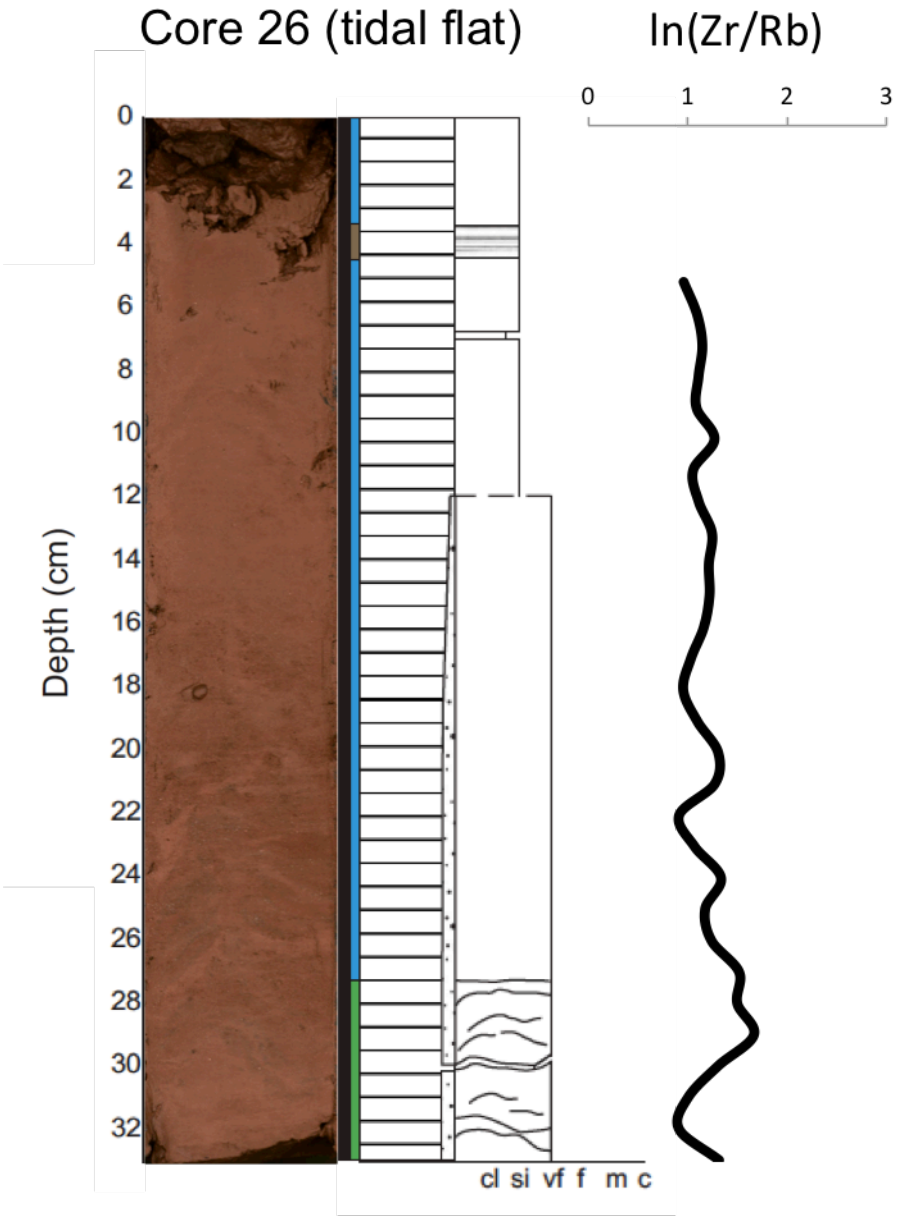

Fig. 45 Composite log of core 26 obtained from the tidal flat.

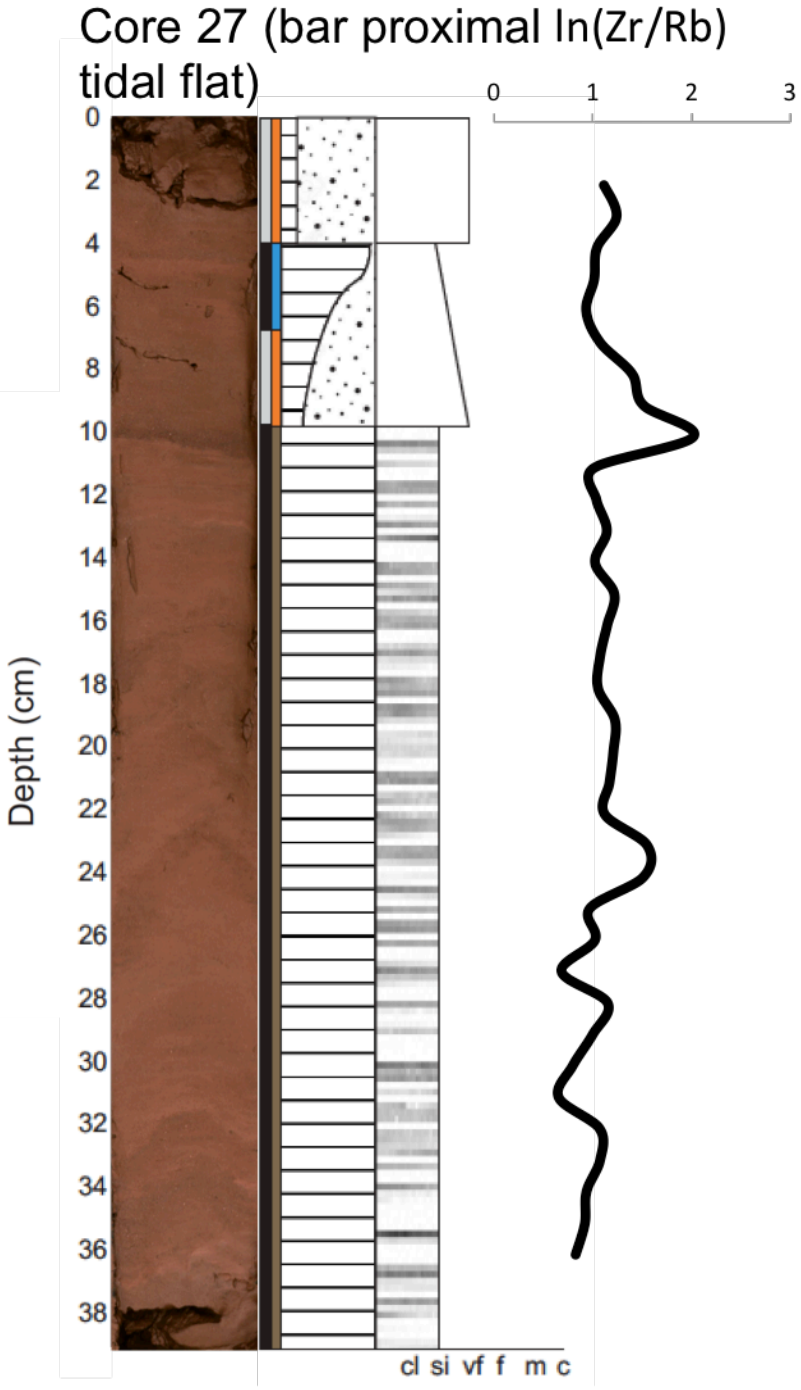

Fig. 46 Composite log of core 27 obtained from a tidal flat close to a point bar.

7. ^{210}Pb and ^{137}Cs dating

Results

The data which makes the basis for the ^{137}Cs and excess ^{210}Pb graphs is found in Appendix A. ^{137}Cs in the point bar core 20 is present though the whole core which is 20 cm long (Fig. 47). In the point bar proximal core 24, ^{137}Cs is not present at all (Fig. 47). The top 5 cm of core 24 was destroyed during opening of the core, so it is not known if ^{137}Cs is present in the top 5 cm. In tidal flat core 26, ^{137}Cs is only present in the upper 25,5 cm (Fig. 47), and in the tidal flat core 2, ^{137}Cs is only present in the upper 6 cm (Fig. 47).

None of the profiles show a regular decrease in excess ^{210}Pb with depth (Fig. 48). Core 20 has excess ^{210}Pb present in the whole core, which is 20 cm long (Fig. 48). Core 24 has excess ^{210}Pb present in 31 upper cm (Fig. 48). Core 26 has excess ^{210}Pb present in 26 upper cm (Fig. 48). Core 2 has excess ^{210}Pb present in the upper 36 cm (Fig. 48).

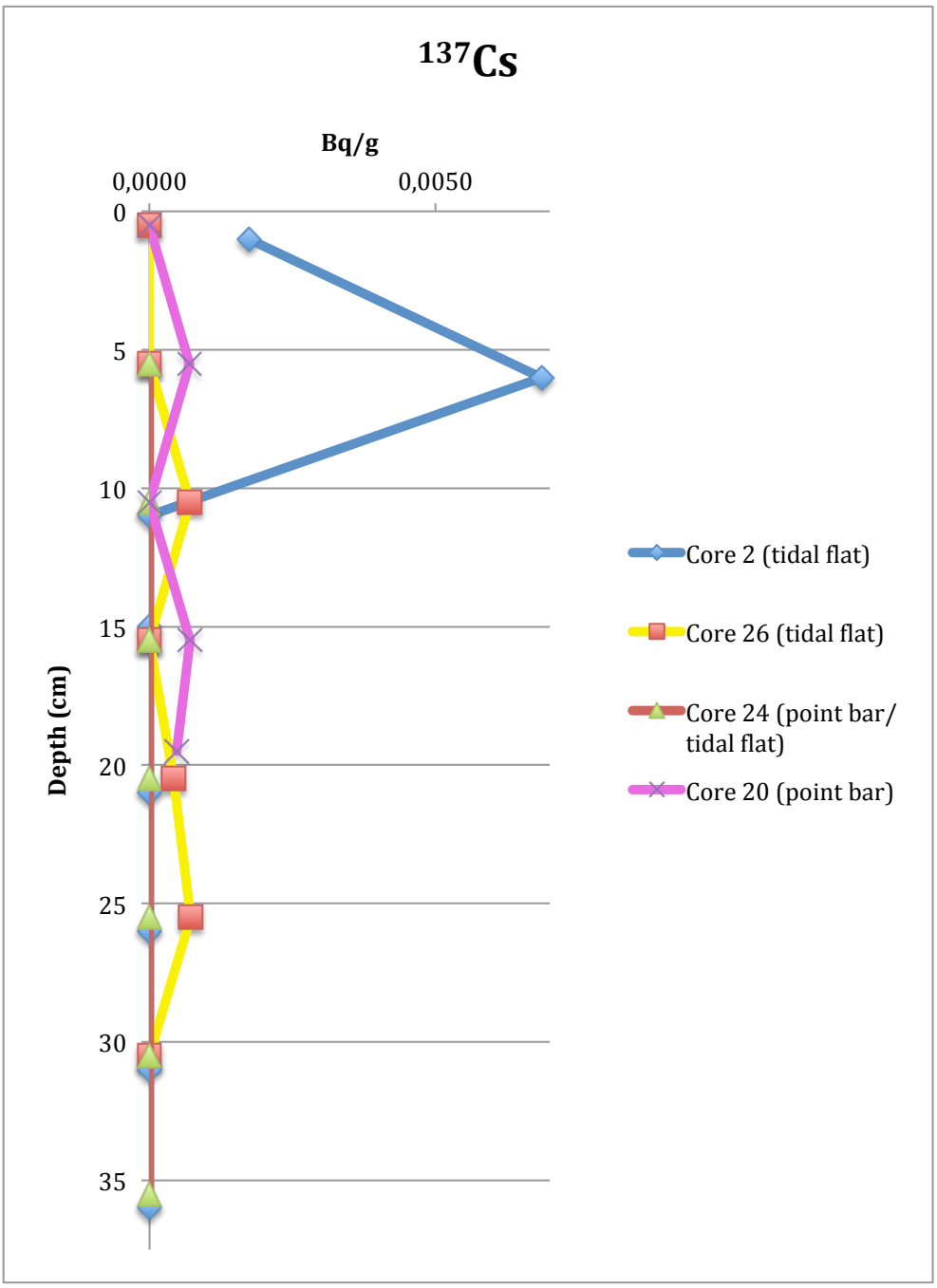

Fig. 47 Graph shows ^{137}Cs measurements of core 2, 26, 24 and 20.

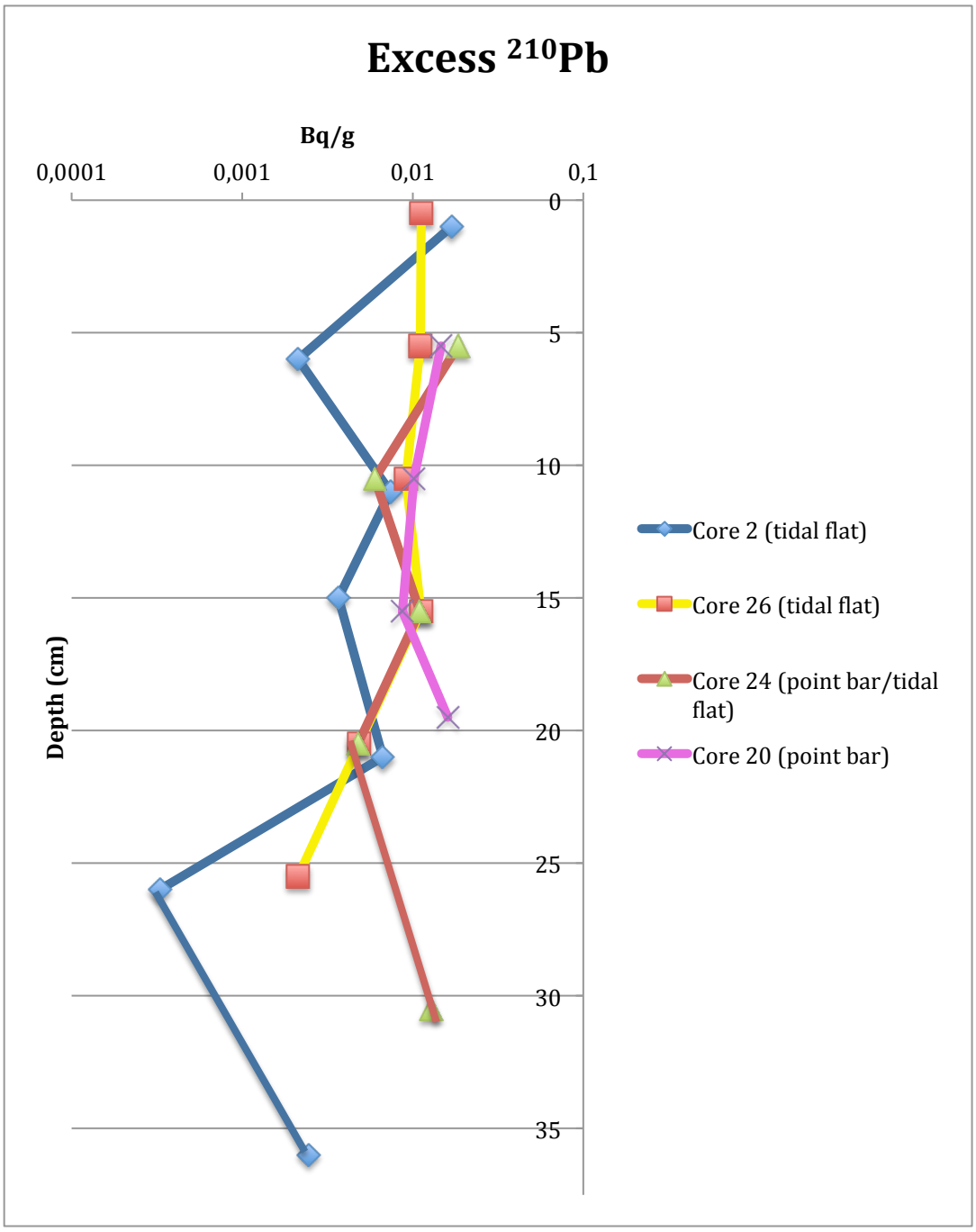

Fig. 48 Graph shows excess ^{210}Pb measurements of core 2, 26, 24 and 20.

Interpretation

The calculations for the ^{137}Cs and excess ^{210}Pb sediment accumulation rate are found in Appendix B. The ^{137}Cs content in the core 20 indicate that the sediment accumulation rate since 1952 has been 0,3 cm/year or more. Due to the missing uppermost 5 cm of core 24, it is not possible to say whether these sediments where deposited before of after 1952. The ^{137}Cs content in core 26 indicate that the sediment accumulation rate since 1952 has been 0,4 cm/year or lower. The ^{137}Cs content of core 2 indicates that the sediment accumulation rate since 1952 has been 0,1 cm/year or lower. This provides an average sediment accumulation rate of around 0,3 cm/year since 1952.

The tidal flat core 26 is placed further out on the delta than tidal flat core 2, and it is therefor expected that the accumulation rate in core 26 is higher than core 2. The outermost part of the fjord-head delta is inundated by the high tides during longer periods than a more land-proximal position, providing more time for sediments to deposit.

The non-regular decline in excess ^{210}Pb through the cores suggests a non-steady accumulation, which is to be expected on tidal flats and tidal bars. The excess ^{210}Pb found in core 20 indicates that the sediment accumulation rate the last century has been maximum 0,2 cm/year. The excess ^{210}Pb found in core 24 indicate that the accumulation rate the last century was 0,3 cm/year or more. The excess ^{210}Pb found in core 26 indicate that the minimum accumulation rate the last century have been 0,3 cm/year. The excess ^{210}Pb found in core 2 indicates that the accumulation rate have been higher than 0,4 cm/year. In average the sediment accumulation rate was around 0,3 cm/year during the last century.

8. Geomorphological map

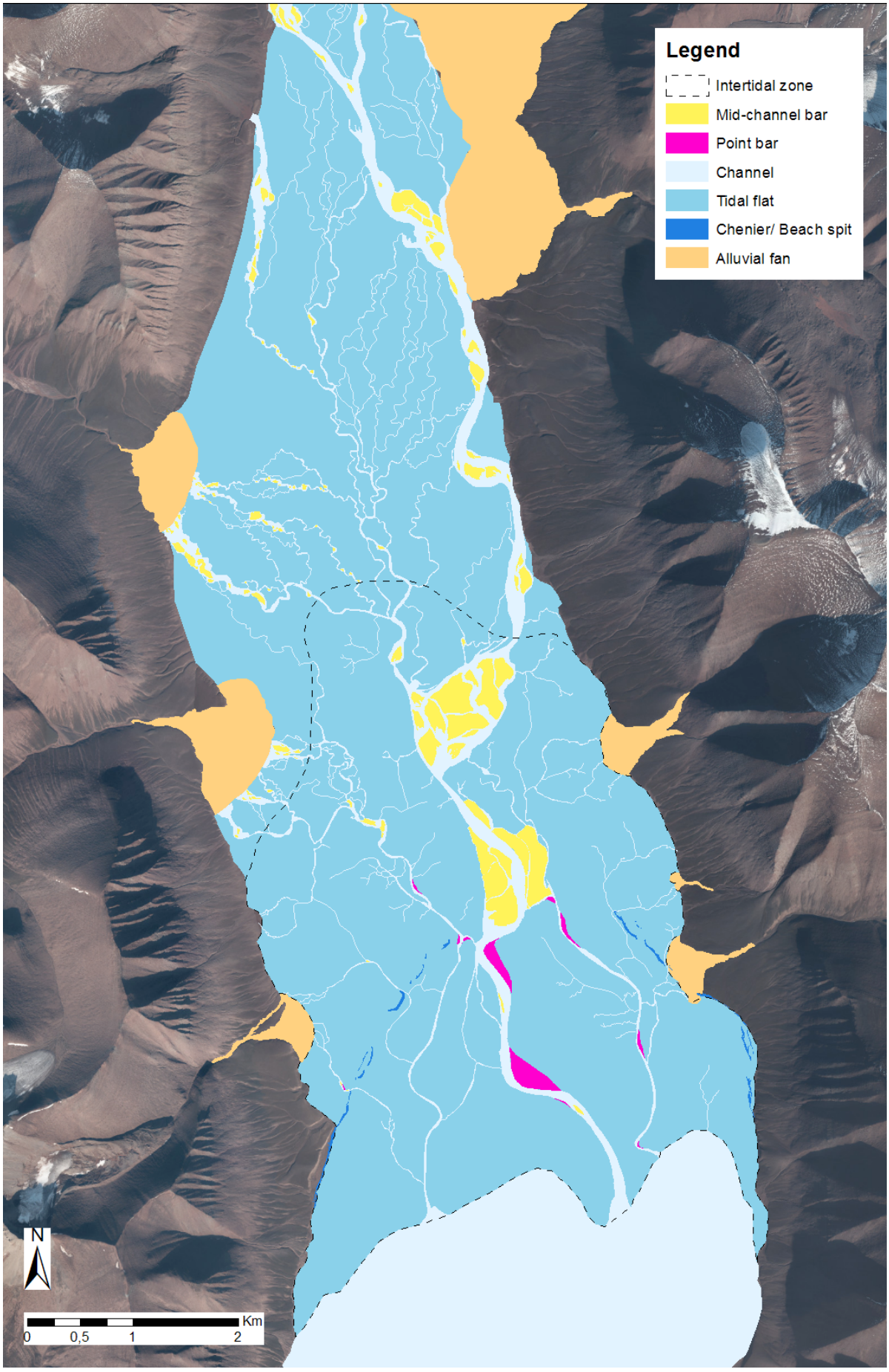

Fig. 49 Geomorphological map of the fjord-head delta in Dicksonfjorden in a scale of 1:40 000.

9. Landforms and surface features

Landforms such as tidal flats, tidal channel, tidal bars and cheniers (beach spits) on the fjord-head delta in Dicksonfjorden have been mapped (Fig. 49), described and interpreted. Surface features that were observed during fieldwork that are not included into the geomorphological map are rill channels, circular depressions, desiccation cracks, animal tracks, kelp with pebbles attached, current ripples and salt flats.

9.1 Tidal flats

Description

Tidal flats, active and non-active constitute the majority of the delta in Dicksonfjorden. The active tidal flats are the tidal flats lying in the intertidal zone (Fig. 50). Non-active tidal flat are formerly active tidal flat, which are not lying in the supratidal zone, out of reach from the highest tides.

Heterolithic mud and sand (facies D), heterolithic clay and silt (facies E), structureless mud (facies F) and deformed mud (facies G) are commonly found within the tidal flat deposits. Current ripple cross-laminated mud (facies B) is sometimes present. The tidal flat deposits are generally fining moving away from the tidal channels. This trend is seen in core transect 1 (core 1-10) (Fig. 18). The amount of very fine and fine sand is decreasing, and in the channel proximal cores, only silt and clay is present. Heterolithic mud and sand (facies D) is therefor not present in the most channel proximal cores (Fig. 18). Both channel proximal and channel distal tidal flat deposits include deformed mud (facies G).

The geochemical element ratio ln(Zr/Br) obtained from the XRF core scanner data shows grain-size changes in the cores (Fig. 20-46). The grain-size is especially useful in regards to detecting grain-size variations in facies only or mostly consisting of mud; E (laminated mud), G (deformed mud) and F (structureless mud). The grain-size proxy makes it easier to detect silty layers and lamina in clayey sediment and clayed layers and lamina in silty sediments. Variations in these fine-grained sediments were difficult to detect only with visual and hands-on observations during the sedimentological logging.

Fig. 50 Tidal flat deposits with desiccation cracks. The tidal flat is getting flooded during rising tide. Person for

Interpretation

The tidal flat deposits are deposited when the tidal flat is flooded during flood, slack and ebb stages of the tidal cycle. They are commonly heterolithic due to the varying capability of the tidal current to transport and deposit sediment. Clay and silt is deposited mainly from suspension during high slack tide condition, and the sand sized fraction is deposited during higher tidal current speeds, during rising and falling tides (Davies 2012). Rapid deposition might occur at times and form units of structureless mud (Collingson and Thompson 1987). Destruction and deformation of original laminations occurs through liquefaction of water-laden sediment and shore ice pushing and scouring (Dionne 1988, 1997, 2011; Dashtgard *et al.* 2014). Some deformation of the sediments might also be due to the coring technic. It is likely that the soft sediment deformation caused by liquefaction is restricted to the channel-proximal areas of the tidal flat, where sediments are more saturated in water. Channel-distal areas of the tidal flat are generally quite dry and firm. Because of this, deformational structures found here are most likely linked to deformation by shore ice during the break up of the shore ice in early summer.

The fining of the sediment, moving away from tidal channel can be explained by a decrease of the tidal current speed due to friction against the tidal flat bed (Dalrymple and Choi 2007). Dalrymple (1992, 2010) states that tidal flats show a general pattern along a transect from the supratidal, through the intertidal and to the subtidal zone going from salt marches, mud flats, mixed sand-mud flats to sand flats. The salt marches were observed during fieldwork in the transition between the supratidal and the intertidal zone. The channel proximal tidal flat deposits are mixed sand-mud flats, while

the land proximal deposits are mud flats. Sandy deposits are confined to the point bars and mid-channel bars, and sand flats are therefor not well developed. This is not in good correspondence to the facies model by Dalrymple (1992), which described well-developed sand flat part of the tidal flats. In Dicksonfjorden, the sediment source is mainly comes from a glaciofluvial rivers system, and this in combination with the bedrock found in the catchment area likely hold the explanation for why the deposits in the Dicksonfjorden delta are especially muddy. Core transect 2 is placed more or less parallel to the channel, and is therefor probably placed inside the mixed sand-mud flat part of the tidal flat. Transect 2 can therefor not be expected to show any clear trend in s sand decrease, as transect 1 does.

9.2 Tidal channels

Description

The width of the tidal channels varies from less than a meter to more than 100 meters (at low tide) (Fig. 51). The maximum depth of the deepest channels is at least 1 meter at low tide. The width of the channel varies enormously with the tidal cycle. Moving from low tide to high tide, the smaller channels merge into larger channels, which at some points merge and flood large parts of the fjord-head delta, covering more than 1 kilometre. From the aerial image from 2011 (Fig. 7 A), which is taken around low tide, the widest channels are about 140 m wide. In some shallow and small channels, a lag of gravel was observed at the channel base (Fig. 52). If lags gravely lags exists in the base of larger and deeper channels is unknown, since it was not possible to access these areas. From the aerial photo from 2011 (Fig. 49), it is also possible to see that the channels widen seaward in to the classic “trumpet” shape typical for tidal channels (Dalrymple 1992, 2010). The large channels close to the fjord are meandering, while the smaller channels further landward are braided.

Fig. 51 Large channel during low tide. A cut bank (left side of channel) and a point bar (left side of channel) are visible. Persons for scale.

Fig. 52 Coarse channel lag in the base of a small channel relatively close an alluvial fan. Shovel for scale.

Interpretation
The gravely lag on the channel base forms due to the high shear stresses occurring here (Dalrymple 1992, 2010). The presence of both braided and meandering channels indicates that the Dicksonelva river system is a combination of these two types of river systems. Braided rivers tend to occur at steeper gradients than meandering rivers (Nichols 2009), and this is a likely cause of why the river system evolves into a more meandering style before entering the fjord, where the gradient of the tidal flat naturally is the smallest. Another reason might that the most seaward part of the channel system gets shaped by tidal currents, while the landward part does not (Dalrymple 1992, 2010).

9.3 Tidal bars

Description
Point bars (Fig. 53) and mid-channel bars (Fig. 54) were observed in the tidal channels. The point bars are generally found in the lower most part of the fjord-head delta, while the mid-channel bars is found closer to land. All of the tidal bars observed were covered in current ripples. The sediment in the tidal bars was saturated in water and acted like quicksand when put force on.

Current ripple cross-laminated sand (facies A) and structureless sand (facies C) are commonly found within tidal bar deposits. Tidal bar deposits proximal to the tidal flat deposits, on the transition to tidal flat deposits, consist of an interfingering of both sedimentary deposits.

Fig. 53 Point bar (location of core 24) with 3D current ripples formed by a current moving seaward. Shovel for scale.

Fig. 54 Mid-channel bar (location of core 22) with 3D current ripples formed by a seaward moving current. The cut bank is visible on the other side of the tidal channel. Shovel for scale.

Interpretation

The tidal bars form at places in the tidal channels where the tidal current decreases enough to deposit sand and mud (Nichols 2009). The water-saturated sediment found in tidal bars makes it likely that deformation through liquefaction occurs here. The presence of point bar and mid-channel bar gives an indication of that the Dicksonelva river system exhibits features from both braided and meandering river systems.

A variety of cross-lamination in sand, and the presences of structureless sand indicate that the tidal bar deposits are transported and deposited by relatively high current speeds. Climbing current ripple cross-laminated sand found in facies A and structureless sand (facies C) indicates rapid deposition from a heavy sediment-laden current (Collins *et al.* 2006; Collingson and Thompson 1987). Sinuous ripples, reactivation surface and structureless sand imply variable flow conditions, which is expected due to tidal action (Dalrymple 1992, 2010; Collingson and Thompson 1987). Soft sediment deformation expressed as lenses and undulating boundaries can be due to liquefaction and shore ice pushing and souring (Dionne 1988, 1997, 2011 and Dashtgard *et al.* 2014). The absence of cross-laminations in the structureless sand (facies C) might also be due to liquefaction and/or ice pushing and souring, destroying the original structures (Dionne 1988, 1997, 2011).

9.4 Rill channels

Description

Rill channels ranging from a few cm to tens of meters in length and a few cm to around 40 cm in depth were observed on the tidal flat (Fig. 55). They have a dendritic pattern spreading toward the tidal flat from tidal channels. Where desiccation cracks are present on the tidal flat, the “fingers” of the rill channels connect with desiccation cracks.

Fig. 55 Large rill channel on the tidal flat connected to a large tidal channel. Person for scale.

Interpretation
After the tidal flat is flooded and ebb starts, the sea and river water runs back into the fjord through the tidal channels (Das 2017). It does this by finding weak zones in the tidal flat (desiccation cracks e.g.) and erodes a channel into the tidal flat through backwasting. The dendritic pattern of the rill channels is the result of large areas of the tidal flat draining though one point, which becomes the main "trunk" of the rill channel.

This implies that the distribution of rill channels on the delta could be used to determine the area that is flooded during spring high tide, maybe also high tide during the equinoxes. The intertidal zone on the geomorphological map (Fig. 49) was drawn on basis of this assumption.

9.5 Cheniers

Description
Several cheniers were observed on the tidal flat (Fig. 56). They consist mainly of pebble and cobble sized sediment, only a little sand. The cheniers are typically made up by several ridges, some parallel to each other. Kelp, shells and driftwood were found both on the seaward and the landward side of the cheniers. Some small plants and moss where found growing on top of the coarse sediment. The maximum height of the cheniers measured where 90 cm, while their length are normally several hundred meters. The cheniers are usually wider than 30 meter. From the geomorphological map (Fig. 49) is it possible to see that the cheniers together make up a horseshoe shape on the delta, with the arc pointing towards land.

Fig. 56 Chenier with logs lying parallel to the landform. Yellow measuring stick (1,5 m) for scale.

Interpretation
Due to the beach like features, such as the parallel ridges and driftwood, it is natural to believe they are formed by wave action. If this is the case, they represent the landward limit on which waves can affect the delta.

9.6 Circular depressions

Description
Circular depressions ranging from a few tens of cm to more than one meter in diameter was observed on large parts of the tidal flat (Fig. 57 and 58). The depressions were sometimes filled with rain and/or seawater. Elevated ridges of a few cm were often surrounding the depressions. Plant remains, pebbles and flocculated mud was normally lying on top of these elevated ridges, while the sediment in the depressions mainly consisted of mud.

Fig. 57 Circular depressions with elevated ridges on the tidal flat. White plastic tube (about 40 cm long) shows coring location of core 18. The depressions are filled with rain and/or seawater.

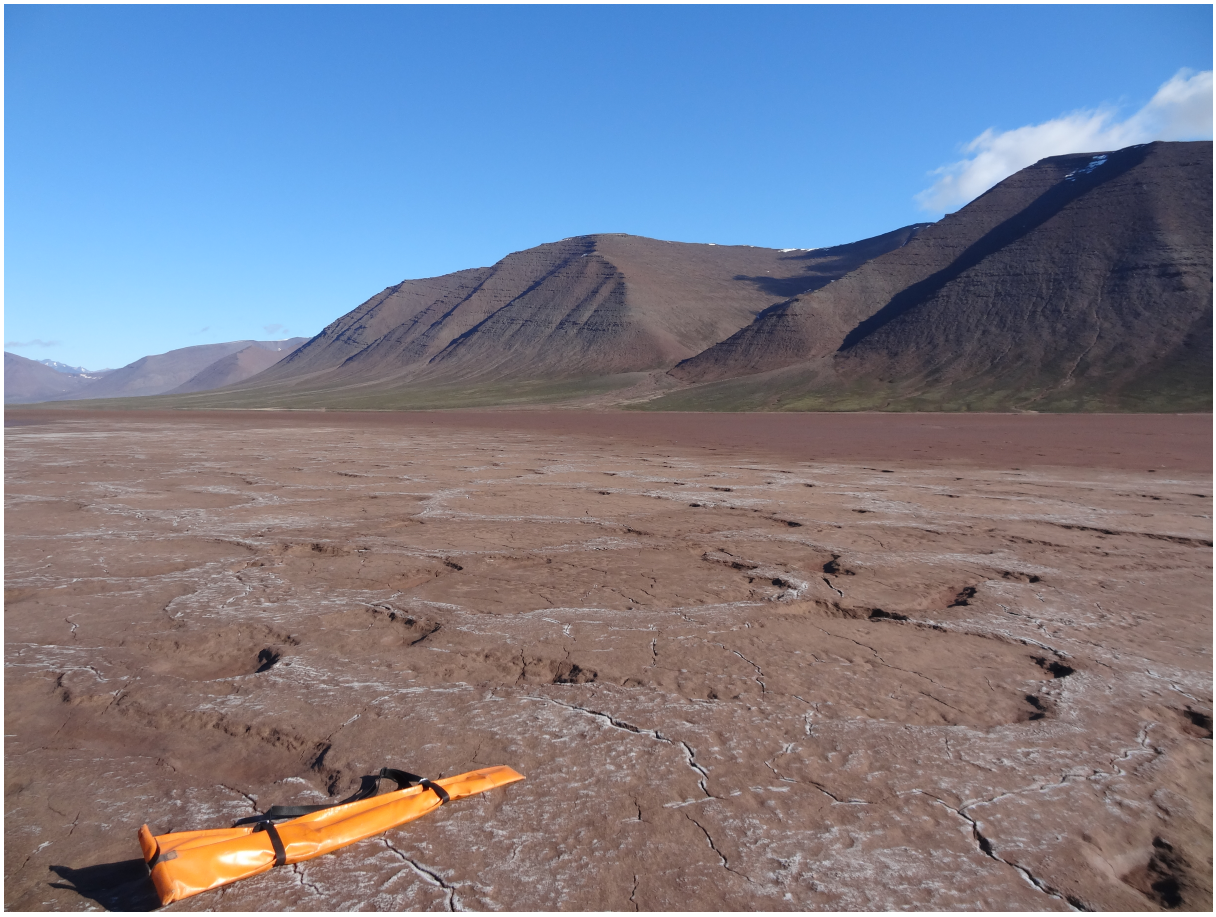

Fig. 58 Circular depressions without elevated ridges on the tidal flat. Salt flats are developing on the tidal flat. Rifle for scale.

Interpretation
Circular depressions that occur on tidal flat are believed to have formed through erosion, scouring and/or deformation by ice cakes (Dionne 1988, 1997). When the shore ice breaks up into ice cakes due to waves and tidal currents, sediments frozen underneath the ice cakes are being transported away with the ice cakes (Dionne 1988). Elevated ridges around the depressions form by scouring and deformation from ice cakes as waves and tides are exerting force on the ice cakes (Dionne 1997). The circular depressions circular depression without a ridge (Fig. 58) is therefor interpreted as a pure erosion and deformation or purely deformation. The erosion and deformation by shore ice is believed to have great impact on the tidal flat deposits on the delta.

9.7 Animal tracks

Description
A variety of animal tracks were observed on the tidal flat on the delta during fieldwork (Fig. 59, 60 and 61).

Fig. 59 Stomach- and claw marks from seals on the tidal flat next to a channel. Pencil for scale.

Fig. 60 Tracks from foxes on the tidal flat. Tracks are a few cm in diameter.

Fig. 61 Polar bear track on the tidal flat. The track is tens of cm wide.

Interpretation
The tracks are interpreted to originate from seals, foxes, birds and polar bears. The tracks might be preserved in the geological record, if the conditions are right (Hallam 1975). Liquefaction of the sediment can occur due to the pressure the various animals exert on the sediments (Nichols 2009).

9.8 Desiccation cracks

Description
A polygonal pattern of desiccation cracks where observed on large areas of the tidal flat (Fig. 62). They where not found on areas close to the channels and the most fjord-ward part of the fjord-head delta.

Fig. 62 Desiccation cracks on the tidal flat on the Dicksonfjorden fjord-head delta.

Interpretation
Desiccation cracks form in clay rich sediment and indicates alternating dry and wet conditions, typical for tidal flats (Davies 2012).

9.9 Current ripples

Description
2D and 3D current ripples were observed mainly on bars (Fig. 53 and 54), but also on the base of shallow channels and on the tidal flat (Fig. 63 and 64). The direction of ripple migration was always seaward or channel-ward. The ripple height varies from millimetres to several centimetres.

Fig. 63 3D, Sinuous crested and isolated current ripples of mud and very fine sand formed by a seaward current (ebb-flow). The diameter of the largest ripples is about 10 cm, while the height is a few cm.

Fig. 64 Small 3D, interference (two currents) ripples in mud. Pen for scale.

Interpretation
The current ripples require moderate flow velocities over a hydrologically smooth bed (Nichols 2012). The current ripples found on the tidal flat have been formed during ebb tide, when the tidal current and river current is both moving in a seaward direction.

9.10 Kelp

Description
Kelp was frequently observed on the tidal flat. Some of the kelp had pebbles attached (Fig. 65).

Fig. 65 Kelp with a pebble attached lying on the tidal flat. Pencil for scale.

Interpretation
Kelp is brought in on the delta by tidal currents and wave action (Carling 2014). Pebbles attached to the kelp can be preserved with the deposits in the stratigraphic record. This shows that ice rafting is not the only way for coarse-grained sediments to end up in fine-grained deposits such as marine sediments and tidal flat deposits.

9.11 Salt flats

Description

Very thin were observed on the tidal flat in periods of relatively warm and dry weather condition (Fig. 66). After a single rain event they were completely gone. The thickness of the salt flats where only a few mm at the most.

Fig. 66 Salt flat on the tidal flat. Persons for scale.

Interpretation

The salt flats form by evaporation of seawater during flooding of the tidal flat (McMacin and Godwin 2017). Due to the thickness of the salt flat, they will most likely not be preserved in the stratigraphic record.

9.12 Grain-size trends on the delta

Description

The mean grain-size of the bulk samples collected from the delta (Fig. 67) show a general trend of increasing mean grain-size moving towards the outskirts of the tidal flat. During fieldwork, it was confirmed through visual observations that the sediments in channels and tidal flats close to the supratidal zone were coarser than the central parts of the fjord-head delta, even sandy and pebbly.

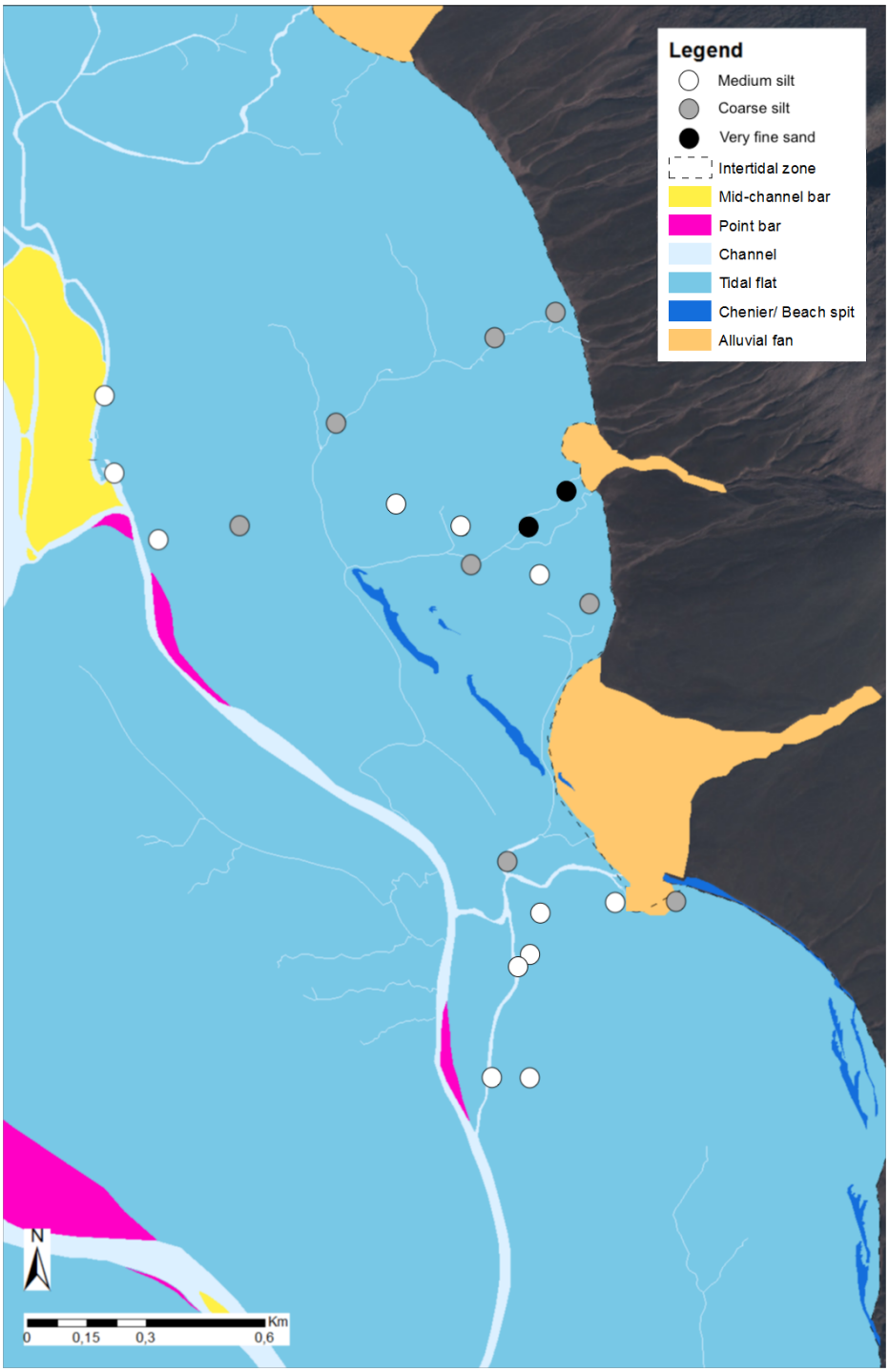

Fig. 67 The map shows the mean grain-size of the bulk samples that was collected from the fjord-head delta.

Interpretation

The trend of increasing mean grain-size moving towards the outskirt of the delta might seem to contradict the observed fining of the tidal flat deposits moving away from the channel. This does not need to be the case. The sandy sediments found on the outskirts of the fjord-head delta, on the transition to the supratidal zone, indicate a sediment input coming from the surrounding mountains, in addition to Dicksonelva. Weathered sediments are likely transported with debris flows, rock falls and/or fluvial processes down the slope of the mountains and in this way contribute to the deposition on the

fringes of the fjord-head delta. During high tide, the relatively coarse grained sediments are redistributed and some of it is transported in rill channels and tidal channels out on the delta in tidal bars and out into the subtidal part of the delta (e.g. delta slope). Because of this, the delta does not show good correspondence to the previously published facies model by Dalrymple (1992).

10. Deposits and processes dominating the delta

10.1 Tidal influence

The deposits on the fjord-head delta in Dicksonfjorden show sedimentological indicators of tidal influence in the form of heterolithic horizontal laminations in tidal flat deposits, which reflect the changing tidal current speeds through the tidal cycles (Davies 2012). A spectrum of bedforms, reactivation surfaces and desiccation cracks together also serve as a strong indicator of tidal influence. This is in good correspondence to the general perception of deposits from tidal systems described by Davies (2012) among others. The position of the delta at the innermost part of a large fjord makes it sheltered from extensive wave action. This allows the relatively small tidal range in the area to be sufficient for influencing the deposits and to form tidal flats on the delta.

10.2 Shore ice influence

Erosion and deformation by shore ice has been documented by the presence of circular depressions on the surface of the tidal flat and deformational structures in tidal flat- and tidal bar deposits. It is therefor clear that there is a substantial influence of shore ice on the delta. The shore ice is likely also serving as a protection from wave action during the winter (Dionne 1988, 1997) (Fig. 68). This is in good correspondence to the few previously published studies from cold region tidal systems, such as the ones by Dionne (1988, 1997). It is starting to become clear that deposits in cold region tidal systems differ considerable from deposits in warm and temperate regions. Knowledge about the deformational structures formed by shore ice can in the future be integrated into a generalized facies model for cold region tidal systems, which can be a useful tool for interpreting environmental and climatic conditions in which ancient sediments may have been deposited.

Fig. 68 The fjord-delta in Dicksonfjorden with a coherent shore ice cover serving as protection from wave action. Picture is taken by Maria Jensen in April 2018.

11. Development of the delta

Description

By comparing an oblique aerial photo from 1938 (Fig. 69) with the on the aerial photos from 2011 (Fig. 7 A) that was used to produce the geomorphological map and a photo taken of the delta during fieldwork in 2017 (Fig. 70), it possible to see that the location of major channels have remained in approximately the same place. Also, it is possible to see the cheniers on the right side of the delta (looking N) have water surrounding them.

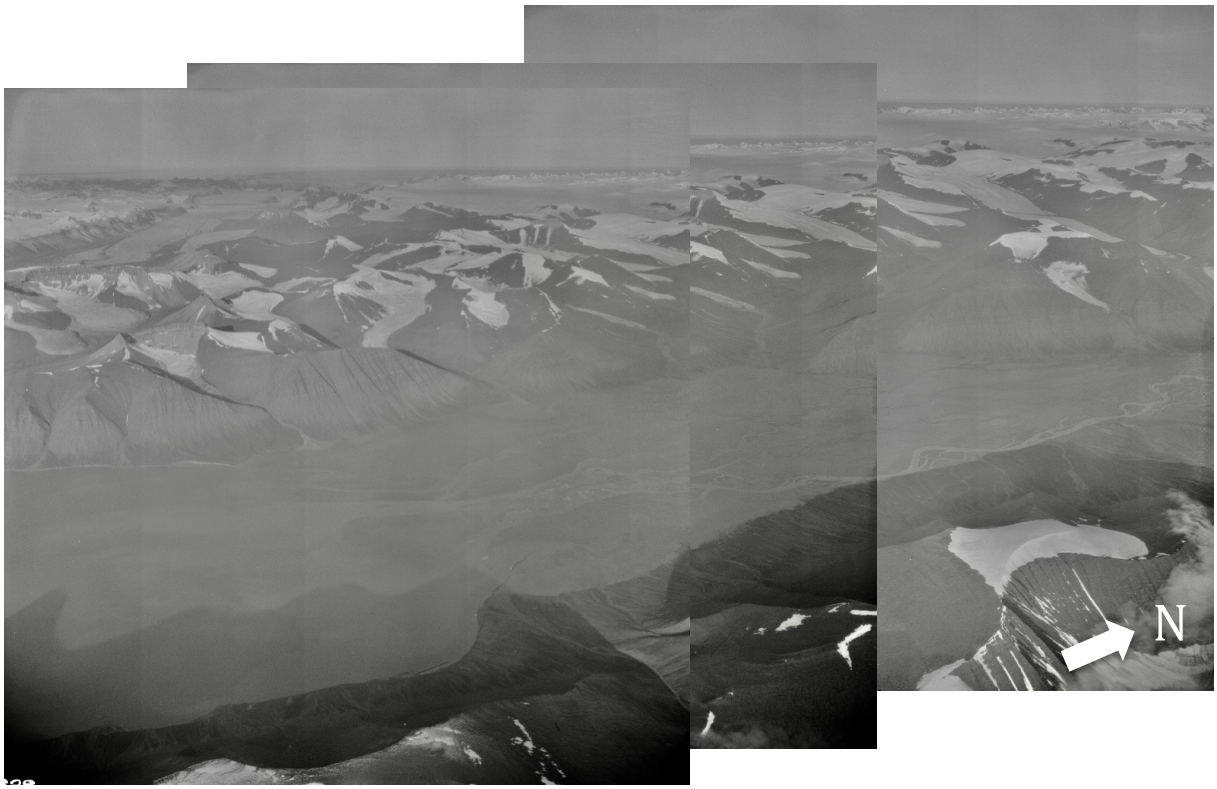

Fig. 69 Oblique aerial photos from summer 1938 showing the delta in Dicksonfjorden during relatively high tide. Source: Norwegian Polar Institute (NPI).

Fig. 70 The fjord-head delta in Dicksonfjorden during relatively low tide on the 2nd of August 2017. The picture is taken from Fiskefjellet Mountain by Astrid Fuglseth Rasmussen.

Discussion

After the tidewater glacier occupying Dicksonfjorden became land based, the delta started prograding into the fjord, probably on top of subglacial sediments. Due to the relative sea-level fall that took place after the last glaciation (Forman *et al.* 2004), the delta prograded into the fjord by forced regression. Indications are strong that the relative sea level in central, west Spitsbergen is still falling (Norwegian Polar Institute 2018). In this case, the delta is still building out into the fjord by forced regression.

As the delta is prograding into the fjord it leaves landward tidal flat areas out of reach from the high tide, making these tidal flat areas supratidal and inactive. As a forced regressive deposit, the delta is likely experiencing fluvial downcutting causing "cannibalization" of the deposits. Older deposits are likely being removed by fluvial erosion and deposited further out on the delta (Posamentier and Morris 2000). It is only the seaward part of the delta that is intertidal (Fig. 49) and that has got active tidal sedimentation on the tidal flats.

The larges similarities the channel system in 1938 and today indicate that the system is relatively stable. Due to the cohesive properties of clay, the sediment is firm and difficult to erode, which might make it difficult for the channels to move laterally.

Since it is not know at what date and time the oblique aerial images from 1938 was taken, it is not possible to determine exactly how high the tides were when the photo was taken. Although, since the cheniers seems to be surrounded by water, it means that the tide most likely was relatively high. The aerial image from 2011 is in contrast taken at low tide, since no water is surrounding the cheniers. This makes it difficult to estimate how much the delta has prograded into the fjord since 1938.

12. Summary and conclusions

- Land forms such as tidal flats, tidal channel, tidal bars, rill channels and cheniers (beach spits) are identified.

- 7 facies are identified which either belong to tidal flat deposits or tidal bar deposits.

- The tidal flat deposits generally consist of muddy laminations, sometimes also sandy laminations, which indicate mainly deposition from suspension during high tide. Deformational structures are very common and are likely caused by deformation by shore ice and liquefaction.

- The tidal bar deposits generally consist of very fine and fine sand, sometimes a little mud. Cross-laminated and structureless sand is present, indicating rapid deposition from a relatively strong heavy sediment-laden current. Deformation structures are present and might be caused by liquefaction or deformation from shore ice.

- Heterolithic horizontal laminations, bedforms, reactivation surfaces and desiccation cracks together serve as a strong indicator of tidal influence in the delta deposits.

- The wave-protected setting in which the delta is situated allows a microtidal range to be sufficient for influencing the delta deposits considerably and forming tidal flats.

- Tidal flat deposits transition from mud flat to mixed sand-mud flats moving in a channel-ward direction, indicating a decrease of tidal current speed due to friction against the tidal flat.

- The ^{210}Pb and ^{137}Cs profiles indicate non-steady deposition in the intertidal zone and that the sediment accumulation rate on average has been around 0,3 cm/year during the last century.

- Circular depressions on the tidal flat and deformational structures in cores indicate that scouring and deformation by shore ice is influencing the tidal flat deposits greatly.

- Rill channels develop on tidal flats due to erosion by ebb tide and their distribution can therefor be used to determine the approximate boundary between the intertidal and supratidal zone.

- Grain-sizes increasing towards the outskirts of the delta indicate a sediment input coming from the surrounding mountains, in addition to Dicksonelva.

- Because of the grain size increase towards the outskirts of the delta and the lack of sand flat deposits in the channel proximal areas of the tidal flats, the previously

published facies model from Dalrymple (1992) does not show a good correlation with the delta.

- An aerial photo from 1938 reveals that major tidal channels on the fjord head delta is located at the approximately same positions as today, indicating that the channel system is quite stable. This is probably linked to the cohesive properties of the muddy tidal flat deposits.

- Due to relative sea level fall that have occurred since the last glaciation, the delta represents a forced regressive deposit.

- The forced regression causes the landward and supratidal part of the delta to slowly increase. Fluvial downcutting and transport of older deposits out on the delta front and slope is likely to be occurring.

12. Suggestions for further studies

- Bathymetric data revealing the subtidal parts of the delta in Dicksonfjorden have been obtained in "Sediment flux from source to sink – the coastal link" project. These data can be used in combination with the aerial photos to create a more comprehensive geomorphological map of the fjord-head delta.

- This study provides insight into the deposits and processes on the tide-influenced fjord-head delta in Dicksonfjorden. More studies of tidal flats in other areas of Svalbard and the Arctic are required to create a generalized facies model for this type of sedimentary environment.

13. References

A guidebook to particle size analysis (n.d.) Horiba Scientific. URL: https://www.horiba.com/fileadmin/uploads/Scientific/eMag/PSA/Guidebook/pdf/PSA_Guidebook.pdf

Ahlborn M, Stemmerik L (2015) Depositional evolution of the Upper Carboniferous – Lower Permian Wordiekammen carbonate platform, Nordfjorden High, central Spitsbergen, Arctic Norway. Norwegian Journal of Geology 95: 91-126

Aplin AC, Macquaker JH (2011) Mudstone diversity: Origin and implications for source, seal, and reservoir properties in petroleum systems. AAPG bulletin 95: 2031-2059

Baas JH (1994) A flume study of the development and equilibrium morphology of small-scale bedforms in very fine sand. Sedimentology 46: 123-209

Baker VR, Kochel RC, Patton PC, Pickup G (1983) Palaeohydrologic analysis of Holocene flood slackwater sediments. (Spec. Publ.) Int Assoc Sedimentol 6: 229–239

Bierman PR, Montgormery DR (2014) Key Concepts in Geomorphology. New York: W.H Freeman

Boggs S (2011) Principles of sedimentology and stratigraphy, Fifth Edition. Pearson Prentice Hall, pp 585

Blomeier D, Wisshak M, Dallmann W (2003). Facies analysis of the old Red Sandstone of Spitsbergen (Wood Bay Formation): Reconstruction of the depositional environment and implications of basin development. Springer-Verlag 49: 151-174

Boròwka M (1989) The development and relief of the Petuniabukta tidal flat. Central Spitsbergen. Polish Polar Research 379 – 384

Boyd R, Dalrymple RW, Zaitlin BA (1992) Classification of clastic coastal depositional environments. Sedimentary geology, pp 139-150

Carling P (2014) The role of attached kelp (seaweed) in lowering threshold of coarse gravel entrainment in tidal flows. Marine Geology 357

Chen J, Chen Y, Liu L, Ji J, Balsam W, Sun Y, Lu H (2006) Zr/Rb ratio in Chinese loess sequences and its implications for changes in the East Asian winter monsoon strength. Geochim Cosmochim Acta 70: 1471–1482

Choi KS (2010) Rhythmic climbing-ripple cross-lamination in inclined heterolithic stratification (IHS) of a macrotidal estuarine channel, Gomso Bay, west coast of Korea: Journal of Sedimentary Research 80: 550–561

Choi KS, Hong CM, Kim MH, OH CR, Jung JH (2013) Morphologic evolution of macrotidal estuarine channel in Gomso Bay, west coast of Korea: implication for the architectural development of inclined heterolithic stratification. Marine Geology 346: 343–354

Choi KS, Jo JH (2015) Morphodynamic of Tidal Channels on the Open Macrotidal Flat, Southern Ganghwa Island in Gyeonggi Bay, West Coast of Korea. Journal of Sedimenatry Research 85: 582-595

Collinson JD, Thompson DB (1987) Sedimentary structures. Second edition. Chapman & Hall, pp 104

Collinson J, Mountney N, Thompson D (2006). Sedimentary Structures. Third edition. Terra Publishing, pp 292

Christiansen HH, Etzelmüller B, Isaksen K, Juliussen H, Farbrot H, Humlum O, Johansson M, Ingeman-Nielsen T, Kristensen L, Hjort J, Holmlund P, Sannel ABK, Sigsgaard C, Åkerman HJ, Foged N, Blikra LH, Pernosky MA, Ødegård RS (2010) The thermal state of permafrost in the nordic area during the international polar year 2007–2009. Permafr. Periglac. Process. 21: 156–181

Croudace IW, Rothwell RG (ed.) (2015) MicroXRF Studies of Sediment Cores, Development in Paleoenvironmental Researce É Springer Science 17

Dallmann WK (ed.) (2015) Geoscience Atlas of Svalbard. Norwegian Polar Institute Report Series 148

Dalrymple RW (1992) Tidal depositional systems. In: Walker RG, James NP (ed.) Facies Models: Response to Sea Level Change. Geological Association of Canada, St. John's, pp 195-218

Dalrymple RW (2010) Tidal depositional systems. In: James NP, Dalrymple RW (ed.) Facies Models 4. Geological Association of Canada, St. John's, pp 201-231

Das GK (2017) Sedimentary structures. In: Das GK (ed.) Tidal Sedimentation of the Sunderban`s Thakuran Basin. Springer, pp 111-112

Dashtgard SE, Pearson NJ, Gingras MK (2014) Sedimentology, ichnology, ecology and anthropogenic modification of muddy tidal flats in a cold-temperature environment: Chignecto Bay, Canada. In: Martini IP, Wanless HR (ed.) Sedimentary Coastal Zones from High to Low Latitudes: Similarities and Differences. Geological Society, London, Special Publications, pp 229-245

Dionne JD (1988) Characteristic features of modern tidal flats in cold regions. In: de Boer PL et al. (ed.) Tide-influenced environments and facies. Reidel Publishing Company, pp 301-332

Dionne JD (1997) Sedimentary structures made by shore ice in muddy tidal-flat deposits, St. Lawrence estuary, Québec. Sedimentary Geology 116: 261-274

Dionne (1969) Action of shore ice on the tidal flats of the St. Lawrence Estuary. Maritime Sediments 4: 113-115

Dionne JD (1971) Polygonal patterns in muddy tidal flats. J. Sediment Petrol 42: 848-851

Dionne JD (1985) Formes, Figures et facieès sèdimentaries glaciels des estrans vaseux des regions friodes. Paleo 51: 414-451

Dionne J (2011) Miniature mud volcanoes and other injection features in the tidal flats, James Bay, Québec. Canadian Journal of Earth Science 13: 422-428

Dougherty AJ, Dickson ME (2012) Sea level and storm control on the evolution of a chenier plain, Firth of Thames, New Zealand. Marine geology 307-310: 58-72

Douglas BC (1991) Global sea level rise. Journal of Geophysical Research Atmospheres 96

Dypvik H, Harris NB (2001) Geochemical facies analysis of finegrained siliciclastics using Th/U, Zr/Rb and (Zr + Rb)/Sr ratios. Chem Geol 181: 131–146

Elverhøi A, Svendsen JI, Solheim A, Andersen ES, Milliman J, Mangerud J, Hooke RL (1995) Late Quaternary Sediment Yield from the High Arctic Svalbard Area. The Journal of Geology 103: 1-17

Eriksen T (2013) Tidal Flat Sedimentation in an Arctic Environment: a Field Study from Braganzavågen. Master thesis, UiO

Fan D (2012) Open-Coast Flats. In: Davis RA, Dalrymple RW (ed.) Principles of Tidal Sedimentology, Edition 1st. Springer, pp 187-229

Flett R (n.d.) Flett Research Radioisotope Services. Retrieved from http://www.flettresearch.ca/Radioisotope.html

Forbes DL, Frobel D (1985) Coastal erosion and sedimentation in the Canadian Beaufort Sea. Current Research, Part B. Geological survey of Canada 85: 69-80

Forman SL (1990) Post-glacial relative sea-level history of northwestern Spitsbergen, Svalbard. GSA Bulletin 102: 1580-1590

Forman SL (2004) A review of postglacial emergence on Svalbard, Franz Josef Land and Novaya Zemlya, northern Eurasia. Quaternary Science Reviews 23: 1391–1434

Forwick M, Vorren TO (2009) Late Weichselian and Holocene sedimentary environments and ice rafting in Isfjorden, Spitsbergen. Palaeo-geography

Forwick M (2013) How to use CRF core scanner data acquired with the Avaatech core scanner at the Department of Geology, University of Tromsø

Hagen JO, Liestøl O, Roland E, Jørngensen T (1993) Glacier atlas of Svalbard and Jan Mayen. Norsk Polarinstitutt 129: 24

Hallam A (1975) Preservation of Trace Fossils. In: Frey RW (ed.) The Study of Trace Fossils. Springer

Hennekam R (2015) High-frequency climate variability in the late Quaternary eastern Mediterranean. Association of Nile discharge and basin overturning circulation dynamics. Utrecht Studies in Earth Science 78

Humlum O, Instanes A, Sollid JL (2003) Permafrost in Svalbard: a review of research history, climate background and engineering challenges. Polar Research 22: 191-215

Humlum O, Christiansen HH, Juliussen H (2007) Avalanched-derived Rock Glaciers in Svalbard. Permafrost and Periglacial Processes 18: 75-88

Humlum O (2002) Modelling late 20th-century precipitation in Nordenskiold Land, Svalbard, by geomorphic means. Norwegian Journal of Geography 56: 96–103

Ingólfsson Ó (2011) Fingerprints of Quaternary glaciations in Svalbard. Geological Society, London, Special Publications 354: 15-31

Ingólfsson Ó, Landvik JY (2013) The Svalbard–Barents Sea ice-sheet – Historical, current and future perspectives. Quaternary Science Reviews 64: 33-60

James NP, Dalrymple RW (ed.) (2010) Facies Models 4. Geological Association of Canada, St. John's

Jensen M, Larsen E, Lysså A, Faucherre S (2014) High Latitide Tidal Environments – Examples from Braganzavågen, Svalbard and their Implications for Facies Models and Stratigraphy. Hedberg Research Conference, Latitudinal Controls on Stratigraphic Models and Sedimentary Concepts, Banff, AB, Canada

Johnson SM, Dashtgard SE (2014) Inclined heterolithic stratification in a mixed tidal–fluvial channel: differentiating tidal versus fluvial controls on sedimentation: Sedimentary Geology 301: 41–53

Jones A, Lewin J, Macklin M (2010) Flood series data for the later Holocene: available approaches, potential and limitations from UK alluvial sediments. Holocene 20: 1123–1135

Kylander M, Ampel L, Wohlfarth B, Veres D (2011) Highresolution Xray fluorescence core scanning analysis of Les Echets (France) sedimentary sequence: new insights from chemical proxies. J Quat Sci 26: 109–117

Landvik JY, Bondevik S, Elverhøi A, Fjeldskaarn W, Manglerud J, Salvigsen O, Siegert MJ, Svendsen J, Vorren TO (1998) The last glacial maximum of Svalbard and the Barents Sea area: ice sheet extent and configuration. Quarternary Science Rewiews Elsevier Science Ltd. 17: 43-75

Landvik JY, Ingólfsson Ó, Mienert J, Lehman SJ, Solheim A, Elverhøi A, Ottesen D (2005). Rethinking Late Weichselian ice-sheet dynamics in coastal NW Svalbard. Boreas 39

Lewin J, Macklin MG (2003) Preservation potential for late quaternary river alluvium. J Quat Sci 18: 107–120

Lønne I, Lyså A (2005) Deglaciation dynamics following the Little Ice Age on Svalbard: Implications for shaping of landscapes at high latitudes. Geomorphology 72: 300-319

Makaske B (2000) Anastomosing rivers: a review of their classification, origin and sedimentary products. Earth-Science Reviews 53: 149–196

Mangerud J, Dokken T, Hebbeln D, Heggen B, Ingólfsson O, Landvik JY, Mejdahl V, Svendsen JI, Vorren TO (1998) Fluctuations of the Svalbard-Barents Sea Ice Sheet during the last 150 000 years. Quaternary Science Reviews 17: 11-42

Martín-Moreno R, Àlvarez FA, Hagen JO (2017) "Little Ice Age" glacier extent and subsequent retreat in Svalbard archipelago. Sage Journals 27: 1379-1390

McMacin M, Godwin W (2017) Sabkha. In book: Encyclopedia of Engineering Geology.

Morales JA, Borrego J, Davies RA (2014) A new mechanism for chewier development and a facies model of the Saltés Island chenier plain (SW Spain). Geomorphology 204: 265-276

Muhammed Z, Bentley SJ, Febo LA, Droxler AW, Dickens GR, Peterson LC, Opdyke N (2008) Excess ^{210}Pb inventories and fluxes along the continental slope and basins of the Gulf of Papua. Journal of Geophysical Research 133, F

[1]Nichols G (2012) The Marine Realm: Morphology and Processes. In book: Sedimentology and Stratigraphy. Second Edition. Wiley-Blackwell, pp 163-178

[2]Nichols G (2012) Clastic Coasts and Estuaries. In book: Sedimentology and Stratigraphy. Second Edition. Wiley-Blackwell, pp 199-214

[3]Nichols G (2012) Processes of Transport and Sedimenatry Structures. In book: Sedimentology and Stratigraphy. Second Edition. Wiley-Blackwell, pp 44-68

[4]Nichols G (2012) Post-depositional Structures and Diagenesis. In book: Sedimentology and Stratigraphy. Second Edition. Wiley-Blackwell, pp 274-296

[5]Nichols G (2012) Terrigenous Clastic Sediments: Gravel, Sand and Mud. In book: Sedimentology and Stratigraphy. Second Edition. Wiley-Blackwell, pp 5-27

Norwegian Polar Institute (2018). Sea level in Barentsburg – annual mean. Environmental monitoring of Svalbard and Jan Mayen (MOSJ). URL: http://www.mosj.no/en/climate/ocean/sea-level.html

Posamentier HW, Morris WR (2000) Aspects of the stratal architecture of forced regressive deposits. Geological Society, London, Special Publication 172: 19-46
Prior DB, Wiseman WJ, Bryant WR (1981) Submarine chutes on the slopes of fjord deltas. Nature 290: 326–328

Rachlewicz G, Szczuciński W, Ewertowski M (2007) Post- «Little ice age» retreat rates of glaciers around Billefjorden in central Spitsbergen, Svalbard. Polish Polar Research 28: 159-186

Rachlewicz G, Szczuciński W (2008) Changes in thermal structure of permafrost active layer in a dry polar climate, Petuniabukta, Svalbard. Polish Polar Research pp. 261-278

Reineck H, Wunderlich F (1968) Classification and origin of flaser and lenticular bedding. Sedimentology 11: 99-104

Reineck HE, Singh IB (1973) Depositional Sedimentary Environments. With References to Terrigenous Clastics, 1st edn. Springer Verlag

Reineck HE (1976) Drift-ice on tidal flats, North Sea. Gèogr. Montrèal 30: 197-200

Salvigsen O (1984) Occurrence of pumice on raised beaches and Holocene shoreline displacement in the inner Isfjorden area, Svalbard. Polar Research 2: 107-113

Schieber J, Southard J and Thaisen (2007) Accretion of Mudstone Beds from Migrating Floccule Ripples. Science 318: 1760-1763

Sisulak CF, Dashtgard SE (2012) Seasonal controls on the development and character of inclined heterolithic stratification in a tide-influenced, fluvially dominated channel: Fraser River, Canada: Journal of Sedimentary Research 82: 244–257

Sumich JL (1996) An Introduction to the Biology of Marine Life, sixth edition. Wm. C. Brown, pp 30-35

Svendsen JI, Mangerud (1997) Holocene glacial and climatic variations on Spitsbergen, Svalbard. The Holocene 7: 45-57

Szcucinski W, Zajaczkowski M (2012) Factors controlling downward fluxes of particulate matter in glacier-contact and non-glacier contact settings in a sub polar fjord (Billefjorden, Svalbard). In: Sherwood LM, Hill P (ed.) Sediments, Morphology and Sedimentary Processes on Continental Shelves: Advances in technologies, research and applications, Wiley-Blackwell Publishing, pp 369-386

Tadahiro S, Okuno J, Hinderer J, MacMillan DS, Plag H, Francis O, Falk R, Fukuda Y (2006) A geophysical interpretation of the secular displacement and gravity rates observed at Ny-Ålesund, Svalbard in the Arctic – effects of post-glacial rebound and present-day ice melting. Geophysical Journal International 165: 729-743

Thomas RG, Smith DG, Wood JM, Visser J, Calverley-Range EA, Koster EH (1987) Inclined heterolithic stratification: terminology, description, interpretation and significance. Sedimentary Geology 53: 123-179

Tidevannstabeller for den norske kyst med Svalbard samt Dover, England (2018) Kartverket 81

Tinterri R (2011) Combined Sedimentary Structures and the Genertic Link Between Sigmoidal- and Hummocky-Cross Stratification. GeoActa 10: 1-43

Tjallingii R, Rohl U, Kolling M, Bickert T (2007) Influence of the water content on Xray fluorescence core-scanning measurements in soft marine sediments. Geochem Geophys Geosyst Geosy Geosyst 8

Tjallingii R, Stattegger K, Wetzel A, Phung VP (2010) Infilling and flooding of the Mekong river incised valley during deglacial sealevel rise. Quat Sci Rev 29: 1432–1444

Turner JN, Jones AF, Brewer PA, Macklin MG, Rassner SM (2015) MicroXRF Applications in Fluvial Sedimentary Environments of Britain and Ireland: Progress and Prospects, pp 228. Chapter 8 in Croudace IW, Rothwell RG (ed.) (2018) MicroXRF Studies of Sediment Cores, Development in Paleoenvironmental Researce É Springer Science 17

Veldkamp A, Kroonenberg SB (1993) Application of bulk sand geochemistry in mineral exploration and quaternary research: a methodological study of the Allier and Dore terrace sands, Limagne rift valley, France. Appl Geochem 8: 177–187

Wang MJ, Zheng HB, Xie X, Fan DD, Yang SY, Zhao QH, Wang K (2011) A 600 year flood history in the Yangtze River drainage: comparison between a subaqueous delta and historical records. Chin Sci Bull 56: 188–195

Weltje GJ, Tjallingii R (2008) Calibration of XRF core scanners for quantitative geochemical logging of sediment cores: theory and application. Earth Planet Sci Lett 274: 423–438

Wlodarska-Kowalczuk M, Szymelfenig M, Zajaczkowski M (2007) Dynamic sedimentary environments of an Arctic glacier-fed river estuary (Adventfjorden, Svalbard). II. Meio- and macrobenthic fauna, Estuarine, Coastal Shelf Science 74: 274-284

Appendix A – Results of ^{137}Cs and excess ^{210}Pb analysis

Core 20 (point bar)												
	depth	mid-depth	range	40K	uncertainit	137Cs	uncertainit	total 210Pb	uncertainit	supported 2	uncertainit	excess 210Pb
	cm	cm	cm	Bq/g		Bq/g		Bq/g		Bq/g		Bq/g
IG1537	0-1	0,5	0,5	0,4408	0,0414	0,0000		0,0261	0,0101	0,0268	0,0021	0,00
IG1538	5-6	5,5	0,5	0,6104	0,0534	0,0007	0,0003	0,0484	0,0153	0,0338	0,0023	0,0146
IG1539	10-11	10,5	0,5	0,4575	0,0419	0,0000		0,0438	0,0145	0,0336	0,0024	0,0102
IG1540	15-16	15,5	0,5	0,4945	0,0433	0,0007	0,0003	0,0442	0,0136	0,0355	0,0023	0,0087
IG1541	19-20	19,5	0,5	0,5448	0,0508	0,0005	0,0006	0,0508	0,0168	0,0347	0,0026	0,0161
Core 24 (point bar/tidal flat)												
IG1553	5-6	5,5	0,5	0,4736	0,0479	0,0000		0,0632	0,0211	0,0448	0,0034	0,0185
IG1554	10-11	10,5	0,5	0,4394	0,0405	0,0000		0,0491	0,0158	0,0431	0,0029	0,0060
IG1555	15-16	15,5	0,5	0,4375	0,0427	0,0000		0,0457	0,0163	0,0347	0,0027	0,0110
IG1556	20-21	20,5	0,5	0,4330	0,0407	0,0000		0,0345	0,0128	0,0297	0,0022	0,0048
IG1557	25-26	25,5	0,5	0,4487	0,0447	0,0000		0,0290	0,0125	0,0292	0,0024	0,0000
IG1558	30-31	30,5	0,5	0,6030	0,0569	0,0000		0,0471	0,0166	0,0343	0,0026	0,0128
IG1559	35-36	35,5	0,5	0,6191	0,0612	0,0000		0,0335	0,0158	0,0345	0,0029	0,0000
Core 26 (tidal flat)												
IG1530	0-1	0,5	0,5	0,6211	0,0562	0,0000		0,0427	0,0146	0,0315	0,0025	0,0112
IG1531	5-6	5,5	0,5	0,5796	0,0541	0,0000		0,0434	0,0154	0,0323	0,0026	0,0111
IG1532	10-11	10,5	0,5	0,5658	0,0544	0,0007	0,0011	0,0397	0,0155	0,0306	0,0026	0,0091
IG1533	15-16	15,5	0,5	0,5826	0,0530	0,0000		0,0410	0,0142	0,0298	0,0023	0,0112
IG1534	20-21	20,5	0,5	0,5534	0,0486	0,0004	0,0006	0,0350	0,0116	0,0302	0,0021	0,0049
IG1535	25-26	25,5	0,5	0,4855	0,0469	0,0007	0,0004	0,0320	0,0128	0,0299	0,0023	0,0021
IG1536	30-31	30,5	0,5	0,5346	0,0513	0,0000		0,0329	0,0136	0,0340	0,0026	0,0000
Core 2 (tidal flat)												
IG1408	0-2	1	1	0,5506	0,0499	0,0017	0,0008	0,0528	0,0176	0,0359	0,0026	0,0169
IG1409	5-7	6	1	0,5518	0,0492	0,0069	0,0011	0,0283	0,0109	0,0262	0,0021	0,0021
IG1410	10-12	11	1	0,5786	0,0503	0,0000		0,0343	0,0117	0,0269	0,0019	0,0074
IG1411	14-16	15	1	0,6109	0,0538	0,0000		0,0321	0,0120	0,0284	0,0021	0,0037
IG1412	20-22	21	1	0,6661	0,0584	0,0000		0,0336	0,0120	0,0269	0,0021	0,0067
IG1413	25-27	26	1	0,7070	0,0617	0,0000		0,0301	0,0113	0,0298	0,0022	0,0003
IG1414	30-32	31	1	0,6868	0,0627	0,0000		0,0282	0,0134	0,0309	0,0025	0,0000
IG1415	35-37	36	1	0,7067	0,0625	0,0000		0,0301	0,0118	0,0277	0,0022	0,0024

Appendix B - Calculations of ^{137}Cs and excess ^{210}Pb sediment accumulation rate

^{137}Cs sediment accumulation rate
Core 20: 19,5 cm/65 years = 0,3 cm/year
Core 24: Calculations can not be done as it is unknown if ^{137}Cs was present in the uppermost 5 cm.
Core 26: 25,5 cm/65 years = 0,4 cm/year
Core 2: 6 cm/64 years = 0,1 cm/year

Average ^{137}Cs sediment accumulation rate: 0,3 cm/year + 0,4 cm/year + 0,1 cm/year = 0,3 cm/year

Excess ^{210}Pb sediment accumulation rate
Core 20: 19,5 cm/100 years = 0,2 cm/year
Core 24: 30,5 cm/100 years = 0,3 cm/year
Core 26: 25,5 cm/100 years = 0,3 cm/year
Core 2: 36 cm/100 years = 0,4 cm/year

Average excess ^{210}Pb sediment accumulation rate: 0,2 cm/year + 0,3 cm/year + 0,3 cm/year + 0,4 cm/year = 0,3 cm/year